[Supplementary material]

Hunter-gatherer metallurgy in the Early Iron Age of northern Fennoscandia

Carina Bennerhag[1], Lena Grandin[2], Eva Hjärtner-Holdar[2], Ole Stilborg[3] & Kristina Söderholm[1,*]

[1] The History Unit, Lulea University of Technology, Lulea, Sweden

[2] The Archaeologists, National Historical Museums, Sweden

[3] Archaeological Research Lab, Stockholm University, Sweden

[*] Author for correspondence: ✉ kristina.soderholm@ltu.se

Materials and methods

Metallurgical material representing ore, metal, slag and technical ceramics were selected and analysed through archaeometallurgical analyses and radiocarbon dating from three archaeological sites in northernmost Sweden where various process steps in the production of iron have taken place. The analyses were carried out continuously as the various sites were found and excavated. The first excavated site is Sangis 730, where forging of iron took place. The second site is Sangis 842, an iron production site that was found a few years later. The third site is Vivungi 723, also an iron production site. The archaeometallurgical analyses of the sites are presented in the OSM in the order in which they were discovered and excavated, in part because this influenced how the analyses were carried out. Radiocarbon datings are presented in Table S5.

Several different archaeometallurgical analytical methods were used for the metallurgical finds from the sites. Analyses were performed primarily on slags and metal, and to a smaller extent on ore and furnace wall (technical ceramics). In general the same analytical method(s) were used for the respective type of material from all three excavated sites, although slight deviations may occur. Some methods are general for several types of material, while others are unique for a material category. For several of the material categories a combination of analyses were carried out (e.g. slags were analysed in both a polarisation microscope and with bulk chemical analytical methods). In the following sections, details on the samples and the methods used are described and, if needed, any deviations are specified.

Sample selection for archaeometallurgical analyses

Extensive archaeometallurgical material was collected from the respective site, of which only a fraction was analysed. The selection was made to provide a basis for describing the raw material (ore), waste (slag and metal waste), material for furnace construction (clay) and product (iron/steel) and for interpreting the processes in iron production and forging that have taken place. In total, 27 samples of slag (Sangis 730: 9 pcs, Sangis 842: 10 pcs, Vivungi 723: 8 pcs), 28 samples of technical ceramic (Sangis 842: 8 pcs, Vivungi 723: 20 pcs), 17 samples of iron waste (Sangis 730: 6 pcs, Sangis 842: 7 pcs, Vivungi 723: 4 pcs), 5 iron objects (Sangis 730) and 3 samples of iron ore (Sangis 730: 1 pcs, Vivungi 723: 3 pcs) were analysed through archaeometallurgical analyses.

Visual inspection

Slags and iron were first inspected visually and characterised with respect to form and type. Slags were also characterised with respect to degree of magnetism. The pieces were divided and the cross section examined to get additional information about composition and whether they were homogeneously or heterogeneously built up. The technical ceramics (furnace walls) were inspected in a corresponding way and samples taken to determine the materials used and their heat resistance. Ores (in this case limonite ores) were studied with a stereo magnifier to get an understanding of contamination from other material (e.g. sand).

Sampling

Slags were cut and sampled for bulk chemical analyses. From the cross-selection also a selection was made for preparation of thin sections for optical microscope. Thin sections are produced from a sawed-away slice of the slag, which is attached to a slide and ground/polished to a microscopically thin sample (approximately 0.03mm). The saw cut is normally placed and oriented so that all included parts are represented. The technical ceramics were divided and sampled for production of thin sections in the same way as slag. Iron samples (and sometimes also slag and limonite ore) were cut and a cross section was mounted in a two-component epoxy resin, and subsequently ground, and polished using diamond pastes to a 3µm finish. Iron samples were etched and analysed using a microscope and in certain cases in an electron microprobe. Ores intended for bulk chemical analyses were sent as bulk samples to an external laboratory. Depending on grain size and possible heterogeneity, the sample quantity varied from just a few grams up to several kilos.

Petrographic/metallographic analyses of slag, technical ceramics, ore and iron using a microscope

Slag, iron and in particular cases limonite ore were examined in a polarisation microscope to see how they are built up. Slag primarily consists of the minerals olivine and wüstite and of glass. Other minerals that occur include magnetite, leucite, hercynite and limonite, and there is often also a small quantity of metallic iron present. Its appearance at microscale shows details of slag formation that reveal under what temperature and oxygen conditions the slag was solidified. This in turn says something about whether the slag was formed inside or outside a furnace, or in a hearth, and whether the process was homogeneous or heterogeneous. The grain size of limonite ore is generally too small to be observed in an optical microscope, but certain textures can be studied.

The petrographic and metallographic examinations were conducted in reflected light (plane-polarised light) in order to identify the material's various components and textural features. The examinations were done with a Zeiss Axioskop 40A polarization microscope (up to 500× magnification) equipped with an integrated computer-linked camera (Zeiss AxioCam MRc5) for continuous digital documentation of the analyses.

Thin sections of technical ceramics were analysed in a polarisation microscope in a similar way as slag. With this method the quantity, grain size distribution and type of natural coarse material (silt and sand) can be determined. Furthermore, the quantity and grain size of any added tempering can be separated and assessed. A mineralogical determination of the coarse fractions in the clay can also be made. The clay's content of iron oxide, mica, ore and other minerals can further be estimated. At magnifications of 600–1000× any occurrence of e.g. diatoms and fossiliferous limestone can be studied.

Iron samples were examined first with respect to any slag content and distribution, after which the iron was etched with 2 per cent nital solution. This affects the metal differently depending on composition and the method was used partly to determine carbon content in iron, whether it is a soft, carbon-free iron, steel (with up till 2 per cent carbon) or cast iron, which contains over 2 per cent carbon.

Bulk chemical analyses of slag and ore

Bulk chemical analyses of slags and ores were performed by ALS Scandinavia (samples from Sangis) and ALS minerals (samples from Vivungi). The analytical methods used were primarily ICP-AES for major elements (oxides) and some metals, and ICP-MS for trace elements including rare earth elements (REE). Regularly, internal standard slag samples are

analysed in order to check accuracy and precision. A total of 43 (Sangis) and 59 (Vivungi) elements were analysed in each sample. The complete result is presented in table form (Table S3) where the major elements are indicated as oxides and the rest as pure elements, even if these actually occur in more complex forms.

Microprobe analysis of slag inclusions and iron

In order to chemically analyse slag inclusions in iron, a Cameca-SX100 (EPMA) electron microprobe with wavelength-dispersive method (WDS) at the Department of Geosciences, Uppsala University was used. In the polished iron sample's slag inclusions, point analyses in the respective phase as well as surface analyses were conducted to quantify the bulk chemical composition of the slag (Table S1). The composition of the metallic iron (Table S2) was also analysed in the microprobe. Operating conditions during runs involved an acceleration voltage of 20kV and an electron beam current of 15nA. The obtained analytical data were related to standards (oxides, sulphides, metals) and ZAF corrected.

Radiocarbon dating

Radiocarbon dating was carried out on charcoal and burnt animal bone material from construction remains and charcoal inclusions in slag, as well as on iron objects and iron waste (carbon extracted from metal). The dated material was pre-treated in various ways depending on material type and weight according to the laboratory protocols of the two radiocarbon dating laboratories used, i.e., Ångström Laboratory in Uppsala, Sweden (Ua) and Poznan Radiocarbon Laboratory, Poland (Poz). Retrieved radiocarbon ages were all calibrated using OxCal v4.4.2 (Bronk Ramsey 2020) and the IntCal 20 atmospheric curve (Reimer *et al.* 2020) and given as age ranges for each dated sample at 2σ. Details on the samples are provided in Table S5.1–S5.2.

Archaeometallurgical concepts and assumptions

The ore used for iron production in a bloomery furnace is normally limonite. Limonite occurs in nature e.g. as bog-iron ore and lake-iron ore, containing up to 62 weight percent iron. Limonite can be considered iron(III) oxide-hydroxide FeO(OH) with varying water content and the minerals goethite, lepidocrocite and ferrihydrite have been demonstrated. Slag primarily consists of the minerals *olivine* and *wüstite* and *glass*. Other minerals that occur include *magnetite, leucite, hercynite* and *limonite*, and there is often also a small quantity of metallic iron present. Olivine is a silicate mineral with the general formula A_2SiO_4, where A

is usually iron (fayalite). The iron oxide *wüstite*, FeO, is also very common primarily in slags from bloomery furnaces, and is formed with reduction of hematite and/or magnetite, and is reduced in turn to metallic iron. Glass constitutes the "residual melt" of the slags and can therefore vary significantly in composition. The iron oxide *magnetite*, Fe_3O_4, can occur instead of wüstite if temperature and/or oxygen partial pressure are sufficiently high. This means that it is possible to distinguish slags that solidified inside or outside a furnace (bottom slag or tap slag) or determine whether these are smithing slags. High aluminum levels in combination with high potassium levels are found in the mineral *leucite*, $KAlSi_2O_6$, which in certain slags can occur instead of the more common glass phase. The grain size of the minerals is also significant, where fine-grained slags show rapid cooling and coarse-grained slow cooling. The latter normally indicates cooling inside the bloomery furnace (Buchwald 1998; Buchwald 2005).

Among the major elements, iron and silicon commonly occur with the highest content in slags from iron production in a bloomery furnace (reduction). In broad terms these elements constitute an indirect measure of the efficiency of the iron production and theoretically this generally results in a high content of silicon in the slag the more iron that has been extracted as metal for the same iron content in an ore. Other major or minor elements (e.g. aluminum, calcium and potassium) may occur in ores as well as in furnace walls and fuel, and contribute to the slag composition. The contribution besides ore is often assessed as marginal but should not be underestimated. Other substances that are considerably more interesting to link to the ore are e.g. manganese, phosphorous, titanium and magnesium. These can occur from a few tenths of a weight percent up to several percent, or in the case of manganese even tens of weight percent (as MnO). Phosphorous is also a commonly occurring element in ores and helps in distinguishing various ore regions. Phosphorous also has a mostly positive effect on the produced (bloomery) iron by contributing to a harder, but still ductile, iron compared with phosphorous-free iron. Phosphorous distributes during the production process between metal and slag, for which reason an elevated phosphorous level in the slags is a signal that phosphorous iron may have been produced. Slag from primary smithing mainly has a composition that corresponds to that with reduction slag (Buchwald & Wivel 1998; Buchwald 2005).

Elements that occur in significantly lower amounts, known as trace elements, may be significant for comparing slags with each other and with ores in order to see if there is a common origin, and if this can be linked to any specific geologic/geographic context. Among these are, for example, barium (Ba), which is often correlated with manganese content (Mn).

Other elements that may be important to compare are nickel (Ni), vanadium (V), cobalt (Co) and chromium (Cr), as well as the group of rare earth elements (REE). Terms used to describe iron include *ferrite*, which is the soft (pure) iron without carbon, *cementite*, which is a compound of iron and carbon (Fe_3C, also called iron carbide), and *pearlite*, which is a structure (texture) built up of laminae with alternating ferrite and cementite. In grey cast iron there are also *graphite laminae* which are thin slices of pure carbon. A structure that is formed during cooling in white cast iron is *ledeburite*, which consists of a mixture of cementite and pearlite. In general a larger quantity of pearlite entails a higher carbon content and harder iron. Occurrence of phosphorous is commonly seen as a superimposed dendritic texture. Phosphorous (in low concentrations) makes e.g. a carbon-free/low carbon content (ferritic) iron harder, but the ductility of the ferrite is retained. High levels of phosphorous are negative however for the quality of the iron. It is also possible to see how the iron has been worked, e.g., if different pieces have been joined together. Such welding can create a seam that is visible as a deviating line in the sample and sometimes also bordered by slag. Different heat treatments such as quench hardening can also be distinguished (i.e. heating with subsequent rapid cooling in, for example, water). The structure thus formed is called *martensite*. Hardened steel can also be tempered (heating up without rapid cooling) to reduce the brittleness and reshape the martensite. Annealing (heating up without rapid cooling of unhardened steel) can be seen in rounder forms of cementite (spheroidising) and leads to a softer, less brittle steel (Devos *et al*. 2000; Heimann *et al*. 2001; Grandin 2016; Dillmann *et al*. 2017; see also Historical Metallurgical Society 2021).

S1: analytical results, Sangis 730

S1.1: slag

After the visual inspection is done, a general division of the material into different categories is made based on the morphology of the slags, with some variations. All slags can probably be defined as various types of smithing slags. A couple of smithing hearth cakes and parts of smithing hearth cakes occur. Among the fragments there are hammer scales formed during secondary forging when objects are worked on an anvil. Among the recorded slags there are also homogeneous and dense slags, built up of several superimposed slag flows, which normally is characteristic in the reduction process, but among those inspected there are examples where the flows have built up forms that occur from smithing. A selection of these slags has been examined and analysed further to clarify from which process stage they

originate. Among the slags that have been microscopically examined there are two main types: a homogeneous slag that has been formed under even and reducing conditions, and a complex slag that has been formed under varying and mainly oxidising conditions. The homogeneous slags are few in number, but with features that are characteristic of reduction slags and contain wüstite, olivine and a glass phase as well as small drops of metallic iron. The other slag type is more frequent in the examined material. This type has a bottom layer of sand and over this normally are also built up in layers with varying proportions between the minerals present, including one or more iron oxides that reflect varied but primarily oxidising formation conditions, also with varying temperatures. All this is characteristic of secondary forging.

Find no. 980, A4

Irregular magnetic slag with imprint of bottom/corner. Weight 128.3g. Sandy bottom area with larger stone melted in, otherwise homogeneous slag (Figures S1–S2). In the microscope a complex piece of slag emerges built up of layers of various materials, but also several layers of the same, or similar, slag with boundary areas of magnetite horizons. In the bottom there is a layer of sandy material dominated by quartz and feldspar grains. Small amounts of slag are also melted into this. The sand layer is not comprehensive, instead there are areas where slag extends down to the same level as the bottom of the sand layer. In the entire sample the slag consists of olivine laminae, a glass phase or local leucite, and iron oxides. The proportions and grain sizes vary heterogeneously, as well as which iron oxide occurs. The grain size is smallest in the bottom layer, then it increases successively until a magnetite horizon is defined against the next slag with finer grains and other proportions (Figure S3). Metallic iron is lacking in the sample. In the lower parts there are magnetite crystals as well as wüstite dendrites. The latter are consistently more fine-grained than the magnetite and are embedded in the olivine crystals, and the dendrites are not homogeneous in composition, but instead contain both a wüstite and a magnetite component. Higher up in the slag a larger portion of dendritic wüstite occurs, but this has plentiful magnetite laminae and magnetite spots. The rounder wüstite forms (Figure S4) as well as the blockier magnetite are complexly built up of both wüstite and magnetite. This is a complex slag that demonstrates varying oxygen access.

Find no. 1112, A4

Irregular, weakly magnetic slag with charcoal imprint and imprint of sandy bottom. Eight pieces, total weight 241.0g. Mainly homogeneous slag (Figures S5–S6) with sand melted in and a couple of pieces with sandy bottom area. In the microscope a slag emerges that is relatively homogeneous (Figure S7). No clear layering can be seen. It contains dendritic wüstite (Figure S8), olivine laminae and a glass phase in approximately the same proportions in the entire section. The grain size is also similar except in the very bottom layer where it is somewhat more fine-grained. Several pieces of charcoal are encased. Scattered drops of metallic iron occur sporadically. In the bottom layer there is fused sandy material with a large proportion of quartz grains. Along the bottom area, and locally along the upper area there are small concentrations of metallic iron; in the bottom together with a thin zone of iron oxides. The homogenous construction of the slags is characteristic of reduction slags or at least slags from early process stages. The occurrence of wüstite, and absence of magnetite, as well as the consistently homogeneous crystals also indicate this.

Find no. 1344, A4

Irregular nonmagnetic slag. Four pieces with total weight 301.2g. The largest piece has bottom and wall of cemented sand, and melted on an inside surface where slag is lacking. In cross-section (Figure S9) a clear layering is visible, which also emerges clearly in the microscope. In a bottom layer (Figure S10), which also extends along the sides, there is an even layer of sandy material that consists mainly of quartz grains but also has grains of feldspar, sandstone and/or quartzite. The grains are not smelted in but some are cracked and between them there is a partially melted matrix containing slag. This slag contains a glass phase and olivine crystals, and in places also fine-grained magnetite crystals. Over the sandy layer there is a layer of slag fused together with the sand layer. The slag layer mainly contains olivine crystals and a glass phase as well as a small amount of fine-grained dendritic wüstite. Within the layer some quartz grains are also melted in. The slag layer changes successively to another slag layer. This is also dominated by olivine crystals. In addition, a glass phase occurs and accumulations of magnetite crystals or more irregular, locally oblong magnetite concentrations (Figure S11). The magnetite crystals are complexly built up in places with varying composition from the core and out toward the edges. All this indicates a complex slag.

Find no. 1521, A4

Convex magnetic slag, with clear form from bottom and sand cemented to it. Weight 383.9g. Almost whole slag, partly sandy bottom layer, partly glassy top area that stands out even more clearly in cross section. It is also striking in the petrographic analysis that the slag is built up of several layers. At the bottom is a layer of sandy material that is dominated by quartz grains but grains of feldspar and sandstone/quartzite are also found. These are fused together by a fine-grained semi-melted matrix. The upper parts of the layer are melted to the lower slag layer, which contains olivine laminae and a glass phase. This slag layer changes successively into a slag layer with large quantities of iron oxides, olivine laminae and a glass phase, locally leucite too. The proportions between the different phases vary but there are no sharp boundaries between them. In the lower part, the iron oxides are dominated by dendritic wüstite but magnetite crystals take over in the upper parts and at the very top there are thin bands of magnetite. Magnetite also occurs sporadically in the lower parts of the slag. There is also wüstite with magnetite laminae in the sample. This is characteristic of a smithing slag that is formed under quite variable oxygen conditions.

Find no. 913, A53

Plano-convex nonmagnetic slag (Figure S12). Weight 146.9g. Homogeneous slag with only sporadically sandy bottom layer but clear strings of slag at the bottom. Charcoal imprint in the bottom and top area. Grey to rust-brown. In cross-section: homogeneous slag, which is denser at the bottom, more porous higher up (Figure S13). The petrographic analysis shows that the slags are mainly homogeneous (Figure S14). Only in a thin lower layer does this deviate by being somewhat more fine-grained and with less iron oxide than in the rest of the slag. In the lower parts olivine crystals dominate with a glass phase and dendritic wüstite in a smaller quantity. Otherwise there is dendritic wüstite, olivine laminae and a glass phase plus a small quantity of droplets of metallic iron. The iron oxide in the slag is almost solely wüstite (Figure S15). Only in a very limited area in the upper part of the slag next to a cavity are there some scattered occurrences of magnetite. The homogeneous construction of the slag and occurrence of wüstite in combination with lack of magnetite is characteristic of slags from the reduction process or early process stages in smithing.

Find no. 3448, A45

Irregular magnetic slag. A total of 20 pieces with total weight 200.9g. Slag with rusty sections and cemented/fused sand. The petrographic analysis shows a heterogeneous slag. The slag is dominated by iron oxides, with smaller amounts of olivine crystals, a glass phase

and leucite. The proportions between these vary frequently through the entire slag. The iron oxides vary (Figures S16–17) from scattered magnetite crystals, both in lower and upper parts, by way of thin wüstite dendrites and compact wüstite concentrations to thin horizontal lobate bands of wüstite with magnetite laminae. Locally complex formations with core of iron oxide(s) also occur. These are overgrown by thin laminae of spinel containing silicon, in turn overgrown by olivine. The complexity of the slag is also seen in the form of zoned olivine crystals, where a thin outer rim deviates from the olivine core's composition. Metallic iron only occurs in a few small drops. Combined this reflects very complex conditions as far as both temperature and access to oxygen are concerned in this smithing slag.

Find no. 3764, A45

Irregular weakly magnetic slag with charcoal imprint. A total of four pieces with total weight 109.1g. Viscous slag. One piece has a sandy bottom layer. The petrographic analysis shows that the slag is built up in layers but without clear contacts between the layers. At the very bottom there is a thin layer of corroded material and secondarily affected slag. In this zone there is a thin film of complex iron oxides. Over this the actual slag begins. In the lower half it is dominated by dendritic wüstite with olivine in smaller quantities and a subordinate glass phase. Higher up the wüstite content is reduced and in the upper parts coarse-grained olivine occurs along with a glass phase and also leucite in places. In the outer parts of the upper half other material is incorporated. At the very top in one half of the sample there is material rich in quartz which is also partially melted and integrated with the slag. In the wüstite-dominant lower layer there are some oblong accumulations of iron oxide that are more compact. In terms of composition this also appears to be wüstite, which may possibly be hammer scale that fell down into the slag and was partly transformed in a reducing environment. Primarily in the upper parts of the slag there is wüstite that contains magnetite laminae. Metallic iron occurs in some scattered droplets only micrometers in size. As an entirety this shows a complexly built-up smithing slag that formed under varying conditions.

Find no. 1763, A29

Irregular weakly magnetic slag with charcoal imprint. Weight 49.7g. Viscous slag with sand melted in, glassy sections, and sandy bottom. The slag is clearly layered in its construction. Petrographic analysis shows that there are three different layers. A lower layer is made up of slag that contains olivine, iron oxide(s) and glass; a middle layer is made up of slag consisting of olivine and glass; and an upper layer consists of sandy (and somewhat coarser)

material with grains of quartz in a glassy matrix rich in silica integrated with slag concentrations. The slag in the bottom, which is somewhat more fine-grained and has cooled somewhat faster than in the higher levels, has in addition fused with the sand grains. The iron oxides are either separate crystals or several together in complex formations. On the one hand there are wüstite dendrites and wüstite dendrites with magnetite laminae, on the other there is magnetite in dendrite-like but more pointed forms. There are also zoned magnetite crystals. All of the complex iron oxides that occur in major parts of the sample suggest that this is a smithing slag that formed under quite variable oxygen access.

S1.2: iron

The largest group of iron specimens is made up of undefinable rusty lumps. Scattered finds that are possibly parts of objects or iron bars also occur, as does slag with a notable percentage of metallic iron. Upon examination in the microscope many of these undefinable lumps turn out to be unconsolidated (i.e. not compacted). They thereby show no signs of advanced working or forging. This indicates that this is waste from rather early stages in the process, either from the bloomery process or when the bloom is cleared of slag. Several of these iron lumps have high carbon content, while two are very low-carbon, i.e., soft iron. Among the objects steel with rather high carbon content is common, but there is also one knife with lower carbon content but elevated phosphorous content.

Find no. 922, A4

Three irregular, rusty magnetic lumps without imprint. Total weight 40g. In the divided section of one of them an irregular core of iron with slag emerges (Figure S18). In the microscope a mixture of coarse-grained slag and spongy metallic iron appears. The slag consists of dendritic wüstite, olivine laminae and a glass phase. There are also a number of cavities. With etching an evenly grained, relatively fine-grained ferrite emerges in the whole sample (Figure S19). Only in a very limited area close to one outside edge are there small quantities of pearlite along with the ferrite. This piece has been lost in an early stage in the process, before the iron has been consolidated properly. Possibly this is a part that has not been in contact with the bloom, or alternatively it was formed in its outer parts. The iron in itself is very homogeneous however in composition; a mainly soft iron completely free of carbon.

Find no. 925, A4

A rusty, irregular, magnetic lump with cemented sand. Weight 4.4g. In the metallographic analysis of the divided section, a core of metallic iron emerges with cavities and corrode areas, surrounded by fragments of pieces of charcoal. The iron sample is covered to a large degree by a thin layer of iron oxides. Outside this is an irregular layer of complex composition with pieces of charcoal and parts of hammer scales that probably are cemented on the iron. Etching of the sample shows the same texture across large parts of the cross section with high carbon content (Figure S20), mostly over 1 per cent. There are coarse grains of pearlite throughout mostly with cementite, locally with ferrite, in the grain boundaries. In some places however, only pearlite occurs. In other areas there are indications that cementite contains phosphorous, but this is not verified by chemical analysis. The small lump consists of steel with high carbon content throughout. It contains cavities which indicates that it has not been extensively worked.

Find no. 7045, A4

Irregular strongly magnetic piece with rusty area, 10.5g. In the divided section an irregular core of iron appears with cavities and spots of rust and/or slag. The metallographic analysis shows that the metallic iron contains cavities and is corroded in spots. The outer edge is also corroded with scattered charcoal and hammer scale fragments baked into the rust layer. There is slag primarily on the outer edges and in connection with larger corroded areas. The slag is mostly rather coarse-grained and consists of dendritic wüstite and a glass phase. In some inclusions there is only a glass phase. With etching a texture emerges that is dominated by pearlite. Normally there are also thin cementite laminae, but locally only pearlite. Thus this is a homogeneous steel with a consistently high carbon content. It contains cavities and has probably not been extensively worked.

Find no. 1840, A53

Oblong iron object or iron bar, strongly magnetic with corroded area, 6.7g. In cross section an irregular core of iron is seen surrounded by rust and with spots of rust and possibly slag in more central parts. The metallographic analysis shows that the sample is dominated by metallic iron, locally corroded. Slag occurs only in a few small areas at the outer edges of the sample and along a border where the iron is slightly spongy. The inclusions consist mainly of a glass phase. In the surrounding slag on the outside olivine also occurs. When the sample was etched a texture emerged that demonstrates a high carbon content. Large areas are made up of pearlite with cementite laminae, but locally, in the core of the sample, there is even

higher carbon content in the form of white cast iron. Overall this piece has high or very high carbon content. It has not been extensively worked and was probably lost early in the process. Cast iron is normally associated with smelting in a blast furnace. Here however this concerns a very limited occurrence, which now and then appears locally in bloomery iron (e.g. in the vicinity of charcoal). Considering that high carbon content is common in all of the investigated material, this sample should therefore not be rejected as more modern, but instead probably belongs to the context generally.
Upon analysis with EPMA (Table S2) of the metal, only iron has been noted in concentrations above the detection limits (carbon cannot be detected with the microprobe used). Slag inclusions that have been analysed (Table S1) consist of a glass phase dominated by silicon. In addition, manganese occurs at rather high or in some cases very high content. Phosphorous however occurs only in very small concentrations.

Find no. 878, A29

Knife, corroded (Figure S21). A cross section has been made through the blade from its back to its edge. The section is oblong and triangular with a base of 4mm and length of 15mm. The metallographic analysis shows that large parts of the triangular cross section are preserved metallic iron. It is corroded at the outer edge, including at the very tip. Slag inclusions run from edge to back, primarily along a central band (Figure S22). The inclusions are small, thin and elongated parallel to the extension of the entire band of slag. They are mostly drawn out in “plastic” condition. The largest, concentrated to the central band, include a glass phase. Among the smaller inclusions are some that contain wüstite. Wüstite also occurs in a number of larger, more irregular, inclusions along the long side. After etching steel emerges with only small variations in composition. In the core, in a band from the edge to the back, almost only pearlite occurs with small quantities of ferrite in the grain boundaries, with a carbon content of about 0.7%. On either side of this, the blade consists of pearlite with somewhat larger quantities of ferrite in the grain boundaries (the carbon content here is about 0.5 per cent). No clear welding lines can be seen between these bands even though a band of slag inclusions borders the contact between them (Figure S23). With electron microprobe the iron was analysed at several points across the full width but no other elements are found in concentrations above the detection limits (Table S2). The slag inclusions vary in chemical composition. Those in the central band, which is dominated by a glass phase (analysis 1b1-1b3 in Table S1), have a large amount of silicon. They are also rich in manganese. The inclusions at the outer rims, which are dominated by wüstite, are dominated by iron while

other elements occur in amounts below 1 weight percent each. In summary, it can be noted that the cross section through the knife blade shows a steel with a somewhat higher carbon content in a central band from the edge all the way to the back. On either side of this central band the carbon content is somewhat lower. Possibly it is forged together from two different qualities, alternatively welded in folds from the same original material with somewhat varying composition creating a laminated structure. The knife is not hardened but has carbon content which is very suitable for hardening. The occurrence of slag inclusions and their oblong, elongated form show signs of extensive forging of the knife.

Find no. 3789, A29

Irregular, magnetic, viscous slag with sandy bottom layer, 7.8g. In cross section a homogeneous, viscous slag appears with concentration of unconsolidated metallic iron. Metallographic analysis of the iron concentration shows that it has a large, centrally located cavity, several smaller cavities, and a number of corroded areas. True slag inclusions cannot be distinguished, however. In the metal there is a texture, fine-grained and resembling dendrite, which possibly is slag. Analyses with electron microprobe show however that it is not slag, but only corroded iron. The metallic iron contains no other elements in amounts above the detection limits (Table S2). With etching of the sample an evenly-grained ferrite emerges in all of the preserved metallic iron, which is not extensively worked and must have been lost in an early stage in the process.

Find no. 1559, A27

Irregular magnetic piece, 8.5g, with rusty area. Metallographic analysis of the trapezoid-shaped cross section shows a core of dense metallic iron surrounded by a thin corrosion layer. Clear bands of slag inclusions appear parallel to the long side of the section, but they bend toward one corner on the longest side. At the opposite base, at the short side parts of the inclusions bend around (Figure S24) from the one long side to parallel with the short side and back to become parallel with the other long side. The inclusions occur partly in thin, partially interrupted bands that contain only a glass phase, and partly in extended bands that consist solely of wüstite. Etching of the sample shows that the carbon content varies somewhat. It is highest in two bands along the long sides (Figure S24) and a central band (up to 0.6–0.7 per cent), and lower in between (0.1–0.2 per cent). The lowest carbon content is seen in connection with the broader slag inclusions. Locally a Widmanstätten pattern can be seen, which shows that the material has been cooled. In summary it can be noted that the iron

(steel) is welded from one piece by means of repeated folding, or composed of at least two different qualities. The difference in the composition may have arisen in early outer edges when these have been welded together (i.e. this has resulted in lower carbon content along weld seams). Alternatively, the iron has originally had this lower carbon content in contact with the slag inclusions rich in wüstite (because of local chemical equilibrium during the reduction). The piece is severed in hot condition from a somewhat larger, possibly nearly finished object.

Find no. 2021

Knife, conserved (Figure S25). A cut has been made through the blade from the edge to the back. The cross section is triangular with the base of 5mm and the height of 23mm. The outer parts, including the edge, are corroded. The metallographic analysis shows that the iron contains a fairly large quantity of slag inclusions. There is both a large central band with broader and more scattered, small and winding inclusions. They are distributed across the whole width of the cross section but are not completely elongated; instead they appear to be evenly distributed. This can possibly be due to intense heating, which has made oblong inclusions become more drop-like. They consist of several phases, possibly wüstite has crystalized along the border to the metal and both olivine and a glass phase can be observed in the majority. A clearly banded structure emerges with etching of the sample (Figure S26). The bands run somewhat unevenly but parallel with the height of the triangular cross section (i.e. from the edge toward the back). These vary in width, composition and grain size. Bands of coarse-grained ferrite alternate with bands of finer-grained ferrite with a superimposed phosphorous texture. Some thin bands of ferrite with small quantities of pearlite in the grain boundaries are also found. A somewhat higher quantity of pearlite is also found in a concentration near the outer rim on the back side. Here pearlite grains dominate with ferrite in the grain boundaries. The absolute edge is lacking, for which reason it is not possible to determine which of all the bands that run out into this, but it seems as if it is a band with ferrite and pearlite. Analyses with electron microprobe (Table S2) show that the iron contains phosphorous in concentrations up to 0.4 weight percent. Cobalt and wolfram possibly also occur, but these amounts are at the detection limit for the respective elements, for which reason their occurrence is more uncertain. The bulk composition of the slag inclusions (Table S1) has been analysed. They are rich in iron but also contain silicon as well as phosphorous (notably high quantity) and manganese.

In summary it can be noted that the knife's content of phosphorous is rather high and has increased the hardness of the material. Phosphorous is not evenly distributed however but is concentrated in some of the bands. Other bands that contain carbon also occur, which also increased the hardness. However, bands that lack both carbon and phosphorous also occur and reduce the hardness. The metal has been heat treated which is seen locally in the carbon-rich areas as a spheroidised texture and by means of the dendritic texture of the phosphorous occurrence.

Find no. 2684

Axe (Figure S27) which is conserved. A cut has been made through the blade at the best preserved edge. The cross section is triangular in form, with a base of 8 mm and a height of 16 mm. The metallographic analysis shows two bands of preserved metallic iron in the triangular cross section that runs parallel out toward the edge, but not all the way out in the edge which is corroded (Figures S28–29). The two bands are separated by corroded iron. In the preserved metal, but also in corroded areas, there are slag inclusions. These are small but collected in concentrations that extend parallel with the preserved metallic bands. The inclusions are dominated by wüstite, usually surrounded by a thin zone of a glass phase. The very thinnest inclusions contain only one glass phase and extremely fine-grained olivine. Etching of the sample shows that iron bands (Figure S29) that reach farthest out toward the tip are made of quenched carbon steel (martensite) which is annealed (but probably not completely) to reduce the brittleness. The other half is also heat treated to the same extent, with quenching and annealing, but the carbon content is somewhat lower, for which reason islands of martensite/pearlite are surrounded by ferrite. In the latter area light bands appear (Figure S28), parallel to and sometimes together with the slag inclusions. These define weld joints, where the iron has been welded together. Electron microbe analyses of the metal show no elements other than iron in concentrations above the detection limits (Table S2). The slag inclusions are consistently very small, but as good representativity as possible has been aimed for in the chemical analyses. Because the inclusions vary in mineral content this is reflected in the chemical composition. Analysis 1a1 (Table S1) is dominated by wüstite, resulting in high iron concentration, but the content of manganese is also noteworthy. The manganese content is even higher in analysis 1a2 (Table S1), which consists of wüstite, glass and olivine. Here the silicon content is also high, and the iron content consequently lower. There is also a notable content of phosphorous. Analyses 1a3 and 1a4 (Table S1) mainly consists of glass and olivine and a small percentage of wüstite. The manganese content of these is also

remarkable. In summary it can be noted that the axe is made of steel. The steel has been heat treated in several stages. In part it has been hardened (i.e. rapidly cooled from a high temperature to get a hard material). An attempt at reduction of the resulting brittleness through annealing has probably been made but the effect is not evenly distributed. The carbon content in the sample was estimated to be sufficient for dating, for which a sub-sample was selected for radiocarbon dating.

Find no. 2771, A27

Oblong object, 45mm. At its thickest 10 × 6mm in cross section, and at its thinnest 5 × 4mm. The cross section in the thickest part is rhombic to rectangular. The metallographic analysis in the microscope shows rather plentiful slag inclusions but these are small and evenly distributed across basically the entire cross section, but a small number are along one side. The inclusions are mainly oriented (Figure S30) along the long side. The elongated inclusions appear to be dominated by a glass phase, but both olivine and glass are more common in the rounder inclusions. Etching of the sample shows that the iron structure is banded (Figure S31) and follows the same pattern as the slag inclusions. The grains are equiaxed in certain parts but elongated in others, and look partially deformed in the vicinity of where the piece is bent. Ferrite dominates but in some bands cementite also occurs, partly along the grain boundaries and partly in round, spheroidised shapes. Electron microbe analysis of the metal shows that it does not contain any elements other than iron in detectable concentrations (Table S2). The slag inclusions are also rich in iron where they consist of olivine, glass and wüstite (analysis 1b3 and 1b4 in Table S1). Those that lack wüstite have more silicon (analysis 1a1 and 1a2). We can also note presence of manganese (at most about 3 per cent MnO). Phosphorous occurs in somewhat smaller concentrations. In summary it is noted that the piece is produced from carbon steel and is built up of several bands with only somewhat varied composition. The metal is relatively rich in slag and the slag inclusions follow the texture of the iron both within and between the bands. Carbon content appears in the form of spheroidised cementite which indicates that the object has been heat treated to reduce potential brittleness.

Find no. 3010, A27

Irregular, magnetic, slag-like piece with rusty surface, 4.9g. In the cross section irregular, unconsolidated metallic iron is seen. In the microscope cavities appear, likewise a number of larger, rounded slag inclusions and a few corroded areas. The slag is dominated by dendritic

wüstite which is fairly coarse, with olivine and glass in smaller quantities. The same type of slag is also surrounding the metal. Etching of the sample shows that the carbon content is consistently very high, around 0.7 per cent. The metal is mostly constituted solely of pearlite. Locally the carbon content is somewhat higher and cementite laminae occur, and in other areas the carbon content is somewhat lower and instead ferrite occurs in the grain boundaries. The material is rather coarse-grained. No elements other than iron have been detected (Table S2) with certainty with the electron microprobe (carbon, observed in metallographic analysis, cannot be analysed with this instrument). One point of analysis gives results for vanadium but the measurement of the background signal in this point is uncertain, for which reason the content should be viewed with caution. The analysed slag inclusions (Table S1) are fairly coarse-grained and large areas have been analysed. The slag, which consists of wüstite, olivine and glass, is dominated by iron with small quantity of silicon. The manganese content is also notable, even if the concentration is only in the magnitude of 2 weight percent MnO. In summary it can be noted that occurrence of large cavities, slag inclusions that are round in shape and the coarse-grained texture indicate that the material has not been extensively worked after the iron was formed. The piece has thereby been lost at an early stage in the process, either in the bloomery furnace or with an initial consolidation of the bloom. The high carbon content means that the piece was prioritised for radiocarbon dating.

S1.3: ore

A number of possible finds of ore were observed. The majority of these are brown-black and loosely cemented, of a sandy nature. They mainly contain iron hydroxides. The occurrence of quartz grains is also common in ore formations. These nonmagnetic iron precipitates have not been roasted (i.e. they have not undergone the preparatory process before ore is placed in a bloomery furnace). A possible ore sample, from the area around A27, was further analysed to see if there is any connection to the iron forging at the site.

Find no. 2917, A27

Irregular, nonmagnetic lump, 9.7g. In cross section a rust-brown, bumpy side appears with somewhat metallic surface. The metallographic analysis shows that the sample is built up of several irregular layers of iron hydroxides of variable thickness. These follow each other either in planar parallel layers or are concentrically built up around a core. There are scattered quartz grains in the layers. Neither metallic iron nor slag has been observed. The sample has a construction that is characteristic of ores. However, such superimposed layers of iron

hydroxides can also be formed on metallic iron that oxidises. There are no remnants however of metallic iron in the sample or original forms that indicate that this was any type of object or iron bar, rather it is irregularly constructed. Considering that, it is probably a lump of ore.

S2: analytical results, Sangis 842

S2.1: slag

The 565 registered slags are reduction slags (i.e, from iron production in a bloomery furnace); stearin slags (Figures S32–33) and bottom slags (Figures S34–35). Some spherical slags are probably drop slags and a special variant of stearin slags that have formed inside the furnace. All slags that have been examined in the microscope have homogeneous appearance with occurrence of the minerals olivine and wüstite plus a glass phase, all of which are characteristic of reduction slags from iron production. There are no indications that forging has taken place at this site.

The slags mainly come from the furnace area and the different layers in the slag heap, but a small number were also found outside and north of this area. All slag types occur across the entire area. Thus it is not possible to distinguish any concentrations in any area; instead it appears as if a similar process has taken place over time and the waste has been spread out continuously.

F83 (SW of the slag pit)

A larger bottom slag with stearin strings on the bottom with preserved thickness. The upper part is somewhat bowl shaped and with relatively low viscosity (Figure S36). The bottom is irregular with many thin stearin strings of slag that have cooled around pieces of charcoal. In cross section a homogeneous, porous bottom slag appears. No metallic iron can be observed. The upper part of the slag, close to its outer edge, has been selected for examination in the microscope (Figure S37). There a rather coarse-grained slag appears. It is generally homogenous although there are minor variations in composition. Mostly the slag is dominated by coarse-grained olivine. Wüstite and a glass phase also occur rather frequently (Figure S38). Metallic iron appears as small droplets, distributed in the slag. Along the upper part there is a thin zone of slag that is dominated by olivine with concentrations of metallic iron, mostly as a thin winding streak, but partly corroded. The slag is coarse-grained and has cooled slowly, in the furnace. Its upper area, with occurrence of metallic iron, indicates that this may have been in contact with the smelted iron (the bloom).

F256 (SW of the slag pit)

Fragment of slag solidified against sandy furnace wall/bottom (?). In cross section (Figure S39) a mostly very dense slag dominates, with only scattered smaller cavities. In contact with the slag there is the partly melted sandy lining on one side and accumulations of metallic iron on the opposite side. The petrographic analysis shows that the slag is rather coarse-grained. It is rich in iron oxides throughout, with olivine laminae and a glass phase to a smaller extent. Locally however the olivine quantity is higher. The iron oxide is mainly wüstite but magnetite also occurs (Figure S40). Wüstite dominates, mainly in the center parts of the slag. In outer edges (Figure S41), as a thin concentrated zone and in contact with the lining, however, magnetite occurs more frequently. The wüstite is not completely homogeneous, but instead contains thin laminae of magnetite (Figure S42). Some slag has also melted into the lining and locally mixed with it. The slag has relatively large grains, which shows a rather slow cooling and crystal growth. It also has a high bulk content of iron (as oxides and silicates), which is also characteristic of slags from bloomery furnaces. But the fact that magnetite occurs together with wüstite indicates considerably more oxidising conditions.

F396 (below lining, within the stone frame)

F396 includes thinner stearin strings cooled against a sandy base. In cross section the slag is dense or somewhat porous, locally with scattered larger cavities, also after charcoal fragments. The slag is mainly homogeneous but locally, along the edges, there are sandy areas melted in. Petrographic analyses show that it is rather fine-grained and consists of olivine laminae, wüstite and a glass phase in very similar proportions through the entire slag (Figure S43). Separate slag flows cannot be distinguished. Metallic iron occurs only as small droplets or irregular formations. All these features are characteristic of slags from the reduction process in a bloomery furnace.

F756 (SW of the slag pit)

Larger stearin slag. In cross section a slag appears that is homogeneous and contains a large number of cavities, both large and small. In the sample, from the slag's outer parts, which were selected for examination in the microscope, the homogeneous feature as well as large number of pores are clearly visible. The slag is rather coarse-grained and dominated by wüstite with a smaller quantity of olivine laminae and glass (Figure S44). In a few smaller, circular areas the proportions are reversed, however. There are also scattered small droplets

of metallic iron. Charcoal pieces are enclosed and along the outer edges of the slag. In places along the outer edge there is also a thin streak with metallic iron. The slag is coarse-grained and has cooled slowly, which is typical for reduction slags from bloomery furnaces.

F757 (SW of the furnace pit)

Bottom slag. The slag is mostly dense but locally there are larger cavities. The sample that was analysed in the microscope comes from central parts of its upper half (Figure S45). The variation of cavities and the homogeneous feature also appears in the microscope. However, the proportions between the included minerals vary somewhat, but without marked contacts (Figure S46). Mostly wüstite dominates with olivine and glass in smaller quantities; locally however wüstite is in minority. There is metallic iron as scattered small droplets and as thin winding streaks in connection to cavities, possibly from charcoal pieces. The slag is mainly homogeneous and has a grain size that shows that it is a reduction slag that has cooled in the furnace.

F931 (SW of the furnace pit)

The bottom slag is rather porous in cross section, locally with large cavities (Figure S47). It also contains a relatively large amount of metallic iron in accumulations both large and small. The examined sample comes from the upper half of the slag, where the iron concentrations are most common. The petrographic analysis shows that the slag is rather homogeneous with relatively coarse-grained structure containing wüstite and olivine in similar quantities. A glass phase is subordinate. The metallic iron appears as spongy accumulations, occasionally in denser concentrations (Figure S48) and as thin winding streaks in connection to cavities. The grain size of the slags reveals that it has hardened slowly in the furnace. The relatively high concentration of metallic iron shows that reduction has also continued within the slag at lower levels in the furnace. Possibly this slag was formed in close contact with the smelted iron/bloom.

S2.2: iron

A total of 55 finds of small irregular magnetic lumps were observed. These commonly have a rust-brown irregular surface. None of them have a weight exceeding 100g, and the majority weigh much less than that. The finds are spread across the investigated area. The majority occur in the north part but some also are found in the south part. The irregular form of the iron lumps (Figures S49, S56 & S60) is characteristic of iron that is lost in connection with

iron production, or initial removal of the iron bloom. Of the seven lumps examined three are homogeneously carbon-free or low-carbon soft iron, two are homogeneous steel with rather high carbon content, while two are more heterogeneous with strongly varying carbon content, ranging from carbon-free iron to steel with similar carbon content as the more homogeneous steel samples.

F161 (SW of the furnace pit)

In cross section a concentration of metallic iron appears, about 15 × 8mm in size (Figure S50). It contains a number of cavities and corroded areas. The slag occurs mostly around the metal and is coarse-grained. In the metallic iron there are a number of small irregular slag inclusions and in one area there is more slag than iron. The slag around the metal is dominated by wüstite. The slag inclusions contain olivine and wüstite in more equal amounts and a glass phase in a smaller quantity. After etching a somewhat heterogeneous metal develops (Figure S51). The carbon content of the iron varies from carbon-free, i.e., ferrite, in the more spongy iron formations in contact with slag to at most about 0.7 per cent on the opposite side. Ferrite or ferrite with a little pearlite dominates in the sample for which reason carbon content in total is only a few tenths of a percent. Locally along one edge and in connection with cavities there is more pearlite. The grains are rather coarse and without orientation, which is indication of slow cooling without any further working. The lump is thereby a somewhat heterogeneous metal, iron–steel and the overall carbon content is probably too low to permit quenching.

F256

The iron sample is made up of one irregular oval concentration of metallic iron, about 13 × 8 mm in size, from a bottom slag. The edges of the iron concentration are somewhat uneven and spongy in contact with the slag. In the central parts the iron is rather dense, with only a small number of cavities and slag inclusions. The slag inclusions are more fine-grained than the surrounding slag and occurs in irregular accumulations. It consists of olivine, wüstite and glass. In the etched sample a rather homogeneous texture of only ferrite, i.e., carbon-free iron (Figure S52) appears. The grain boundaries are, however, in places, clearly marked, probably due to occurrence of cementite. The grain size and shape of the ferrite is partly limited by the quantity of slag, for which reason the ferrite is coarser in the areas free of slag and somewhat more fine-grained in slag-containing areas where the grain boundaries are restricted by the slag inclusions. Overall this is a homogeneous low-carbon, almost carbon-free iron.

F629 (central/north in the furnace area)

The lump contains a small, irregular, rectangular concentration of metallic iron, about 8 × 6mm in size. In the cross section there are a number of larger cavities and corroded areas (Figure S53). On the other hand the occurrence of slag is low, around the iron as well as within it. The few slag inclusions are small and rich in silicate(s). In the etched sample a steel emerges with high carbon content throughout (Figures S54–S55), close to 0.7 pre cent. The metal is mostly coarse-grained and is dominated by pearlite, locally with a little ferrite in the grain boundaries. In one area the carbon content is even higher with cementite laminae in and between the grains of pearlite. At very high magnification yet another fine laminar texture emerges which possibly can be due to a phosphorous content. In relation this there is an additional phase that probably contains both manganese and phosphorous, but this needs to be confirmed by chemical analysis. After analysis the iron lump thereby turns out to be a steel lump, with high carbon content throughout.

F759 (central in the furnace area)

The find is dominated by metallic iron, with only a small amount of slag (Figure S57). The iron concentration in the cross section is irregularly rectangular 18 × 10mm in size. The metallographic analysis shows that it is surrounded by a streak a few millimetres wide of relatively fine-grained slag that consists of olivine laminae, dendritic wüstite and a glass phase. Slag inclusions are lacking but there are plenty of corroded areas that have the form of slag inclusions, along with corroded areas that are probably along the grain boundaries of the metallic iron. After etching a metal with carbon content throughout emerges. The sample is dominated by pearlite; locally with some cementite; in other parts with ferrite, in the grain boundaries. The steel is mostly coarse-grained. Generally the carbon content is highest centrally in the sample and generally decreases somewhat towards the edges, although there are exceptions to this (Figure S58). Locally, along one outer edge the carbon content is even lower where ferrite dominates and pearlite is subordinate. In summary it can be noted that the find is steel, with carbon content normally alternating around 0.7 per cent, but locally only a few tenths of a percent, elsewhere above 0.8 per cent.

F833 (central/south in the furnace area)

In the find there is a small concentration of metallic iron, irregular in shape and about 9 × 8mm in size. The sample is constituted of metal or corroded metal. There is no slag around

the metal, only corrosion products and secondarily attached material such as sand and fragments of carbon. Slag inclusions are rare but locally there are inclusions rich in wüstite. The etched metal shows a coarse-grained texture with low carbon content (Figure S59). The sample varies from only ferrite to ferrite with a little pearlite. At most the carbon content is only some tenths of a percent. The iron lump thereby has low carbon content and is a soft iron.

Id 242 (from the hearth area in the south)

In the cross section (Figure S61) a larger concentration of metallic iron appears, about 14 × 12 mm in size, with a rather straight side. The metallic iron is surrounded by a thin film of corroded material. In the iron there are also large corroded areas and quite a few cavities. The quantity of slag varies from areas with large inclusions of olivine, wüstite and glass, to areas where slag is lacking. Etching shows that the metallic iron in the sample has a heterogeneous composition (Figure S62). Mostly ferrite dominates (i.e. it is carbon free or low in carbon). In the outer edges, however, the carbon content increases significantly in a short distance to at least 0.7 per cent, locally even higher with pearlite and cementite in the grain boundaries. The grain size is somewhat smaller, without being fine-grained. The lump has a varying carbon content with both soft iron and harder steel.

Id 243 (from the hearth area in the south)

In the cross section (Figure S63) a larger concentration of metallic iron emerges, with some large cavities. The sample is irregular and about 17 × 13mm in size. Metallographic analysis shows that the metallic iron is surrounded by coarse-grained wüstite-dominant slag. There is also similar slag in larger, irregular inclusions, as well as a number of smaller inclusions that are rounder in shape. These contain the same minerals but are finer grained. The etched sample shows iron that is dominated by ferrite (i.e. carbon-free iron) (Figure S64). Locally there is a somewhat elevated carbon content with a little pearlite in the grain boundaries. The find is thus a rather homogeneous, carbon-free, soft iron, with only a locally marginally elevated carbon content.

S2.3: technical ceramics

The fragmentation of the sintered material/technical ceramics varies from small fragments up to larger ‘furnace wall’ parts (F956, F957), of which F957 was found *in situ* in the top of the furnace. Most of the finds originate from the slag heap. Besides size, the fragments primarily

vary with respect to thickness, occurrence of slag on the inside, and to what degree they were subjected to reduction or oxidation. There is also a variation in the sorting of the sintered material, which is mainly seen in the occurrence of clay clumps (Figure S65, F466) and large sand grains (Figure S66, F138). Remnants of several blowing holes occur in the sintered fragments, and in most cases the rounded blowing hole opening appears to be shaped (Figure S67). Besides blowing holes, no traces of other construction elements have been observed (e.g. stakes, wickerwork, stone) in the sintered wall fragments. The abovementioned technological variation can be summarised into three types:

1. A large amount of the sintered materials found consists of concave-convex "shards" less than 15mm thick but up to 200 × 200mm in size (F956, F957). They consist of slag layers (from thin to centimetre thick) with a layer of clayey(?) sand sintered on the convex outside. The outside is often oxidised. This type of material occurs in the furnace and in both layers of the slag heap.
2. Thicker concave-convex pieces of sintered/partly vitrified material without slag on the inside or with only a very thin layer of slag are also common in the slag heap. The largest fragment is about 130 × 100mm, thickness 15–27mm. Among these fragments there are some scattered ones that seem to consist of two layers (for more detail see discussion of samples below). It is common that the fragments, sometimes even the outside surface layer, are reduced.
3. A small group of fragments, possibly from a separate furnace construction (F620, F702, and possibly F565), differ through a clearly vitrified inside. The fragments are small and only up to 10mm thick (Figure S68). The vitrified inside is consequently reduced to a black colour, while the outside varies from reduced to oxidised burnt. Several of the fragments include parts of a blowing hole and could be fit together with each other and with a slag.

For a more detailed study, six fragments of type 2 and 3 were selected.

F282:1081

The fragment 75 × 50× 20mm in size (66g) encompasses parts of a blowing hole with an estimated diameter of 40mm. The inside is lightly concave and covered by a thin layer of slag. The outside, which is convex in one direction and concave in another, consists of sintered sand. The sand is partly reduced (grey), partly oxidided (light red). The core is very

vesicular closest to the inside. It is reduced with features of red where iron inclusions in penetrating slag have rusted. The material seems to contain a fair amount of clay and is well-sorted with grains up to 1.5mm.

F105:1081

The fragment 90 × 55 × 30mm in size (96g) encompasses parts of a blowing hole with an estimated diameter of 30mm (Figure S67). The blowing hole seems inclined in relation to the inside. The inside is lightly concave and smooth with scattered small vesicles. The outside is convex with a concavity around the blowing hole. It consists of sintered sand and is reduced (grey) with the exception of the concave part, which is oxidised to a light red colour. The core is vesicular and partly vitrified. It is reduced to a grey-black colour. The material is relatively well sorted with grains up to 4mm.

F494:693

The fragment 45 × 30 × 20mm in size (32g) has a lightly concave inside with a thin layer of slag. The outside consists of sintered, clayey sand and is reduced to a grey-brown colour. The core is vesicular and reduced to a grey-black colour with features of red, possibly from penetrated slag with rusty iron inclusions. The material is unsorted with grains up to 4mm.

F398:1335 (outside the stone frame)

The fragment 80 × 45 × 40mm in size (88g) varies horizontally in thickness from 15–40mm. In the thick part, structures in the fracture indicate two, 16–20mm-thick layers (Figure S69). The outer of the two layers is slightly higher in one place than the inner one and demonstrates a smooth, sintered inside similar to the one on the inside of the inner layer. This may indicate that the inner layer has been added as a repair of the wall in a furnace that has already been used once. The inside with mixed slag is concave, smooth with scattered small vesicles and reduced (grey). It has an estimated diameter of 140mm, which is in agreement with other diameters of 150–200mm estimated in connection with the find recording. The convex outside consists of sintered sand and is mottled reduced/oxidised. The core is very vesicular with the largest vesicles closest to the inside. It is reduced to a grey-black colour with features of red, possibly from penetrated slag with rusty iron inclusions (see discussion, however). The material is unsorted with grains up to 4mm.

F622:693

The fragment 50 × 50 × 25mm in size (98g) consists of sintered material with a thin layer of slag and a slag lump on the inside (Figure S70). Structures in the fracture indicate two layers. The inside is plane and coated with reduced grey slag. The plane outside consists of grey-reduced, sintered sand. The core is partly vesicular and vitrified closest to the reduced (black) inside. The material is unsorted with grains up to 5mm.

F620:201

The fragment 40 × 40 × 10mm in size (18g) encompasses parts of a blowing hole with an estimated diameter of 25 mm (Figure S68). The inside is plane to lightly concave and vitrified. The plane outside consists of reduced (grey), sintered sand with the exception of a zone around the blowing hole which is oxidised to a light red colour. The core is heavily vesicular and reduced to a black colour. The material is unsorted with grains up to 3–4 mm. Selected for thin section analysis were fragments F398 (TS 1), which could provide information about the occurrence of several layers in the construction or repair layers, and F620 (TS 2), which probably represents a separate structure, possibly with another construction.

F398 (TS 1)

The thin section as well as the cut cross section confirm that the furnace wall fragment consists of two layers. The cross section (Figure S71) shows two clearly delimited layers, where the first calculated from the inside of the furnace is more compact, although with larger scattered vesicles. The thin section shows a vitrified activity area with plentiful slag on both layers, which is best seen in a photo of the specimen (Figure S72). This entails that the inner layer can be interpreted as a repair of an existing furnace wall.

In the primary, 15mm-thick layer, the slag remnants have penetrated up to 10mm in (Figure S73). The layer consists of sand grains up to 3mm in size (the next five largest grains have an average size of 2.3mm) in a vitrified matrix (Figure S74). In the outer part of the furnace wall where the heat impact has been less, several small pockets of finer-grained material that has not been vitrified are seen. These are what is left behind from the clayey silt/fine sand that has made the sand formable in damp condition.

In the later, 9–15mm-thick layer the slag has penetrated up to 5mm in (Figure S75). The activity layer of glass and slag also encompasses a round metal drop 0.01mm in size. The layer has been made by sand with grains up to 2mm in size (the next five largest grains have an average size of 1.7mm) which has been held together by finer-grained material, still seen

in small pockets furthest away from the heat source (Figure S76). The material in the later layer thus consists of on average smaller sand grains than in the primary layer. Another difference, which may be of interest for the iron production process, is that the slag inclusions in the later layer are yellow-brown and compact (Figure S72) while the slag in the older layer is black and 'granular.'

The thin section analysis shows that a later furnace may consist of repairs of parts of an existing furnace wall. Alternatively a completely new furnace has been built in an older furnace by daubing on a new layer, about 15mm thick, on an existing, slag-covered furnace wall. For this a plastic mass was required (i.e. that the clayey sand with the right quantity of water was formable).

F620 (TS 2)

The other thin section shows the deviating, 6–7mm-thick furnace wall consisting of sand of approximately the same coarseness as the later layer in F398 (TS 1), but with a higher content of clayey silt (Figure S77). The maximum grain size of the grains of sand is 2 mm. The higher percentage of finer-grained material is a necessary prerequisite for shaping this thinner wall. There is quite a bit of slag in the vitrified layer on the inside including several metal drops (Figure S78).

S2.3.1: reference samples

Three samples of sand from the area have been tested for their qualities as construction material for a furnace wall. Two of the samples, 1PM 1579.1335 and 1PM 1417.1335, have been collected within the stone frame and in the work pit. The samples originate from the construction and the probability that they actually represent the material that has been used is therefore good. On the other hand there is a risk that the material has already been affected by heat to such a degree that any clay in the sand has lost its plastic characteristics (>400 degrees Celcius for a longer time). The samples consist of unsorted, grey-brown to brown sand with rock fragments up to 7–8mm in size. The test showed that the samples have no or very little plasticity and cannot be used for furnace construction. A third sample, 1VM 1733, is collected outside the archaeological site area adjacent to Fix no. 3. This consists of unsorted, brown silt/fine sand/sand with scattered rock fragments up to 10mm in size. The test indicated that the material has limited plastic characteristics. It is possible to form a clump in your hand, even if it cracks up easily. This means that one should be able to build a furnace wall in stages with intermediate brief drying periods.

S2.3.2: technical ceramics in summary

The find registration and special recording showed agreement that sintered material could be divided into three main types. No fragments within any of these type groups showed traces of other material that could have been included in a furnace wall construction (i.e. stake or stone imprints). The consistently thicker fragments of type 2 are more often more reduced, which could indicate that they originate from a part of the "furnace wall" that is more protected from oxygen supply. It is reasonable to assume that this concerns the lower part of the furnace wall. Those parts of "furnace wall" of type 3 (F703) that were in contact with slag (F702) are also clearly reduced. The standing "furnace wall" part from the furnace chamber (F957 in context 1335) and the similar F956 show the upper parts of the furnace with blowing hole where the sintered material is thin and oxidised on the outside.

The petrographic analysis of two samples showed that the sand that was used as building material in the furnace walls also contains finer material, probably with a certain proportion of clay which gave the sand some plasticity. This is most evident in sample F398, where an older furnace wall was supplied either with a repair or a completely new inside layer.

The test of the plastic characteristics of three sand samples gave a result that silt-sand deposits in the vicinity of the furnace contained sufficient fine-grained material including clay to be shaped with the addition of a small quantity of water. If built in stages with brief drying in between, it would be possible to build up a clay wall. At least up to a certain temperature penetrated iron and also slag products may have served as adhesive on the clayey sand in that the fluxing characteristics promoted sintering of clay/silt/fine sand grains. In the thin section of the thick furnace wall (F398), in both layers small isolated vitrified areas are seen inside the material that may be the result of such a process.

S3: analytical results, Vivungi 723

Of a total of over 40 find listings; four slags, two iron samples and one ore have been analysed from furnace area 2 and area 3, respectively. In addition, samples of technical ceramics from both areas were selected and analysed.

The analyses of slag in the microscope clearly show that all eight slags are relatively simple in composition. All are fine-grained, relatively homogeneous, and mainly consist of the three phases of wüstite (which dominates), olivine and glass. Metallic iron is observed only very sparsely. They are all characteristic of reduction slags from iron production in a bloomery furnace. The four iron samples (two from each furnace area) are all very rich in carbon and

relatively poor in slag inclusions. The assumed ore 2347 was a rusty piece of iron with a small quantity of slag and other cemented material and has therefore been treated as an iron sample.

S3.1: slag

Slag id 1676

Slag sample id 1676 from the slag heap in furnace area 2 is seen in the microscope to be relatively fine-grained, porous and somewhat heterogeneous where wüstite normally dominates, but in areas is only subordinate (Figure S93). High magnification shows that the light wüstite grows dendritic over the other slag phases, which consist of grey olivine crystals with an intermediate darker residual melt of glass (Figure S94). Metallic iron occurs only sparsely and then as very small droplets, primarily at the outer edge of the slag (Figure S95) while neither leucite, magnetite or hercynite is observed.

Slag id 2616

Slag sample id 2616 comes from the furnace chamber in furnace area 2 and consists of a very fine-grained, homogeneous slag relatively rich in small pores. The slag is dominated by light wüstite (Figure S99), which grows dendritic over both grey olivine and intermediate dark residual melt (Figure S100). In very high magnification (Figure S101) it can be perceived that the dark residual melt, besides glass, contains microcrystals of (probably) olivine. No leucite, magnetite or hercynite can be observed in the slag.

Slag id 1809

Slag sample id 1809 from the slag heap in furnace area 2 is both fine-grained and homogeneous with relatively few pores. However, several flows can be observed (Figure S96). The slag is dominated by light dendritic wüstite which grows over grey olivine crystals with an intermediate dark residual melt, probably of glass (Figure S97). No leucite, magnetite or hercynite can be observed, and metallic iron is only found sparsely at the outer edge of the piece of slag, where wüstite is lacking (Figure S98), possibly due to the presence of oxygen.

Slag id 2825

Slag sample id 2825 comes from the slag heap in the slope below the furnace in area 2 and is a very fine-grained and homogeneous/dense slag (Figure S102). The iron oxide wüstite (light) dominates and grows dendritic over grey olivine crystals and a dark intermediate

residual molten mass, probably consisting of glass (Figure S103). In very high magnification metallic iron is observed, but then only sparsely and at the surface of the slag, where it can also be observed that wüstite decreases in concentration (Figure S104). No leucite, magnetite or hercynite can be observed in the slag.

Slag id 1973

Slag sample id 1973 from the slag heap in furnace area 3 is fine-grained, porous and relatively homogeneous, however, several flows can be perceived (Figure S105). The slag is dominated by light wüstite which grows dendritic over both olivine and dark residual melt of glass; only in places is wüstite seen to be subordinate (Figure S106). Metallic iron is found only very sporadically and the slag appears to lack leucite, magnetite and hercynite completely.

Slag id 2398

Slag sample id 2398 is from the slag heap in the slope in furnace area 3 and is already seen in low magnification to be totally dominated by very fine-grained light wüstite (Figure S107). Parts of the outer edge of the slag have lower concentration of wüstite, however, and there grey olivine laminae with dark intermediate glass dominates instead (Figure S108). This is a secondary effect. Metallic iron is only observed very sparsely and the slag appears to lack leucite, magnetite and hercynite.

Slag id 2854

Slag sample id 2854 is from the interior of the furnace in area 3. In low magnification (Figure S109), it is observed that the slag is very fine-grained, relatively porous and mainly dominated by dendritic growing wüstite (Figure S110). However, there are areas/flows where wüstite is subordinate and the slag is instead dominated by grey olivine laminae and dark intermediate residual melt of glass (Figures S109–S110). There is metallic iron only very sparsely and no leucite, magnetite or hercynite are observed.

Slag id 2861

Slag sample id 2861 is from the interior of the furnace in area 3 and is a fine-grained slag with relatively large amount of small pores. The slag is dominated by light dendritic wüstite (Figure S111) which grows over grey olivine laminae and dark residual melt of glass (Figure

S112). Metallic iron is observed only sparsely and then normally close to the surface (Figure S112). The slag lacks leucite, magnetite and hercynite.

S3.2: iron

Iron id 2347

Iron sample id 2347 (which was first interpreted as a piece of ore) comes from the slag heap in furnace area 2. The polished sample shows that the iron is corroded with few slag inclusions (Figure S113). However, slag is observed at the outer edge of the sample, and then together with sparse streaks of metallic iron (Figure S114). In the microscope this slag is seen to consist of very fine-grained grey olivine and a large percentage of dark residual melt, probably of glass. Etching of the iron sample (Figure S115) shows that it is very rich in carbon and dominated by pearlite (except in the outer rim) and should therefore be considered as steel.

Iron id 392

Iron sample id 392 is from the slag heap in furnace area 2. The polished sample shows a relatively corroded/porous iron (Figure S116) with pale yellow laminae, which is also observed in adjacent rust (Figure S117). The iron contains only very small amounts of slag and then as small, irregular inclusions. Etching demonstrates a very high carbon content (Figure s118) showing that the pale yellow laminae consist of free cementite, which appears completely preserved in surrounding rust (Figure S119). The iron sample can be considered high-carbon steel.

Iron id 1759

Iron sample id 1759 is from the slag heap in furnace area 3. In low magnification it is seen that the metal is both porous and heavily corroded and that it has a few larger slag inclusions (Figure S120). In very high magnification it is perceived that the enclosed slag seems to consist of mainly rounded wüstite with a dark intermediate matrix, probably of glass (Figure S121). After etching of the sample it is seen that the iron is very high in carbon and dominated by brown-blue pearlite (Figure S122). In high magnification it is seen that the light phase that appears together with pearlite consists of cementite, which dominates the sample in places and in places ledeburite texture is observed (Figure S123). The iron sample can be considered very high-carbon steel, in places almost white cast iron.

Iron id 2942

Iron sample id 2942 is from the slag heap in furnace area 3 is corroded and porous (Figure S124). Slag inclusions consist of olivine with dark intermediate glass and a small quantity of wüstite (Figure S125). Etching of the sample shows that it is high in carbon, as the texture pearlite is seen to completely dominate the sample (Figure S126). In very high magnification (Figure S127) scattered grain boundaries of carbon-free iron are observed (i.e. ferrite with so-called feather texture). The iron sample can be considered steel.

S3.3: ore

Ore id 688

Only bulk chemical analysis of ore sample id 688 (bog-iron ore of cake type) approximately 2.5m NE of the furnace in area 2 have been carried out (Table S3), as microscope analyses are not considered able to provide additional information.

Ore id 2382

Ore sample id 2382, which represents coin type lake-iron ore, comes from about 4.5m NW of the furnace in area 3 and was primarily analysed for the purpose of establishing its chemical composition. This ore was also supposed to carry important information about how this type of ore is formed. Therefore, a polished sample was prepared and selected for studies in the microscope (Figure S128). In the microscope it is observed how the ore grew concentrically, where variations in composition resemble rings on a tree (Figures S129–S130). In Figure S128 and S129 it is also seen how sand grains have been incorporated in the ore during growth. In very high magnification it shows how various components in the ore, mainly various iron hydroxides, vary heavily (Figure S130). The variations probably reflect seasonal fluctuations, which change both the chemistry of the water and the speed of the ore formation.

S3.4: technical ceramics

S3.4.1 Furnace area 2

Id 560 (Rn 0 outside furnace)

Fragment A: 47 × 40 × 10mm. A piece resembling a lining with a concave side with iron slag sintered on and a convex outer side/contact surface. The latter side is for the most part a

fracture but near one edge there is a small smooth portion. One of the longer edges has a rounded, melted profile with transition to attached slag on the inside. The rough, sandy material is clearly sintered, probably under reducing conditions. No obvious temperature gradient.

Fragment B: 105 × 55 × 25mm (in two parts). Oblong piece with a concave side with thick iron slag sintered on and a convex outer side/contact surface. On one part of the latter there is some sintered-on or penetrated iron slag and on the outside of the slag a thin layer of red fired clay. Alongside this, the convex surface is relatively smooth with an impressed (?) curved furrow that is concentric with a rounded depression at the edge of the piece about 10mm away. This unevenly rounded depression (with a small slag remnant sintered on) has been interpreted as a bellows hole (diameter <20mm) and the concentric furrow would then be an impression of the bellows nozzle or a tuyere. An even more uneven but larger depression in the transition between the two parts of the fragment could then be a similar hole possibly plugged up at one stage by the outer red burnt layer. The coarse, sandy material is vitrified and vesicular, probably under reducing conditions. No obvious temperature gradient.

Id 592 (Rn 0 outside furnace)

Fragment A: fragment of stone from stone frame with a 80 × 55 × 15mm-large furnace wall fragment sintered on. Obvious concave inside with a little slag on the thickest part of the furnace wall fragment. The thinner part is covered by a slag coating that is also found on parts of the inside of the stone frame fragment. It is hard to determine macroscopically, but it seems more probable that this latter part of the coating represents slag penetrated through a crack in the furnace wall or behind it than that this should mark an earlier functional surface later covered by a repair layer. The coarse, sandy object is vitrified and vesicular, probably under reducing conditions (material of the same type as Id 560 Fragment B). No obvious temperature gradient.

Id 1649 (Rn1 outside furnace)

Fragment A: eight small fragments (the largest is 25 × 20 × 9mm) of coarse, sandy material like Id 560 and 592 above. Different surfaces are difficult to distinguish. One fragment also seems to have been sintered/melted secondarily. The material is vitrified and vesicular, probably under reducing conditions. No obvious temperature gradient.

Fragment B: one small fragment (25 × 20 × 30mm) consisting of a piece of stone from a stone frame, vitrified furnace wall (at least about 20mm thick) and slag. The coarse, sandy material is vitrified and vesicular, probably under reducing conditions. No obvious temperature gradient.

Fragment C: three furnace wall fragments with a clearly lower fired, partly oxidised, convex outside, of which the largest fragment is 53 × 45 × 11mm. The rest of the furnace wall thickness is either sintered or heavily vitrified. The largest fragment has slag coating on the inside. A round depression in one of the edges of a fragment is probably not a remnant of a bellows hole. There is a fracture here and in several places intruding slag appears to have deformed the fragment. Of the two other fragments, one has a black vitrified inside without slag but with suggestion of a shaped edge, which makes it very like a forge lining fragment (cf. the piece in Ogenhall 2015: 23). The coarse, sandy material has, in one case, a single temperature gradient with an approximately 2mm-wide oxidised zone farthest out, followed by a vitrified, vesicular zone in the rest of the fragment's thickness. TCT-sample.

Fragment D: three somewhat larger pieces (the largest is 69 × 40 × 23mm) have a convex outside which is oxidised fired to sintered followed (inwards) by a black vitrified section with a number of small or a few large vesicle formations. On the inside and partly penetrating into the furnace wall there are sintered lumps of iron slag. The coarse, sandy material has a clear but simple temperature gradient with a vitrified, vesicular zone up to 40 mm wide followed by a 3mm-wide, oxidised fired zone (i.e. the rest of the thickness of the piece). Sample Ts 1.

Fragment E: the largest piece of furnace wall (85 × 50 × 19 mm) has a convex, partly sintered, partly oxidised outside followed by a black, vitrified, vesicular part on which a larger lump of slag sits, which in one place has penetrated deeply into the furnace wall. A calculation of the diameter of the wall from the bend of the outside results in 0.39–0.40m corresponding to a furnace space at this location of 0.35–036m in diameter.

Id 2270 (slag heap)

Fragment A: this large fragment (110 × 105 × 35mm) consists of a piece of the stone frame and an up to 35mm-thick furnace wall on one part of the surface. The furnace wall material is black and vitrified with larger and smaller vesicle formations. The inside is clearly concave. The reason for the large thickness of the wall appears to be a repair layer, about 10mm thick,

that covers a surface of about 40 × 35mm on the inside. This repair layer as well as part of the original furnace wall behind/underneath seems to have been split off with a reduced profile as a result. Several of these breakages have a coating of slag, which indicates that the furnace has been used after/while these damages arose. The coarse, sandy material is vitrified and vesicular, probably under reducing conditions. No obvious temperature gradient. Sample Ts 2.

Id 2819 (slag heap)

Fragment A: the fragment is 60 × 40 × 10 mm in size with an obvious ½ bellows hole. The original diameter of the hole was almost 4 cm. The convex outside is partly sintered, partly oxidised, such as id 1649, D while the concave inside has slag sintered on. Slag has also penetrated into the furnace wall. The coarse, sandy material is vitrified and vesicular, probably under reducing conditions. No obvious temperature gradient.

S3.4.2: furnace area 3

Id 2585 (in the furnace chamber)

Fragment A: the fragment is 73 × 52 × 15mm in size with an obvious ½ bellows hole. The original diameter of the hole was about 35mm. The outside is oxidised fired and has a straight to slightly convex form in addition to a concavity around the bellows hole, presumably an impression of the bellows nozzle itself (?). There is a clear temperature gradient with an outer oxidised zone about 4mm thick transitioning to a reduced fired zone about 3mm thick, further into a sintered, reduced zone about 5mm thick and finally a vitrified, slightly vesicular zone about 3mm thick. The inside is concave, especially in relation to the bellows hole. It can best be interpreted as a deformity that occurred in connection with the bellows nozzle (?) having been squeezed onto/into the furnace wall. The inside surface is vitrified without obvious slag inclusions. The clay is medium coarse, silty and fine-grained with scattered large grains of sand. Thus, it appears to be clearly finer than the material that has consistently been used for furnace wall on the area 2 furnace. Sample Ts 3.

Fragment B: the fragment is 65 × 55 × 12mm in size with an obvious ½ bellows hole. The original diameter of the hole was about 42mm. The outside is oxidised fired and has a straight to slightly convex form besides a concavity around the bellows hole, presumably an impression of the bellows nozzle itself (?). There is a hint of a temperature gradient similar to

the one in fragment A. An oxidised zone 3–4 mm wide on the outside can be identified. This is followed by a sintered zone. The piece has however been secondarily burnt, which is seen by rounded fractures and an oxidised, somewhat vesicular inside. There is no counterpart here to the deformity around the bellows hole on fragment A. Clay is medium coarse, silty and fine-grained with scattered large grains of sand.

Id 2610 (working pit outside furnace)

Fragment A: the fragment is 60 × 50 × 15mm in size with an obvious ½ bellows hole. The original diameter of the hole was about 35mm. The convex outside is oxidised fired while the edge of the bellows hole is vitrified like the inside. There is a clear temperature gradient from a vitrified, vesicular zone about 5mm wide at the inside to a 7mm-wide sintered zone followed finally by an oxidised zone up to 3mm wide. The concave inside is vitrified with a little slag inclusion. A small fragment of furnace wall material is sintered on to the inside. This is most likely a fragment that has broken loose during the process and then has attached here, rather than representing remnants of a repair layer. The clay is medium coarse, silty and fine-grained with scattered large grains of sand.

Id 2854 (the furnace chamber)

Fragment A: the fragment is 75 × 49 × 20mm in size. The thickness decreases from 20mm at the one end to about 6mm at the other end. The convex outside is very uneven and appears unworked. The inside is flat /concave with slag coating and scattered lumps of slag sintered on. It is lower fired in a primarily reduced atmosphere which may be due to the fact that this part of furnace wall belongs to the lowest part of the shaft. There is a temperature gradient from a sintered/melted, very vesicular inner zone (up to 16mm thick in the thickest part of the furnace wall fragment) to a lower fired (reduced) zone up to 4mm thick on the outside. A similar simple temperature gradient is also seen in the narrowest part of the furnace wall (about 4mm melted, vesicular zone and a lower fired zone, 2mm wide) which indicates that the temperature effect and/or the fluxing effects of the metal were correspondingly smaller close to the narrower part. The clay is medium coarse, silty and fine-grained with scattered large grains of sand. Sample Ts 4, TCT sample.

Id 1703 (slag heap)

The find consists of two fragments, the larger of which is described.

Fragment A is 70 × 35 × 35mm consisting of furnace wall with slag layers on the inside and penetrated slag almost splitting off a part of the furnace wall. The unsplit part of the furnace wall is 15 mm thick and has a melted, slightly vesicular zone 6mm wide, followed by a reduced, vesicular zone 5–6mm wide and an oxidised zone 1–2 mm wide. The clay is coarse, silty and fine-grained with scattered large grains of sand.

Id 1745 (slag heap)

The fragment, 35 × 35 × 15mm in size, consists of a slag layer 10mm thick and a furnace wall 5mm wide where a 2mm-wide zone next to the slag is sintered, reduced and vesicular while the 3mm-wide outer zone is oxidised. The clay is medium coarse, silty and fine-grained with scattered large grains of sand.

Id 1749 (slag heap)

The find consists of two fragments, the larger of which is described.

Fragment A is 45 × 25 × 22mm in size, consisting of a slag layer up to 14mm thick on the inside of a furnace wall about 8mm thick. The latter displays a sintered, vesicular zone about 4mm wide, followed by an oxidised zone about 4mm wide. The clay is medium coarse, silty and fine-grained with scattered large grains of sand.

Id 2932 (slag heap)

The find consists of four fragments, of which the largest is described.

Fragment A is 80 × 40 × 20mm in size, consisting of a slag layer about 5mm thick on the inside of a furnace wall 15mm thick. The latter shows a melted, vesicular zone about 10mm wide, followed by a reduced, vesicular zone 4mm wide followed by an oxidised zone 1–2mm wide. The clay is coarse, silty and fine-grained with scattered large grains of sand; cf. ID 1703 above.

Id 2952 (slag heap)

Fragment A is 56 × 40 × 35mm in size, consisting of a slag layer up to 25mm thick on the inside of a 18–20mm-thick furnace wall. The latter shows a melted zone about 12mm wide, with scattered large vesicles followed by a sintered, reduced, vesicular zone 4–5 mm wide followed by an oxidised zone 2–3 mm wide. At the very end a remnant of stone frame stone is sintered on. The clay is coarse, silty and fine-grained with scattered large grains of sand; cf. Id 1703 above.

Id 2970 (slag heap)

The find consists of four fragments, of which the largest is described.

Fragment A is 95 × 65 × 50mm in size, consisting primarily of a large piece of stone frame and a slag layer up to 35mm thick on the inside of a furnace/lining 10mm thick at most. The latter shows a reduced, very vesicular zone about 6 mm wide followed by an oxidised zone about 3mm wide. The clay is medium coarse, silty and fine-grained with scattered large grains of sand. In some places there is clearly direct contact between slag and stone frame, which is seen even more clearly on one of the other fragments in the find (Figure S131).

S3.4.3: comparisons between furnace area 2 and 3

There are clear differences between the furnace wall material from the two furnaces. Macroscopically a difference is seen in the coarseness of the clay used – coarse in the furnace in area 2 and medium coarse to coarse in the furnace in area 3, but not as coarse as in the furnace wall fragment from the furnace in area 2. This may have had some effect on the other differences between the samples presented above (Table S4) depending on how this has affected the thermal characteristics.

With respect to dimensions, the furnace walls in the furnace in area 2 go up to 25mm in thickness while the thickest fragment from furnace area 3 is 20mm thick at most. This, however, hardly represents any significant difference in the dimensions of the shaft. Several fragments from furnace area 2 include pieces of stone frame sintered on, and larger or smaller lumps of slag sintered on the inside are also common among the fragments from the furnace in area 2. This does not occur among the fragments found in the furnace in area 3, while both phenomena are common in fragments from the slag heap in the furnace in area 3. This is primarily of significance for the internal history in the furnace in area 3. A rather clear difference in temperature effect is seen in that the furnace walls from the furnace in area 3, much more often have clear temperature gradients and only in some cases have a broader, vesicular sintered/melted zone, while the corresponding zone on the walls of the furnace in area 2 take up almost the entire thickness and are very clearly melted. This difference may be due to the thermal characteristics of the clay (see S3.4.5.3: thermal analyses), but may also be an expression of higher process temperatures (see S3.4.5.3: thermal analyses) and/or a longer lasting temperature influence in the furnace of area 2 (possibly because of repeated use). Where the fragment Id 2819 A, from the furnace area 2 with bellows hole is concerned, this is also clearly more heat influenced (and has attached slag) than similar fragments with

bellows hole from the furnace in area 3. This may have two different reasons. The bellows hole on the furnace in area 2 may have been placed lower (closer to the slag formation zone) than the holes in the furnace in area 3. Alternatively, the difference may be that the furnace in area 2 has been used more times and slag has been allowed to accumulate reaching the level of the bellows hole.

S3.4.4: construction of the furnaces in area 2 and 3

Furnace area 2

An indication of the shaft's dimensions is given by one of the largest fragments in find Id 1649. A diameter calculated on the curvature of the outside is 0.39–0.40m, corresponding to a furnace space at this place of 0.35–0.36m in diameter. The thickness of the furnace shaft has been up to 20mm.

The fragment Id 560 B, furnace area 2, has a depression in the edge that has been interpreted as a bellows hole. The furrow on the outside, which is concentric with the depression, speaks for that interpretation. Speaking against that interpretation is the fact that the hole in that case is crooked, that there is a similar depression alongside, and that the diameter would be under 20mm. When compared with find Id 2819 A, found in furnace area 2, where the opening is obvious with a calculated diameter of 4 cm and the three examples from the furnace in area 3 with calculated diameters of 35–42mm, it becomes even less probable that fragment Id 560 B has a bellows hole.

Furnace area 3

The furnace wall fragments from this furnace constitute a greater part of the finds of technical ceramics in terms of weight than the material attributable to furnace in area 2. The furnace wall's thickness up to 20mm and the occurrence of sintering together with the stone frame indicates a construction similar to the shaft in the furnace in area 2. In relation to the number of fragments, however, there seems to be a greater number of bellows holes (three with diameters between 35 and 42mm in the studied selection) than in the furnace in area 2. This may mean that the furnace was equipped with several air holes or that the wall part containing the air inlet was a separate part that was replaced relatively often. As mentioned above, the furnace wall fragments from the furnace in area 3 are consistently less temperature affected, which is probably due to the number of runs with the same shaft (the flux effects on the inside of the shaft become stronger when the furnace is re-used). There are several fragments, however, from the slag heap with a wider vitrified zone, which indicates multiple

firings with the same shaft. The finds in and around the furnace in area 3 may very well represent only the last shaft, which was only used once or at the most twice before the furnace was abandoned. The consistently fewer broader vitrified zones but above all the lack of repairs indicates that the clay shaft in this furnace was replaced more often than in the furnace in area 2. A few shaft fragments such as ID 2970 indicate that in some places the shaft had the form of a lining of the inside of the stone frame rather than an actual structural furnace wall. The upper parts of the shaft may have rested mainly on the upper edge of the stone frame, which may have produced a simpler construction demanding less clay.

S3.4.5: clay samples from furnace area 2 and 3

S3.4.5.1: furnace area 2

1PL2794.2439(clay samples within the furnace chamber)
Fine-grained material with some grains of sand (including angular stone grains). Large charcoal component (the largest pieces removed and as much as possible otherwise).
Sample I – Shapeable with addition of a little water.

1PL2618.2439(clay sample collected within the furnace chamber under a charcoal layer)
Fine-grained material without visible grains of sand. Small amount of charcoal.
Sample II – Shapeable with addition of a little water. Low plasticity.

2PL2294.1853(clay sample from slag heap)
Fine-grained material with some grains of sand. Small amount of charcoal.
Sample III – Barely shapeable with addition of a little water. Low plasticity. Seems to have a greater amount of non-plastic material.

S3.4.5.2: furnace area 3

2PL2402.2087(clay sample outside furnace)
Fine-grained material with some grains of sand. Small amount of charcoal and a slag fragment.
Sample IV – Shapeable with addition of a little water. Smaller coarse fraction than in the furnace in area 2, but approximately the same plasticity.

1PL2858.2842(clay sample from the outer edge of the slag pit)

Fine-grained material with some grains of sand. Some clay pellets.
Sample V – Shapeable with addition of a little (more) water. Very low plasticity (possibly parts of the material already burnt).

2PL2411.2087(clay sample outside furnace)
Fine-grained material with some grains of sand. Some fresh organic material.
Sample VI – Shapeable with addition of a little water. Plasticity between what is seen in IV and V.

S3.4.5.3: thermal analyses of clay samples from furnace area 2 and 3
The thermal analyses were conducted by Prof. A. Lindahl, Ceramic Research Laboratory, Lund University, and the results have been evaluated and interpreted by SKEA.

Clay samples I–VI
The production of the test briquettes from the three clay samples from furnace area 2 and the three clay samples from furnace area 3 made it clear that besides a high content of silt and sand, the samples also contained some fresh organic material and charcoal which at least in the latter case ought to be contamination from the workshop environment. For that reason there could also be small, already burnt lumps of clay in the samples influencing plasticity and possibly firing properties.
During thermal analysis, where the samples were fired in 100-degree steps from 200°C upward, samples I, II and IV disintegrated at a temperature between 200 and 300°C. Samples III, V and VI retained their form up to 400°C, but at 500°C the briquettes were so broken up that the thermal analysis could not be continued in the usual way (Figure S132). Up to 500°C, the colour development for the three more stable samples was similar. Because of the contamination (especially the charcoal) the Munsell readings, however, can hardly be compared with the results for the two furnace wall samples.
The reason for this very unusual instability in the clay samples is most likely a high content of already fired material, which means that the quantity of plastic clay that can hold the briquette together is too small during the transformation from clay to ceramics, resulting in accelerated crack formation.
In order to get an impression of the refractive characteristics of the clays, despite this problem, a “gravel” was collected consisting of mixed material from clay samples I–III for a sintering test (50-degree intervals above 1000°C). It showed that the sintering (in the form of

a darkening of the colour) starts at 1150°C, vitrification at 1300°C and a glass phase is reached at 1350°C (Figure S132).
As a result of the collapse of the briquettes it was not possible to produce samples for thin section analysis of the clays. For a petrographic analysis of the clay raw material, purer samples must be collected.

S3.4.6: furnace wall samples from furnace area 2 and 3

Relatively low fired parts of furnace wall Id 1649 from the furnace in area 2 and of furnace wall Id 2854 from the furnace in area 3 were analysed thermally, partly through TCT up to 1200°C (colour development) and partly through sintering test from 1000°C (shininess, form). The TCT analysis shows rather small colour changes between 200 and 600°C for the two samples. At 700°C the colour has changed in a more decisive way, which shows that the low fired part of the furnace wall has been fired to between 600 and 700°C. The subsequent colour development in the two samples is also in good agreement. Sintering effects in the form of darkening of the colour appears for both samples at 1000°C while melting starts in both cases at 1250°C (Figure S133). At 1300–1350°C the samples have entered a glass phase. The sintering interval is thus the same for the two samples and their refractivity is of the same quality. Differences in usage traces between the two furnaces therefore ought to relate to differences in the iron production process and/or in the number of repeated runs with the same furnace wall.
Clay samples I–III have almost identical thermal characteristics with the two furnace wall samples. The sintering begins at a slightly higher temperature and melting starts at about a 50-degree higher temperature. The similarity is sufficient to make it probable that the clay samples are of the same material that was used in the furnace walls.

S3.4.7: working temperature of the furnaces

On the inside of several of the furnace wall fragments from the furnace in area 3, a slightly melted, deformed surface is seen, which according to comparison with the results of the thermal analyses should correspond to a temperature between 1150 and 1200°C with a certain proviso for the flux effect of the iron contaminants. The majority of the furnace wall fragments from the furnace in area 2 have thick vitrification on the inside, but this is most likely due to the more effective flux effect from the metal when the furnace was re-used than to higher process temperature.

S3.4.8: microscope analysis of thin section

For thin section analysis, Id 1649 (from the furnace chamber) and Id 2270 (from the slag heap) from furnace area 2 and Id 2585 and Id 2854 (both from the furnace chamber) from furnace area 3 were selected. The material found in the slag heap in furnace area 3 was not available at the time of sampling. The four thin sections of two furnace wall fragments from each of the two furnaces consist in two cases (Ts 3 and 4, both furnace area 3) of a single layer, in one case (Ts 1, furnace area 2) possibly of two layers (wall + repair?) and in one case (Ts 2, furnace area 2) of at least two layers (wall + repair). This means that the account below applies to five to six separately studied materials.

S3.4.9: sorting and mineralogy

The three or four layers of material in samples Ts 1 and 2 from the furnace in area 2 all consist of a coarse, unsorted clay, rich in silt and also in large grains of sand. The maximal grain sizes are 2.4–10.2mm. The Ts 1 sample is divided between a sintered outer layer and a melted inner layer. The difference in the sorting of the non-plastic inclusions is marked. The volume percentage of sand is 33 per cent in the outer and 13 per cent in the inner vitrified layer. It is well known that inclusions of silt size and the majority of fine sand grains as well as the majority of other minerals melt in connection with the vitrification so that only larger grains of quartz and certain types of feldspar are left. In this case, however, the larger grains of sand are also fewer in the melted zone and there are some small inclusions of slag close to the transition between the two zones. For these reasons it is suspected that the inner melted layer represents a later repair. If however one looks at the relationship between sand fraction and average maximal grain size (average for 5 next-largest grains) then it appears that the grain size is the same for the clay in the two parts of sample Ts 1 (Figure 4). Then it is solely the quantity of sand that differentiates them. The most probable explanation for the difference is then that the entire sample is one layer that was heavily changed in the inner part by the vitrification. The diagram shows that there is also a minor difference in the sorting between the two layers in sample Ts 2, but in this case the structure shows two distinct layers – the furnace wall and a repair layer.

The less heat-affected parts of the clay in the total of three layers in Ts 1 and 2 have a very similar mineralogical composition with quartz (some with quartzitic structure), different types of feldspar and some dark minerals, partly in conglomeration and partly as separate grains. The latter encompass various types of amphiboles and pyroxenes – changes because of the temperature effect make it difficult in most cases to decide more precisely which

mineral this concerns – alongside markedly many and partly large grains of zircon, sometimes in conglomeration with ore. Changes because of the temperature effect make it difficult in most cases to decide more precisely which mineral this concerns The clay is rich in iron oxide with a number of concentrations of iron oxide. Mica content, organic material and fossils cannot be assessed because of the high temperature, which even the lower fired parts of the furnace wall were reached.

The clays in the two samples from the furnace in area 3 can also be designated as coarse, even if the percentage of sand is considerably lower (sand fraction 8 per cent and 13 per cent, respectively) than in the samples from the furnace in area 2 (Figure S134).

The clay in Ts 3 is furthermore better sorted than in any of the other samples. The mineralogical composition is the same, however, where the content of zircon grains can be pointed out in particular. In both cases, parts of the samples have been fired to a temperature so much lower than that of the samples of the furnace in area 2 (<700–800°C) that some biotite is still to be seen in the fine-grained sand fraction. A similar element of biotite was reasonably also present in the more highly fired clay in Ts 1 and Ts 2.

Two pieces of technical ceramics that appeared during a survey of the area in 1993 have previously been studied (Ogenhall 2015). The fragment analysed consisted of two layers of clay (wall + repair) sintered onto a stone fragment. Despite the interpretation then as a piece of a stone-built forge with lining (at the base of the form), it is most probable that this is also a furnace wall fragment including a piece of the stone frame. The clays in the two layers have basically the same mineralogical composition as the clays in the four samples above, including the marked content of zircon. They are not, however, as rich in sand as the clays in the samples from furnace area 2 and with their average maximal grain sizes of 1.4 and 1.6 mm they more resemble the clays in the furnace wall fragments from the furnace in area 3. We also find a conspicuous component of zircon in the quartz-rich granite that constitutes the sintered stone fragment. A significant portion of the stone material in the clays can therefore be crumbled stone of the same origin as the stone frame.

As mentioned, it was not possible to fire any of the samples of the clay specks in the area and thereby not possible either to make thin sections of the fired clay samples for a mineralogical comparison. Because clay is not available at the find site, it is in any event more interesting to compare with the nearest known occurrences of clay. The soil type map from the Swedish Geological Survey (scale 1:250 000) for the area shows that there is clay-silt about 10km north of the investigation site. The stone fragment of granite attached to the analysed furnace

wall fragment is in good mineralogical agreement with the clays, which may indicate that stone as well as clay have been obtained within the same area.

S3.4.10: building structures and temperature gradients

The two samples from the furnace in area 3 consist of a single layer of clay where the temperature effect resulted in a single temperature gradient from a 3–5 mm wide vitrified zone facing the furnace space (with larger/smaller quantities of slag sintered on) across a 7–10mm wide reduced, sintered zone (with larger or smaller vesicles), to a narrow, oxidised, lower fired, outer zone (Figure S135).

Furnace wall sample Ts 1 (furnace area 2) constitutes, as already mentioned, probably only a single layer but with a different temperature gradient (see data sheet). The melted zone is about 10mm wide with many intrusive slag inclusions, while the reduced, sintered zone is up to 7mm wide. The broader melted zone with more slag is most likely the result of more runs of this furnace than what the analysed fragments from the furnace area 3 represent.

Penetrating slag containing iron from the first firing, will during a subsequent firing, flux the furnace wall material so that the melted zone is widened. The reduction in the percentage of sand grains in this zone also indicates a repeated process.

Sample Ts 2 (furnace area 2) is exceptional. Macroscopic observation of the cross-section that emerged with the production of the thin section and the observation of three slag horizons in the thin section clarified that the furnace wall fragment consists of an original wall with two successive repairs with at least one run of the furnace after each repair (Figure S136). The 25mm-wide piece that is contained on the slide represents the two repairs and a slag horizon between the original furnace wall and the first repair. In some places, however, a small part of the original furnace wall remains on the slide, sufficient for the observation that this was made from the same clay as the two repair layers. This is supported by macroscopic observation of coarseness and sorting. The two repair layers are 13mm and 10mm thick respectively. The vitrified zone on the most recent repair is up to 6mm thick while the corresponding zone on the first repair is up to 3mm and very mixed with slag. This could suggest that after the first repair the furnace was only run a few times before a new repair was required.

These repairs have presumably only covered limited parts of the inside of the furnace wall where it was considered necessary to reinforce and smooth out the old furnace wall surface. This tallies with the fact that certain fragments demonstrate the simple structure like Ts 1,

some part of a repair (like the previously analysed loose find fragments) and some more substantial repairs like Ts 2.

S3.3.4.11: differences between the furnaces in area 2 and 3

The basic design of the two furnaces with stone frame and clay lining/shaft wall appears to be the same, even if there may be differences in how the clay shafts looked. The clay that was used for the furnace in area 2 is consistently coarser and more poorly sorted than that used for the furnace in area 3 even if there is a variation in the quantity of fine sand in the material in the furnace wall fragments from the latter area. The analysed clays are, however, in mineralogical agreement. A more important difference is that the fragments from the furnace in area 2 more often have a wide vitrified zone and/or one or more repairs. Because the thermal analysis did not show any differences in the refractive characteristics of the clays and the process temperature has been the same, the differences in temperature effects and repair can be explained by the fact that (different versions of) the clay shaft in the furnace in area 2 were run more times and repaired before it was replaced by a new one, while the clay shaft in the furnace in area 3 may have been replaced after each or only a few runs without repairs. The shaft of the furnace in area 3 was possibly built more simply with a thinner clay lining of the stone frame and around the bellow hole(s?) with the upper portion of the shaft resting on the stone frame, which may have meant that only the lower parts needed to be exchanged. This is a very uncertain hypothesis because parallels as well as experiments are lacking with such a design. If the furnace shaft in the area 3 was replaced more regularly than was the case with the furnace shaft in area 2, this ought to have entailed a greater need for clay raw material for the furnace in area 3.

S4: bulk chemical analyses, Sangis 730, 842 and Vivungi 723

Bulk chemical analysis has been done of a selection of slag and ore samples from site Sangis 730 (smithing slags), site Sangis 842 (reduction slags from a furnace area) and site Vivungi 723 (reduction slags from the two furnace areas 2 and 3). The combined results are briefly presented in this section, supported by a few diagrams. Selected elements are brought up but not every individual sample is specifically discussed here. Complete analytical results are found in Table S3. Primarily a comparison is made between the sites in question to see whether there are differences and/or similarities within them or between them.

S4.1: major and minor elements

The results from the bulk chemical analysis show that the analysed slags are dominated by iron (the majority are distributed between about 71 and 95 wt%) (given as Fe_2O_3 in Table S3) and silicon (11–21 wt% SiO_2). The slags from Sangis tend toward the higher iron content in the range, but reduction slags from all three furnaces areas show a distribution. An analysed stray find of slag from Vivungi 723 deviates with somewhat lower iron and higher silicon content. Iron and silicon are the elements that normally dominate in slags from bloomery iron production during the Iron Age. In comparison with other reduction slags from Sweden (Figure S137) we see that these show even greater variation.

Among other major elements, aluminium occurs, which varies from about 1 to over 3 wt% Al_2O_3 for the majority, and potassium, most of which occurs in amounts below 0.7 wt% K_2O. A reduction slag from Sangis 842 and the stray find from Vivungi 723 deviate with somewhat higher amounts of both (Figure S138). In general, the amounts of both aluminium and potassium are somewhat lower in the slags from Sangis than in those from Vivungi. Compared with Iron Age reduction slags in Sweden they are however among those that have the lowest content of both of these elements. Aluminium and potassium can occur in ore as well as in clay furnace walls, and the amounts are at a corresponding level in the analysed "lake" ore (Swedish *sjömalm*) from furnace area 3 in Vivungi 723, for which reason any contamination from the furnace wall is probably small. The bog-iron ore from furnace area 3 in Vivungi has significantly lower amounts, however.

S4.2: manganese and phosphorus as indicators

Manganese is an element that occurs commonly in bog-iron and lake ores and can vary from a few tenths to tens of percent in ores as well as slags. This variation can be seen in reduction slags from bloomery furnaces from major parts of Sweden (Figure S139) where amounts of 5–10 wt% are rather common, and scattered examples with even higher content of manganese occur. The analysed reduction slags from Sangis and Vivungi have content of manganese at most about 5 wt% MnO. The manganese content is generally higher from the two furnace areas in Vivungi, also including the stray find of slag from the area (similar variation; about 3.5–5.5 wt% MnO), but lower in the reduction slags from Sangis 842 (which vary between 1.5 and 2.3 wt% MnO). The smithing slags from Sangis also contain manganese (2.7–5.0 wt% MnO) in the same order of magnitude. The occurrence suggests that these are probably from primary forging, when the slag is mostly melted out of the iron bloom, rather than formed from secondary forging, for which reason the primary smithing slag can be considered to chemically correspond to a reduction slag.

Both types of ore that have been analysed from Vivungi also contain manganese, but in various amounts. The lake ore from area 3 has higher manganese content (3.8 wt% MnO) and the bog-iron ore from area 2 somewhat lower (1.1 wt% MnO). This means that the ore from area 3 has manganese content in the same order of magnitude as the slags from both furnace areas. The ore from area 2, however, with lower manganese content, has no corresponding low manganese content in any of the analysed slags from the site.
Phosphorus is also an element that commonly occurs, in varying amounts, in ores (cf. the method text). A difference can be noted between the slags from furnace area 2 and 3 from Vivungi, where those from area 2 consistently have a somewhat higher content (0.4–0.6 wt% P_2O_5), while the slags from area 3 vary between over 0.1 and 0.3 wt%. The reduction slags from Sangis 842 overlap with the two from Vivungi (0.25–0.5 wt% P_2O_5). The smithing slags from Sangis 730 demonstrate greater difference between them, where some have the same level as the slags from Sangis 842 while two have somewhat higher amounts (0.7 and 0.9 wt% P_2O_5 respectively). Corresponding levels are also seen in the stray find of slag from Vivungi 723. Both of the analysed ores are more uniform with amounts of under 0.4 wt% P_2O_5, i.e., between those as measured in the slags from the two furnace areas in Vivungi.
The slags from the two furnace areas at Vivungi have similar manganese content, but differences in phosphorus content, with somewhat higher amounts in those from area 2. No occurrence of phosphorus iron has been noted however in Vivungi. From the forge in Sangis 730, with two slags with somewhat higher amount of phosphorus, some occurrence of phosphorus is also noted however in the metal (see the sample description). Compared with reduction slags from Sweden it can be noted that the phosphorus amounts connect to the large group of reference slags that have content below about 1 wt% (Figure S139).

S4.3: major and trace element correlation: Mn and Ba as an example

An element which in limonite ores (lake and bog-iron ore) is commonly correlated to manganese is the trace element barium. This means that the higher the manganese content in the ore, the higher the barium content is expected to be too; a relationship which in broad terms is also inherited by the slag formed (Figure S140). The reduction slags from Vivungi, which have higher manganese content than the reduction slags from Sangis 842, also have as expected higher barium content (about 2500–5000ppm). The lake ore from furnace area 3 is also within the same range, while the bog-iron ore from furnace area 2 with significantly lower manganese also has significantly lower barium content (almost 800ppm). All the reduction slags from Sangis 842 have barium content under 580ppm. Some of the smithing

slags from Sangis 730 have somewhat higher amounts, at most about 1500ppm, but this too is clearly lower than in the slags from Vivungi. It is interesting to note that the slags from furnace area 2 as well as 3 show a large, but similar, variation in amounts. But the proportions, or ratio, between manganese and barium is more constant (Figures S140–S141). Here a difference from the slags from Sangis can be noted. These have a different relationship between manganese and barium, where the barium content increases less with increased manganese content compared with in the slags from Vivungi. There is also a greater difference within the group of slags from Sangis 842. The smithing slags from Sangis 730 however demonstrate a similar pattern. It is also worth noting, however, that the lake ore from Vivungi, which has significantly lower content of manganese as well as barium compared with the lake ore and the slags from Vivungi, has a similar ratio between manganese and barium.

Similar differences in the ratio between manganese and barium are noted between several regions with limonite ores, not just in Sweden but also in Norway, e.g. in Oppland (Grandin 2016).

S4.4: rare earth elements (REE)

Other trace elements significant for the ability to distinguish various ore formation areas are the rare earth elements (REE) lanthanum (La) to lutetium (Lu). The proportions between these are mainly preserved from the bedrock from which the ore has been formed and in time inherited by the slag. The signature that these show is thereby a good indication of a relationship between slags, and between slags and ores.

In part these can be treated as a group where their total contents are interesting, while the mutual relationships between them can also be compared. The pattern that emerges (Figure S142) is that there is a variation within each group of slags. The slags from the iron production site in Sangis 842, however, has as a group a somewhat higher total content of REE than the slags from both furnace areas in Vivungi, which are harder to distinguish; those from area 2 show greater variation, but also include the more concentrated slags from area 3 where the ores consistently have lower amounts. Because these elements are expected to be concentrated in the slag, compared with in the reduced metallic iron, this difference is reasonable.

The smithing slags from Sangis 730 are generally at the same total level as the reduction slags from Sangis 842, but with two clear differences; the slags from Sangis 730 have a (large) positive cerium anomaly (Ce) and greater negative europium anomaly (Eu) –

signatures that are expected to be inherited from the bedrock from which the ores have been formed and whose relationship does not change during production and forging (if no other material with other signatures is added). The positive cerium anomaly is clearly distinguishable in the slags from Sangis 730 (Figure S143). The slags from Vivungi however have a weak negative cerium anomaly, which besides the total contents, also distinguishes them from the slags from Sangis 842. In addition, this anomaly is possibly more pronounced in the slags from furnace area 3 than those from furnace area 2.

S4.5: chromium (Cr), nickel (Ni), cobalt (Co) and vanadium (V)

A few trace elements that often occur in slags and reflect occurrence in the ores and in turn can reflect various types of rock in the ore formation area are chromium (Cr), nickel (Ni), cobalt (Co) and vanadium (V). These elements can also be reduced into the metallic iron during the process, for which reason their occurrence in the slags is not directly comparable but nonetheless good indicators of occurrence or absence of them. Among these there is a clear difference between slags from Sangis and Vivungi. The slags from Sangis 730 and Sangis 842 have consistently higher Ni (about 20ppm) and lower Co (<10ppm) than the slags from Vivungi (Figure S144). The latter consistently have significantly lower Ni (<10ppm). They do indeed vary in Co (about 15–55ppm), but consistently at higher levels than in both reduction and smithing slags from Sangis. Chromium appears to vary similarly in all reduction slags. Where vanadium is concerned, the amounts are somewhat lower in the reduction slags from Sangis 842 (about 30ppm) than from Vivungi (about 30–40ppm), although there are exceptions (Figure S145). The slags from Sangis 730 however have significantly higher amounts of vanadium (>75ppm), and among these there is also the highest amounts of nickel (e.g. an outlier with >300ppm).

S4.6: bulk chemical analysis in summary

The variation within each geographically defined group of slags shows reasonable, and expected, differences within a locality and how important it is to analyse several slags from each context. There is a clear difference between the reduction slags from Sangis 842 and Vivungi 723, but also a clear difference between furnace area 2 and 3 in Vivungi.

The differences are probably mainly related to differences in the raw material, i.e., the ore, besides the differences seen in the Fe-Si relationship.

Differences are demonstrated as far as manganese content is concerned and the ratio between manganese and barium between slags from iron production in Sangis and the two furnace

areas in Vivungi. The latter however are not completely identical, and differences for example in phosphorus content and in REE suggest that different ore deposits have been used also in Vivungi.

- MnO and Ba: these are higher in Vivungi than in Sangis.
- MnO/Ba: in area 2 and 3 at Vivungi this is very similar between them, but different compared with in Sangis.
- Phosphorus content: this varies within both areas 2 and 3 at Vivungi, but is generally higher in 2 than in 3 (but no phosphorus iron is noted!). Even higher phosphorus is noted in the stray find of slag.
- REE: slags from Sangis 730 and Sangis 842 have higher total content than those from Vivungi.
- REE: slags from Sangis 730 have pronounced positive cerium anomaly and negative europium anomaly, which is lacking in slags from Sangis 842.
- REE: slags from Vivungi differ from slags from Sangis 730 and 842, but between themselves are also somewhat different, i.e., with weak negative cerium anomaly for slags from furnace area 2 (i.e. those that also have lower phosphorus).
- V, Cr, Ni and Co: the two furnace areas 2 and 3 in Vivungi have varying V, Cr, Ni and Co within the same order of magnitude. The cobalt content is possibly somewhat skewed toward higher amounts in area 3.
- V, Cr, Ni and Co: the slag from both sites in Sangis have significantly higher Ni and lower Co than those from Vivungi, possibly also somewhat lower V, but a similar variation in Cr. The slags that probably are smithing slags from Sangis 730 have consistently higher amounts of V but otherwise demonstrate the same order of magnitude as the reduction slags from Sangis 842.

Figure S1. Find no. 980 from A4. Bottom/edge, with fused sandy material and an attached stone (The Archaeologists, National Historical Museums, Uppsala, Sweden).

Figure S2. Find no. 980 from A4 in cross-section. Over the sandy bottom layer a slag that looks homogeneous emerges (The Archaeologists, National Historical Museums, Uppsala, Sweden).

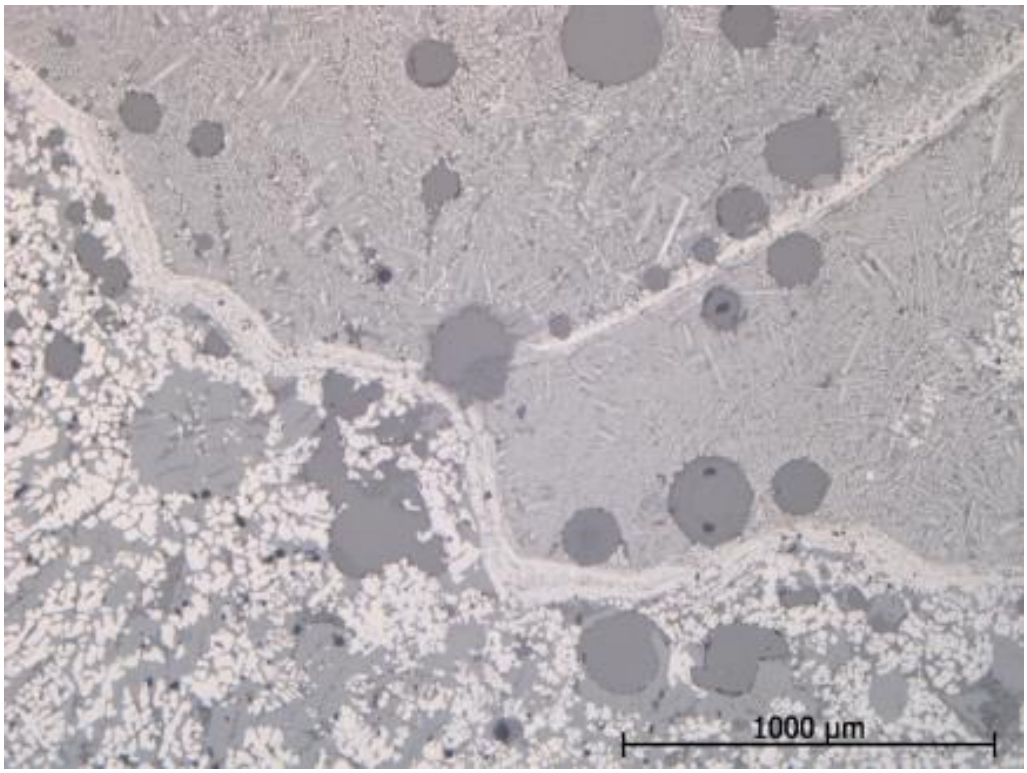

Figure S3. Find no. 980. In the microscope a complex slag emerges. Layers with different slag composition alternate. They are defined by magnetite concentrations (light bands) (The Archaeologists, National Historical Museums, Uppsala, Sweden).

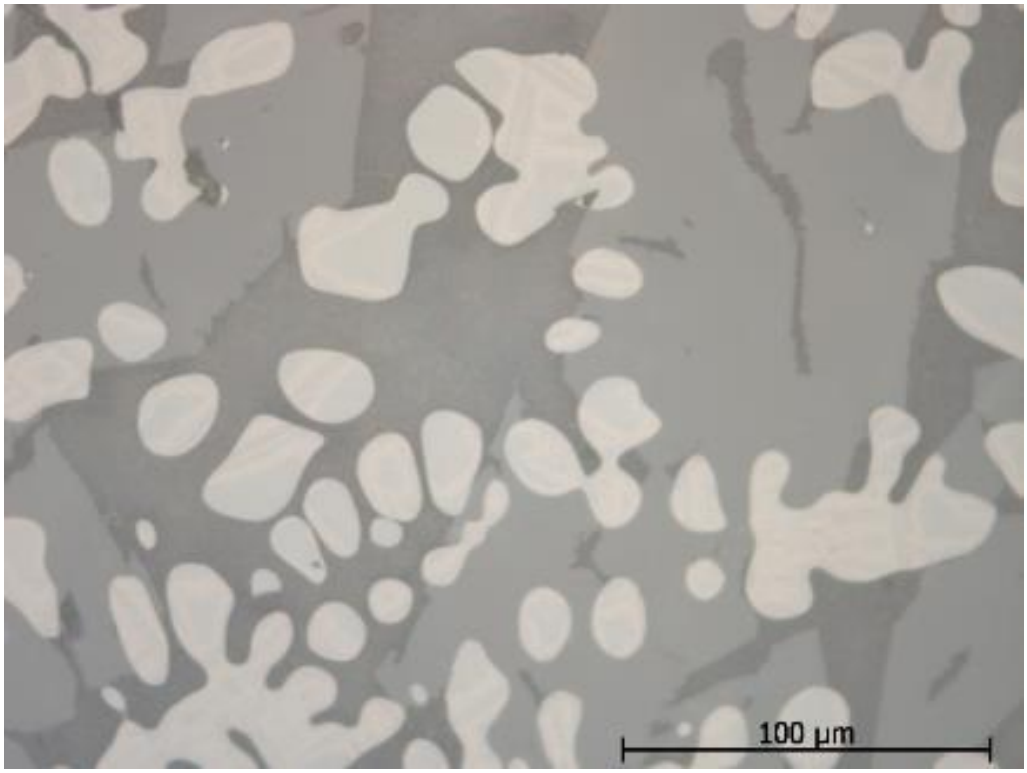

Figure S4. Find no. 980. Detail of dendritic wüstite (light) with some darker laminae of magnetite. Around the wüstite there are olivine laminae (light grey) and a glass phase (darker grey) (The Archaeologists, National Historical Museums, Uppsala, Sweden).

Figure S5. Find no. 1112 from A4. Homogeneous slag without clear bottom forms (The Archaeologists, National Historical Museums, Uppsala, Sweden).

Figure S6. Find no. 1112 in cross-section. Homogeneous slag (The Archaeologists, National Historical Museums, Uppsala, Sweden).

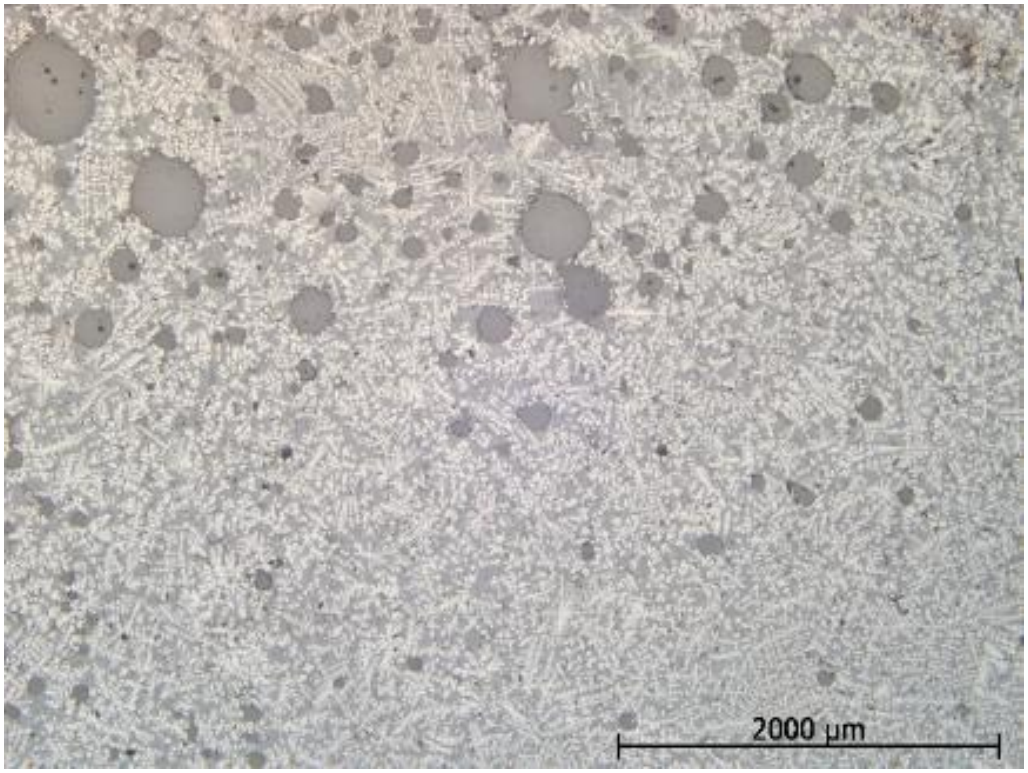

Figure S7. Find no. 1112. The slag is homogeneous even at microscale. It consists of dendritic wüstite (light), olivine laminae and glass (two grey phases). The round, grey areas are cavities (The Archaeologists, National Historical Museums, Uppsala, Sweden).

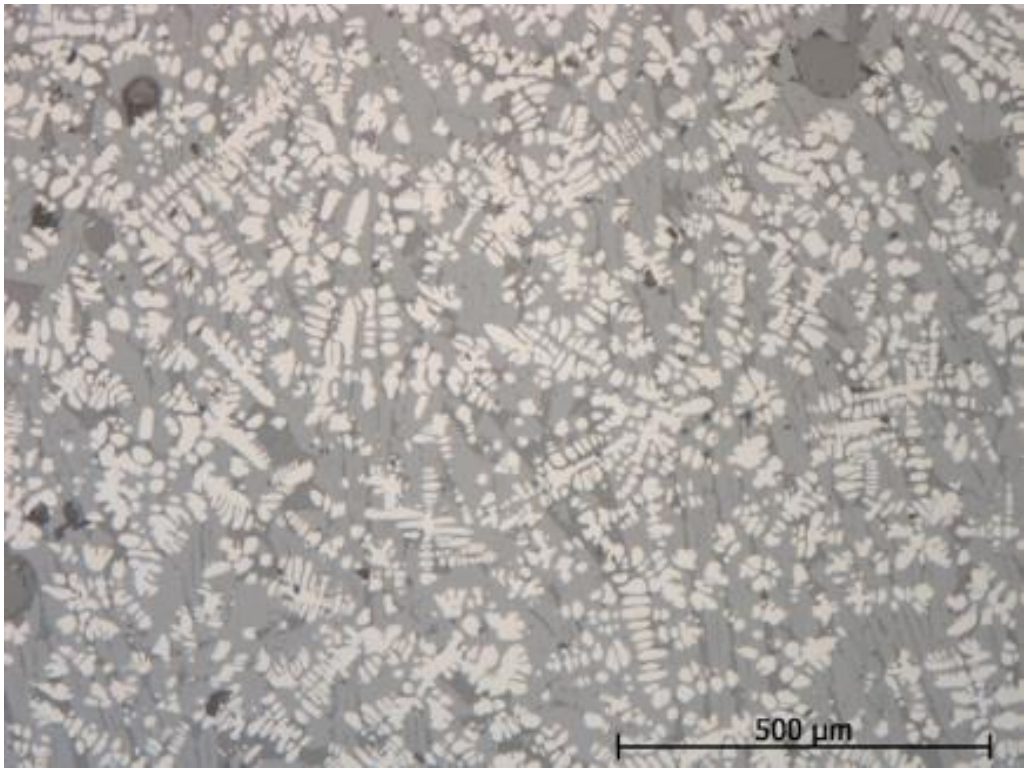

Figure S8. Find no. 1112. Detail from previous where olivine (lighter grey) can be distinguished from glass (darker grey) and where it appears that the white wüstite is homogeneous in composition (The Archaeologists, National Historical Museums, Uppsala, Sweden).

Figure S9. Find no. 1344 in cross-section. In the bottom and along the edge a sandy/gravelly layer, followed by slag (The Archaeologists, National Historical Museums, Uppsala, Sweden).

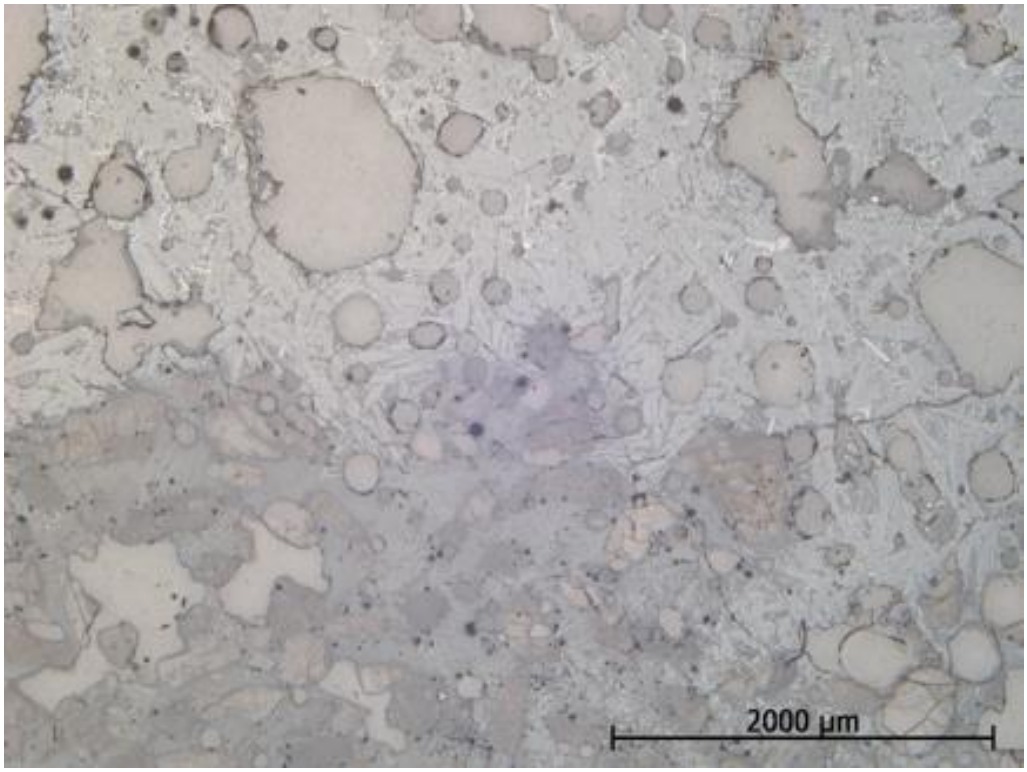

Figure S10. Find no. 1344. Detail from bottom where the quartz grains in the lower part have partially melted into the slag, which has melted down into the sandy layer. The slag is dominated by olivine (light grey) and glass (darker grey) (The Archaeologists, National Historical Museums, Uppsala, Sweden).

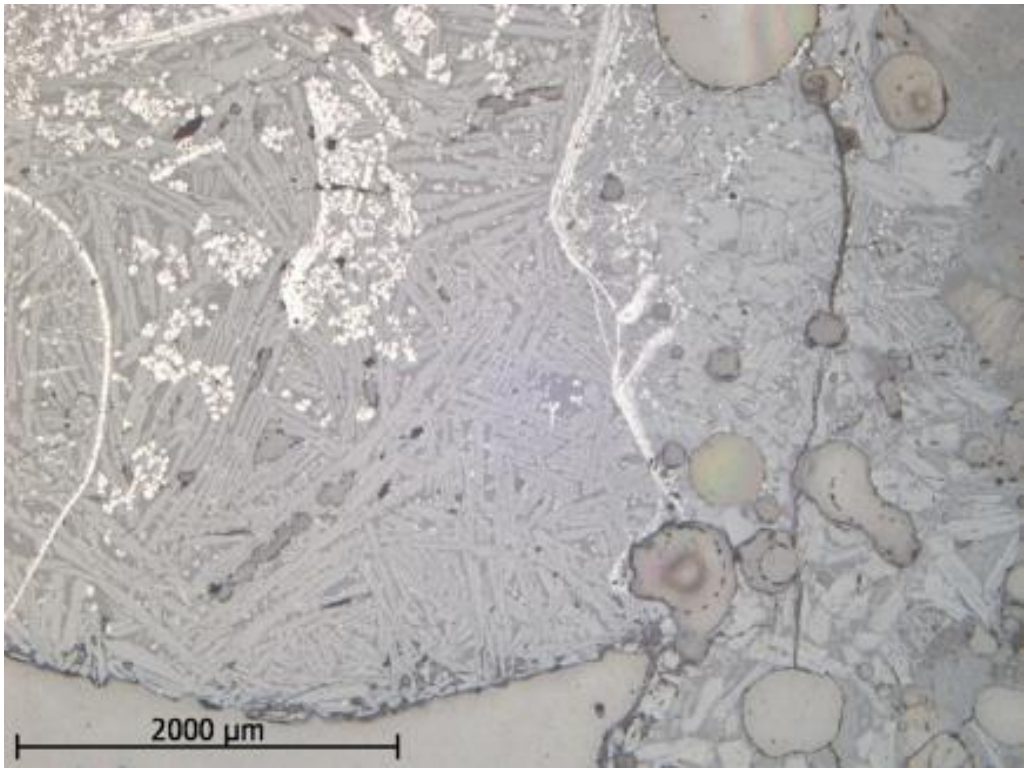

Figure S11. Find no. 1344. In microscale a complexly built-up slag emerges with varying mineral content and occurrence of magnetite (light oblong bands) (The Archaeologists, National Historical Museums, Uppsala, Sweden).

Figure S12. Find no. 913 from A53. Top side (The Archaeologists, National Historical Museums, Uppsala, Sweden).

Figure S13. Find no. 913 in cross section. A homogeneous slag that lacks bottom layer of sand (The Archaeologists, National Historical Museums, Uppsala, Sweden).

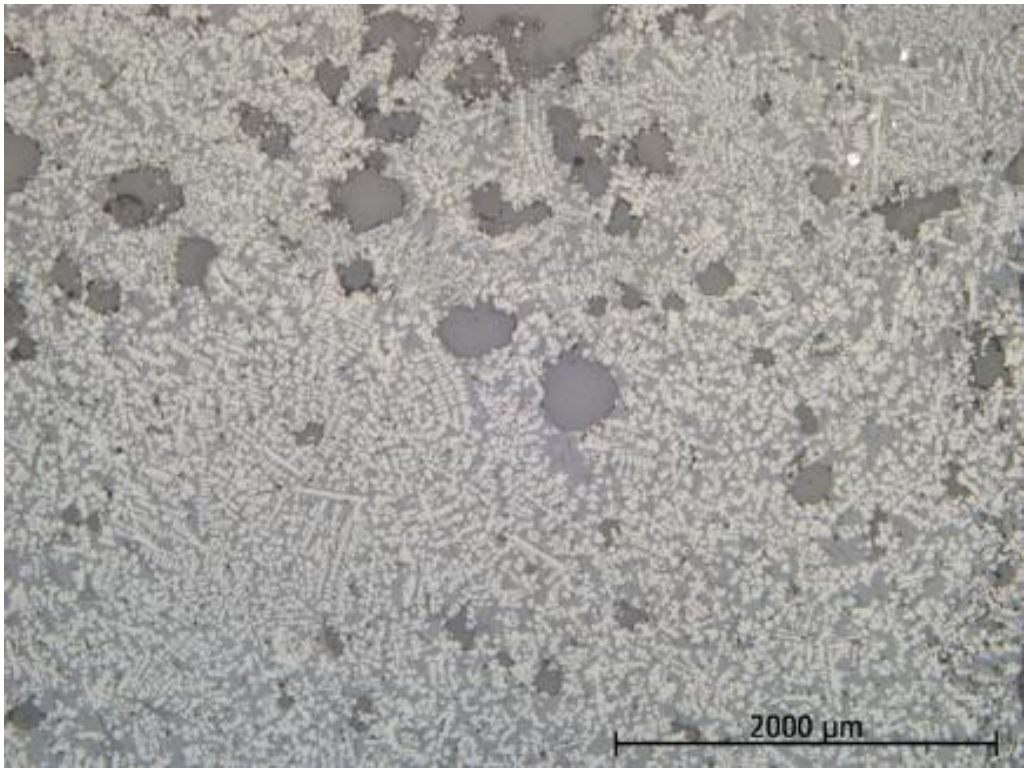

Figure S14. Find no. 913. Even at microscale a very homogeneous slag appears with wüstite (light), olivine (light grey) and glass (darker grey). At the top right are some white droplets of metallic iron (The Archaeologists, National Historical Museums, Uppsala, Sweden).

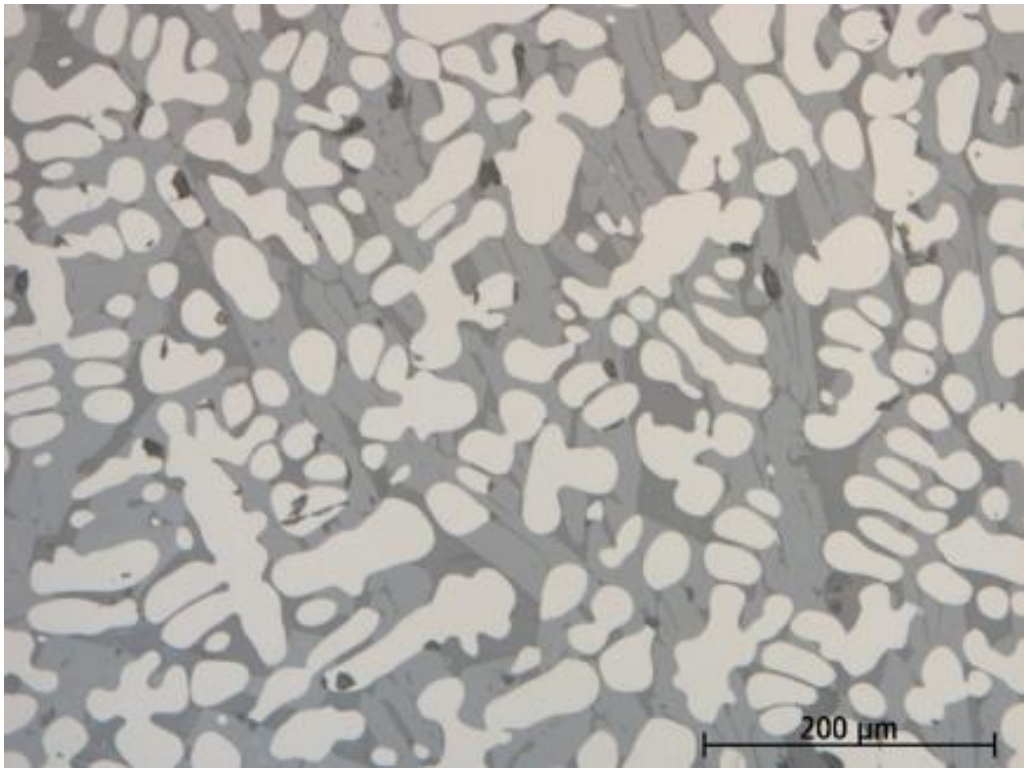

Figure S15. Find no. 913. At high magnification it can be seen that the dendritic wüstite (light) is homogeneous in composition. Here olivine (light grey) and glass (darker grey) also appear clearly (The Archaeologists, National Historical Museums, Uppsala, Sweden).

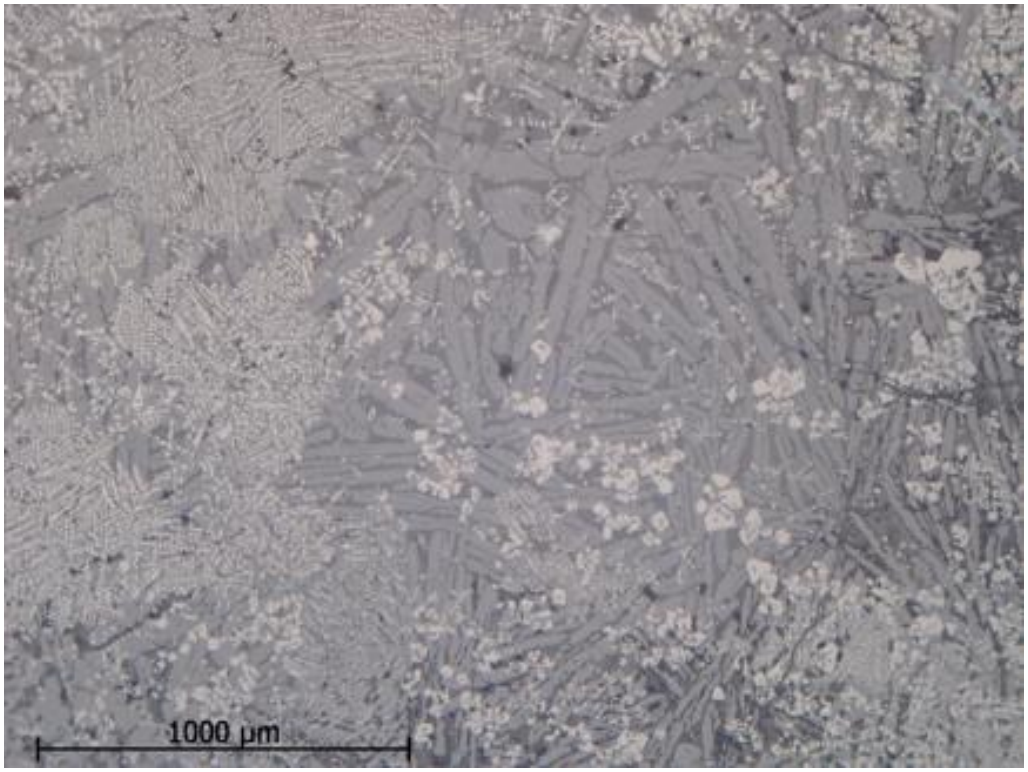

Figure S16. Find no. 3448. Complex slag with varying proportions between the minerals included. To the left there is wüstite (light oblong shapes), to the right more magnetite (light blocky crystals) (The Archaeologists, National Historical Museums, Uppsala, Sweden).

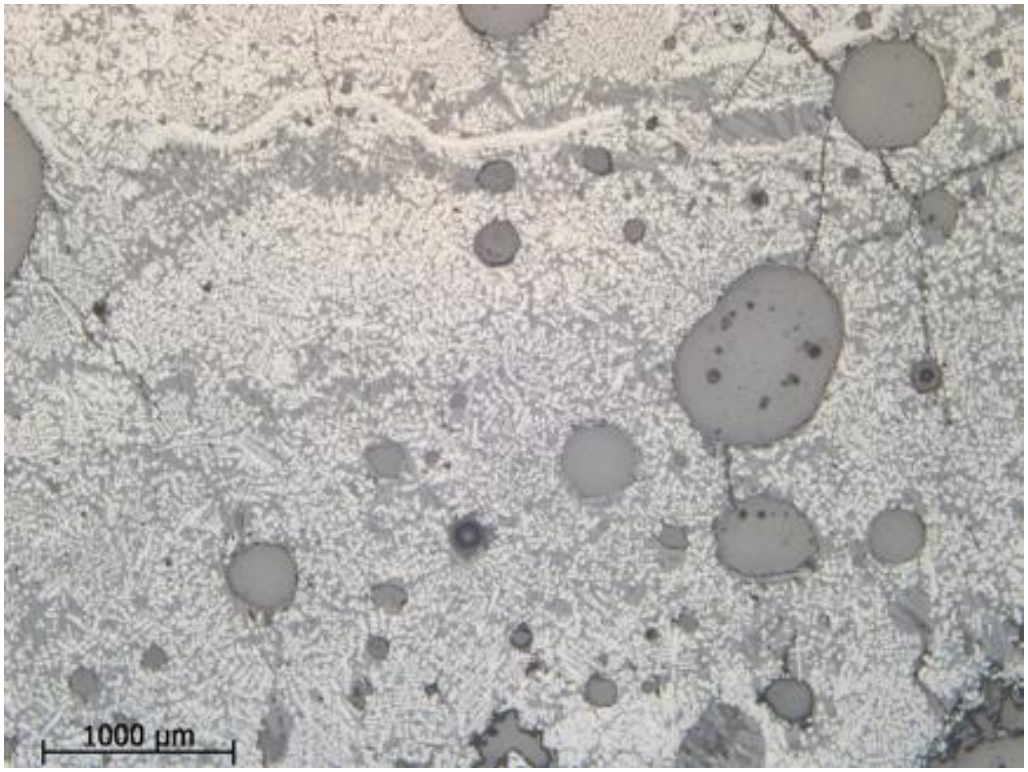

Figure S17. Find no. 3448. Overview of area in the slag with high total iron content where several types of iron oxides occur, e.g. magnetite in the clear bands (The Archaeologists, National Historical Museums, Uppsala, Sweden).

Figure S18. Find no. 922 from A4. Spongy iron (light) and slag (darker) (The Archaeologists, National Historical Museums, Uppsala, Sweden).

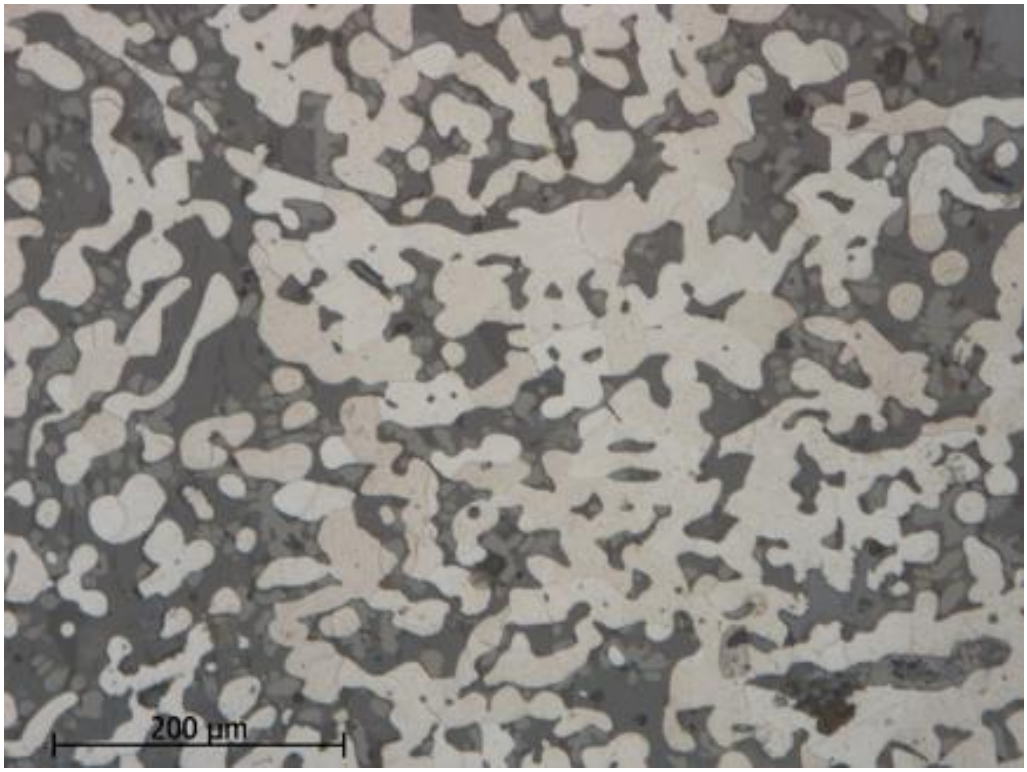

Figure S19. Find no. 922. Micrograph of etched sample. The spongy iron is ferritic (faintly brown-coloured field) and surrounded by slag (The Archaeologists, National Historical Museums, Uppsala, Sweden).

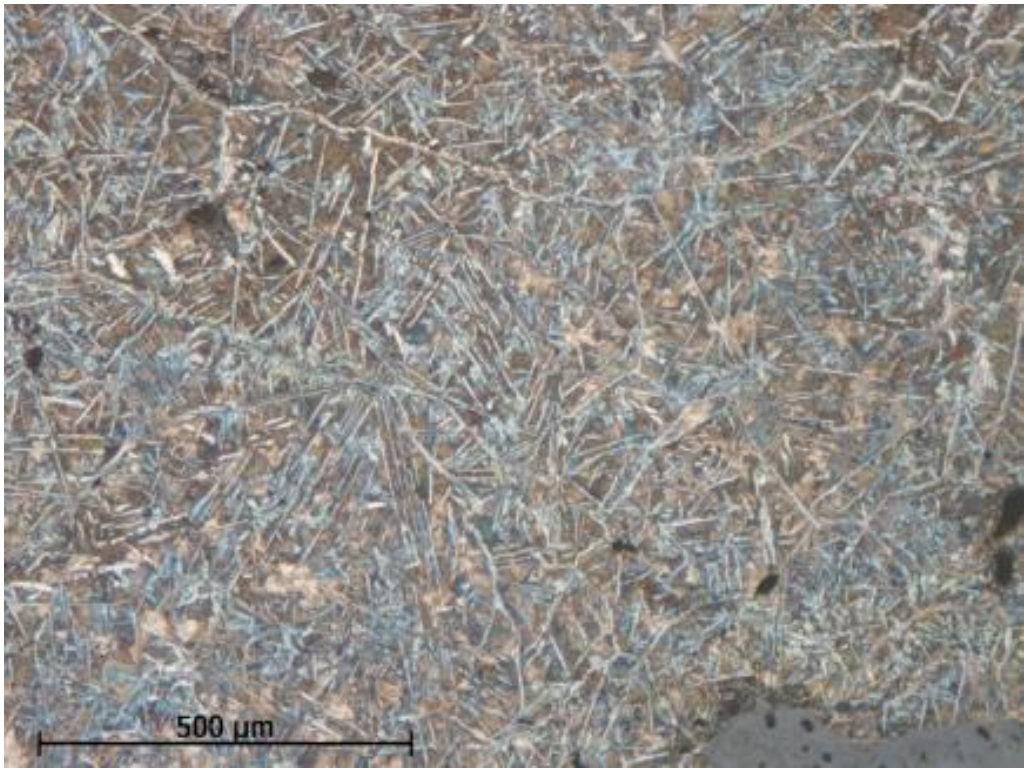

Figure S20. Find no. 925 from A4. Micrograph of etched sample. Iron with high carbon content. The sample consists of pearlite (speckled) and cementite (light laminae) (The Archaeologists, National Historical Museums, Uppsala, Sweden).

Figure S21. Find no. 878. A knife. The line shows the cross section through the blade which has been analysed (see following figures) (The Archaeologists, National Historical Museums, Uppsala, Sweden).

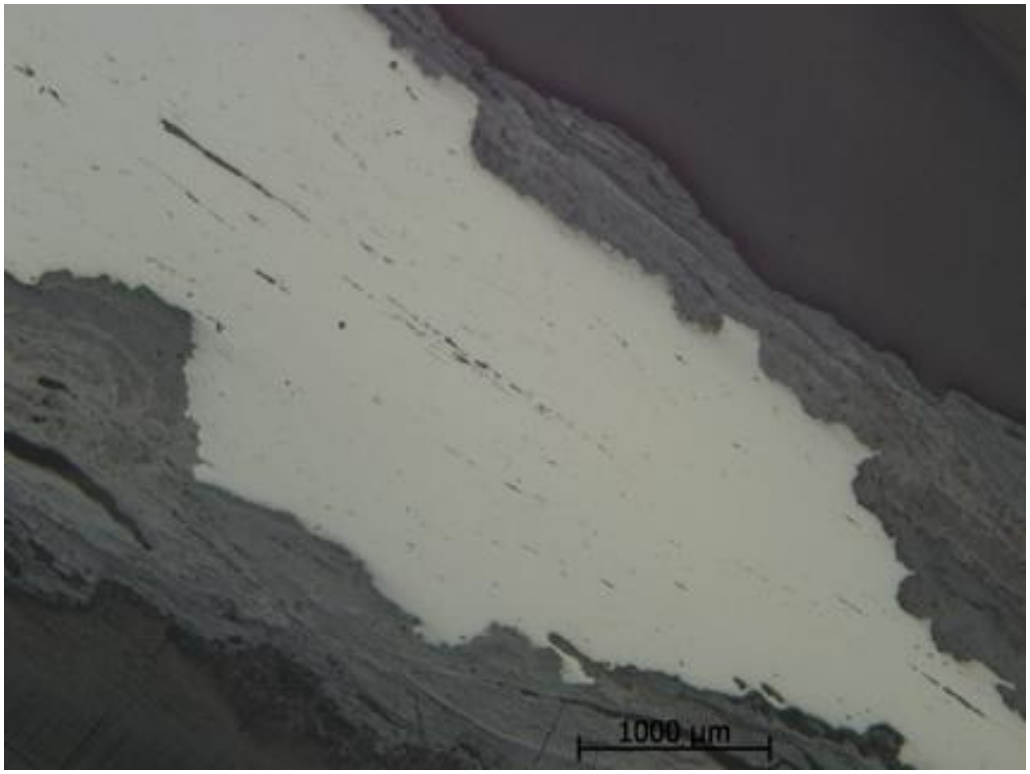

Figure S22. Find no. 878. Micrograph, unetched sample. The knife in cross section, near the edge. The intact metallic iron is light. The outer grey parts are mainly rust. The smaller grey or black, parallel and elongated formations are slag inclusions (The Archaeologists, National Historical Museums, Uppsala, Sweden).

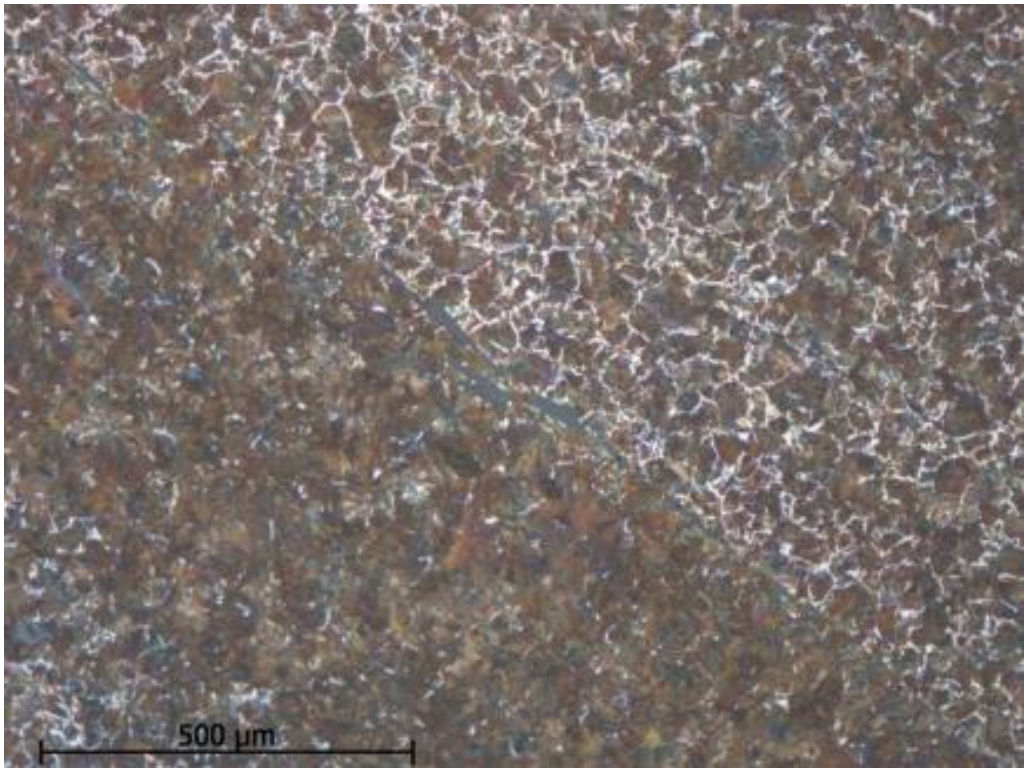

Figure S23. Find no. 878. Micrograph, etched sample. The knife in cross section, central. Slag inclusions are seen as a grey diagonal band. The metal below the band mainly consists of pearlite. On the top side of the slag inclusions there is pearlite and a little ferrite (light borders) and here the carbon content is somewhat lower (The Archaeologists, National Historical Museums, Uppsala, Sweden).

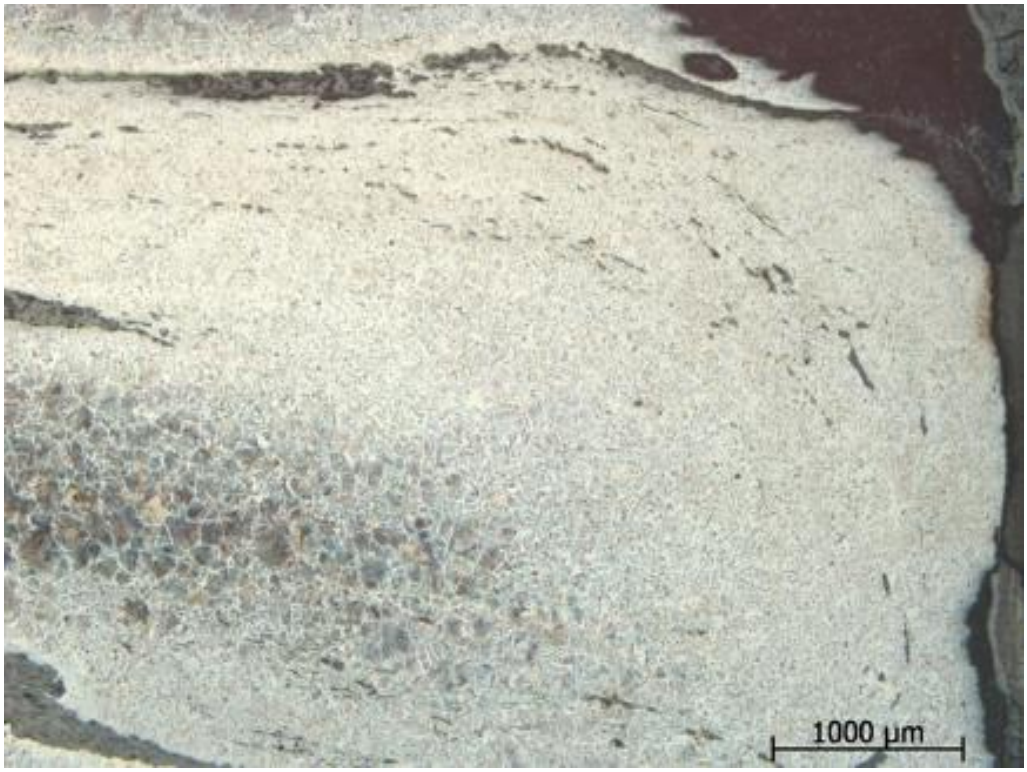

Figure S24. Find no. 1559. Micrograph of etched sample. Slag inclusions bend around the outer edges of the find. Along these the carbon content is lower (light areas). More centrally the carbon content is higher (speckled area to the left) (The Archaeologists, National Historical Museums, Uppsala, Sweden).

Figure S25. Find no. 2021. A knife. The line shows the cross section through the blade which has been analysed (The Archaeologists, National Historical Museums, Uppsala, Sweden).

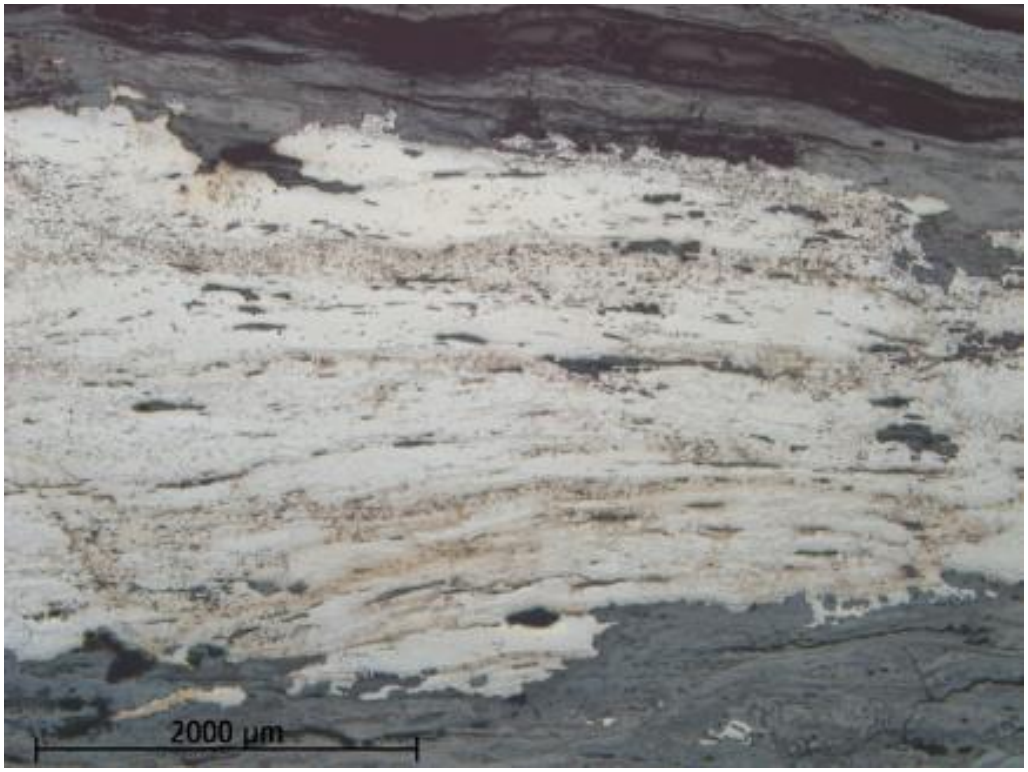

Figure S26. Find no. 2021. Micrograph of etched sample. Detail of the cross section close to the edge. The upper and lower grey areas are rust. The small extended central grey areas are mostly slag inclusions that run from the edge, at right, toward the back, at left. The metal is banded (laminated), parallel to the slag inclusions and is constituted of alternating bands of ferrite (light) and ferrite with phosphorous content (faintly brown coloured). Scattered bands of ferrite with small quantities of pearlite also occur (in the upper half) (The Archaeologists, National Historical Museums, Uppsala, Sweden).

Figure S27. Find no. 2684. Axe. The lines indicate the area that has undergone metallographic analysis and where sample has also been taken for dating (The Archaeologists, National Historical Museums, Uppsala, Sweden).

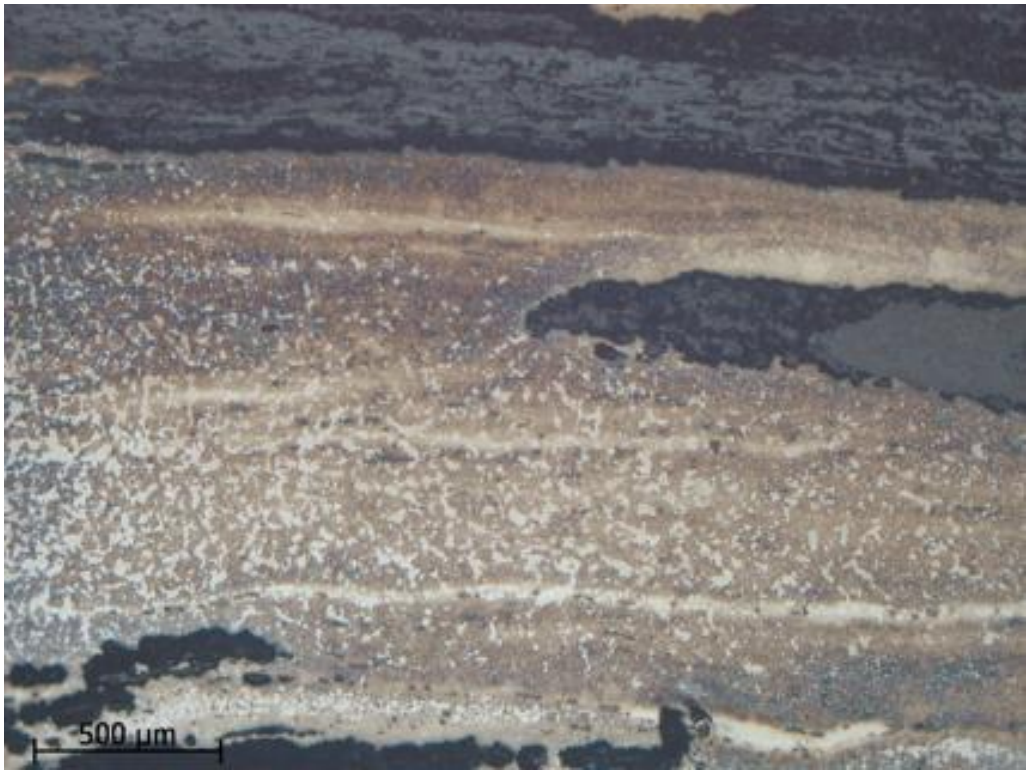

Figure S28. Find no. 2684. Micrograph of etched sample. Detail from cross section of the axe where the light lines indicate weld seams where the steel has been forged together. The grey areas are rust (The Archaeologists, National Historical Museums, Uppsala, Sweden).

Figure S29. Find no. 2684. Micrograph of etched sample. Detail from the edge of the axe where it is mostly corroded (grey). A narrow band of metal is preserved. It consists of hardened steel (brown-blue shades) (The Archaeologists, National Historical Museums, Uppsala, Sweden).

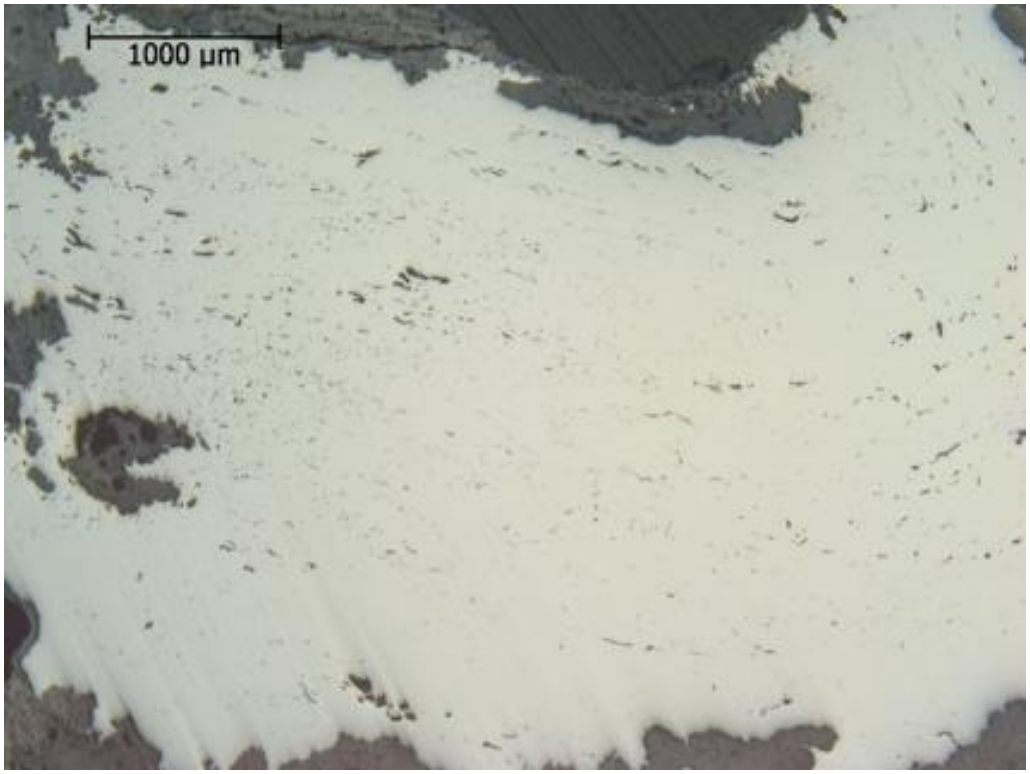

Figure S30. Find no. 2771 from A27. Micrograph of unetched sample. Cross section where plentiful slag inclusions (grey-black) follow a parallel structure through the metal (The Archaeologists, National Historical Museums, Uppsala, Sweden).

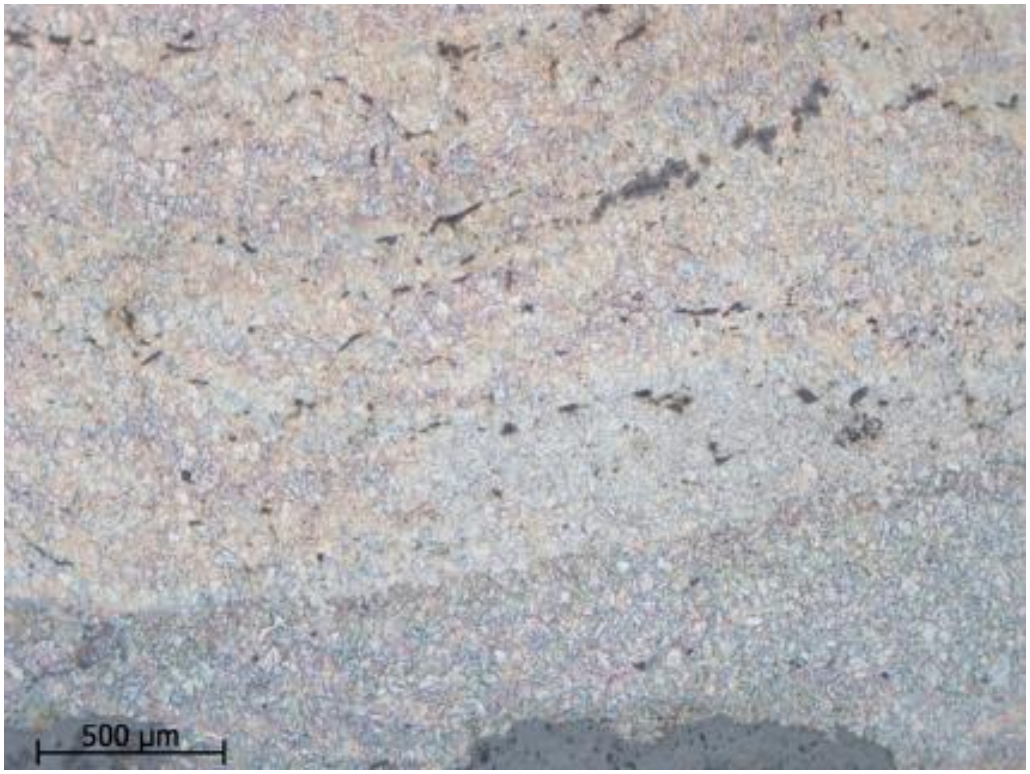

Figure S31. Find no. 2771. Micrograph of etched sample. The iron is banded parallel with the inclusions. The carbon content in the steel is similar in the various layers (The Archaeologists, National Historical Museums, Uppsala, Sweden).

Figure S32. F930, example of stearin slag with a few larger slag strings (The Archaeologists, National Historical Museums, Uppsala, Sweden).

Figure S33. F930, stearin slag in cross section with a few small pores (i.e. a dense slag) (The Archaeologists, National Historical Museums, Uppsala, Sweden).

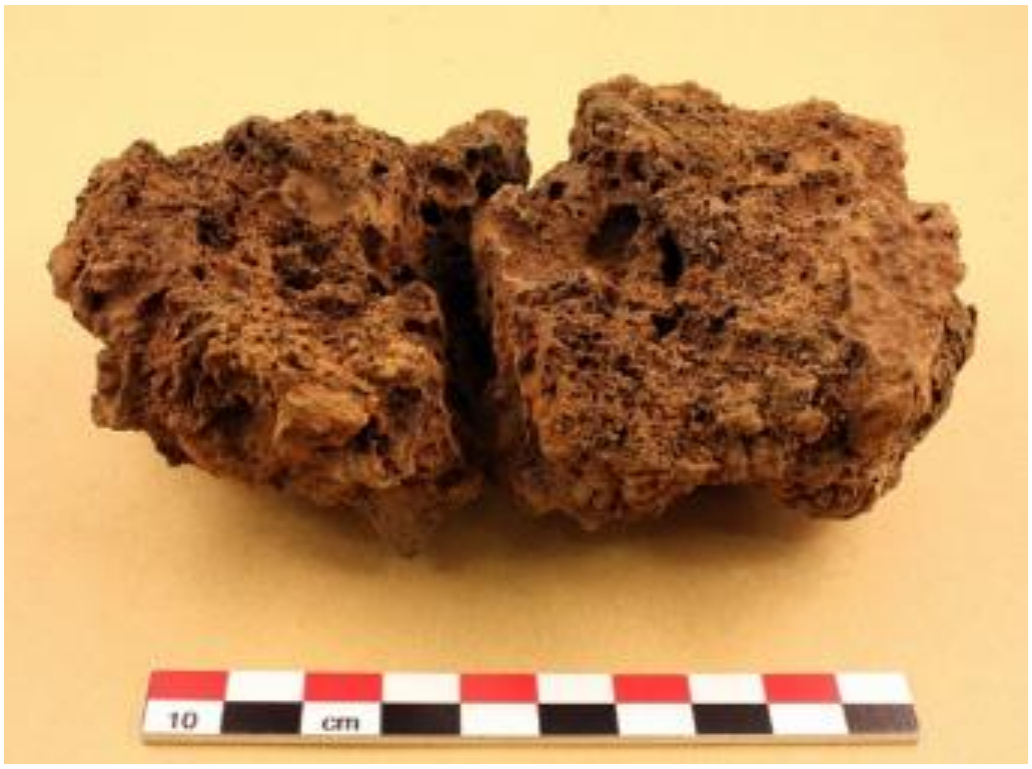

Figure S34. Bottom slag F491, seen at an angle from above with weakly bowl-shaped upper area (The Archaeologists, National Historical Museums, Uppsala, Sweden).

Figure S35. Bottom slag F491 where stearin strings of slag are seen on the bottom area (The Archaeologists, National Historical Museums, Uppsala, Sweden).

Figure S36. Bottom slag F83, seen from the side, with weakly bowl-shaped upper area (The Archaeologists, National Historical Museums, Uppsala, Sweden).

Figure S37. F83 in cross section; a rather porous slag. The square shows the part that has been examined in the microscope (The Archaeologists, National Historical Museums, Uppsala, Sweden).

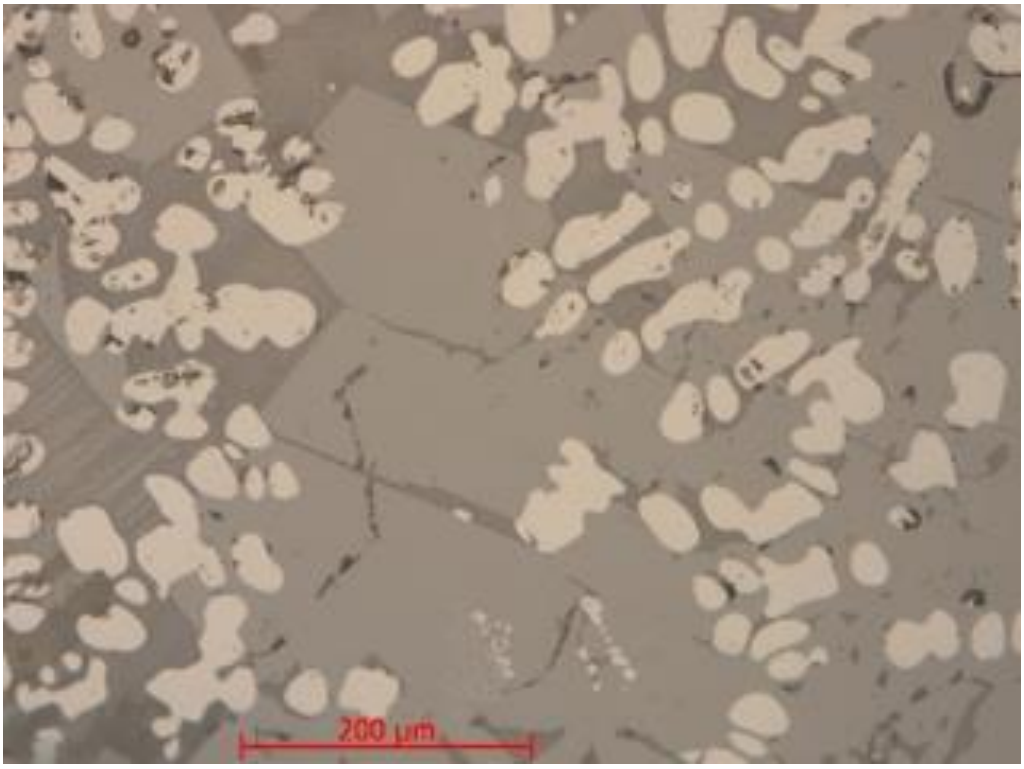

Figure S38. Bottom slag F83. The slag contains coarse olivine laminae (light grey), wüstite (light) and a glass phase (darker grey). Micrograph of polished surface (The Archaeologists, National Historical Museums, Uppsala, Sweden).

Figure S39. Slag F256 in cross section. The box shows the part of the slag that has been examined in the microscope. In the circle is the iron concentration that has also been analysed (The Archaeologists, National Historical Museums, Uppsala, Sweden).

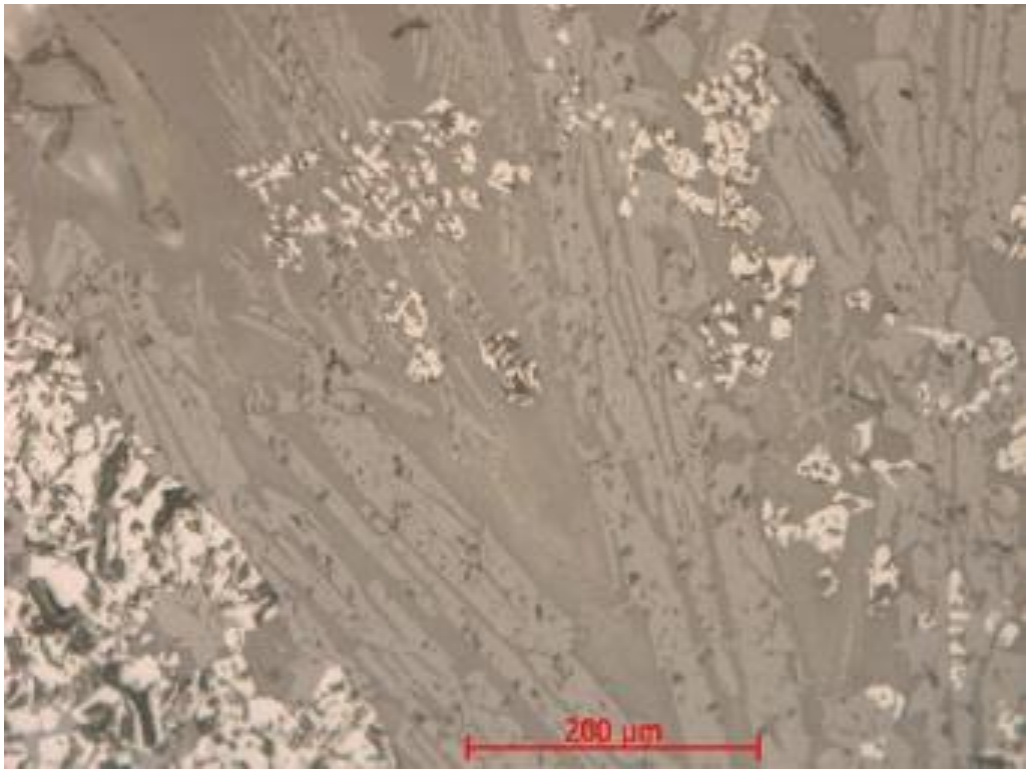

Figure S40. Detail from central parts of slag F256. Here olivine (light grey) and a glass phase (darker grey) appear to dominate. The iron oxide (light), which is magnetite, is somewhat blocky in shape. Micrograph (The Archaeologists, National Historical Museums, Uppsala, Sweden).

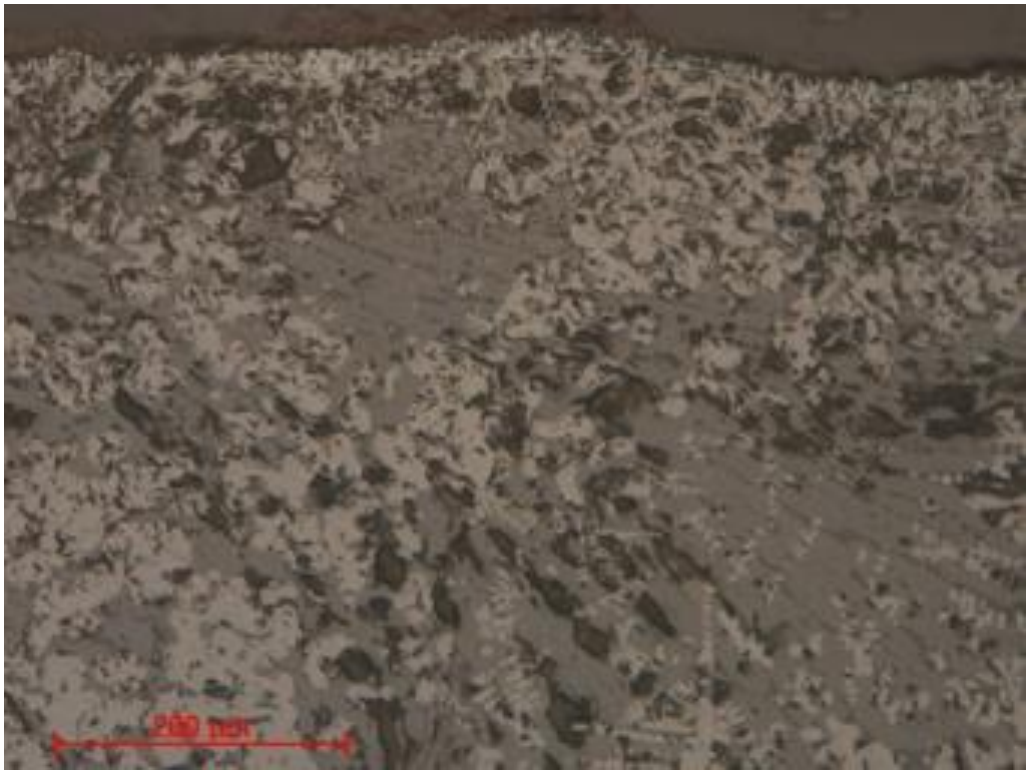

Figure S41. Detail from slag F256 at its outer edge. The thin light edge at the top of the picture is dominated by magnetite. Micrograph (The Archaeologists, National Historical Museums, Uppsala, Sweden).

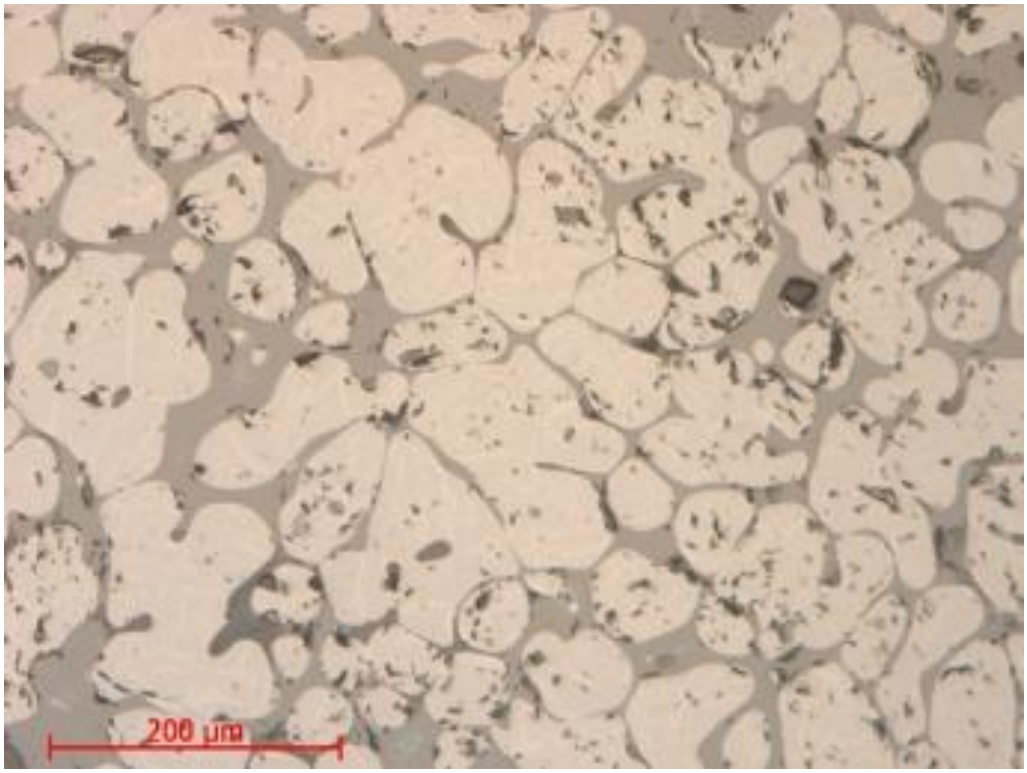

Figure S42. Detail from F256 of wüstite (light) with thin laminae of magnetite (somewhat lighter). Surrounding grey phases are olivine and glass. Micrograph (The Archaeologists, National Historical Museums, Uppsala, Sweden).

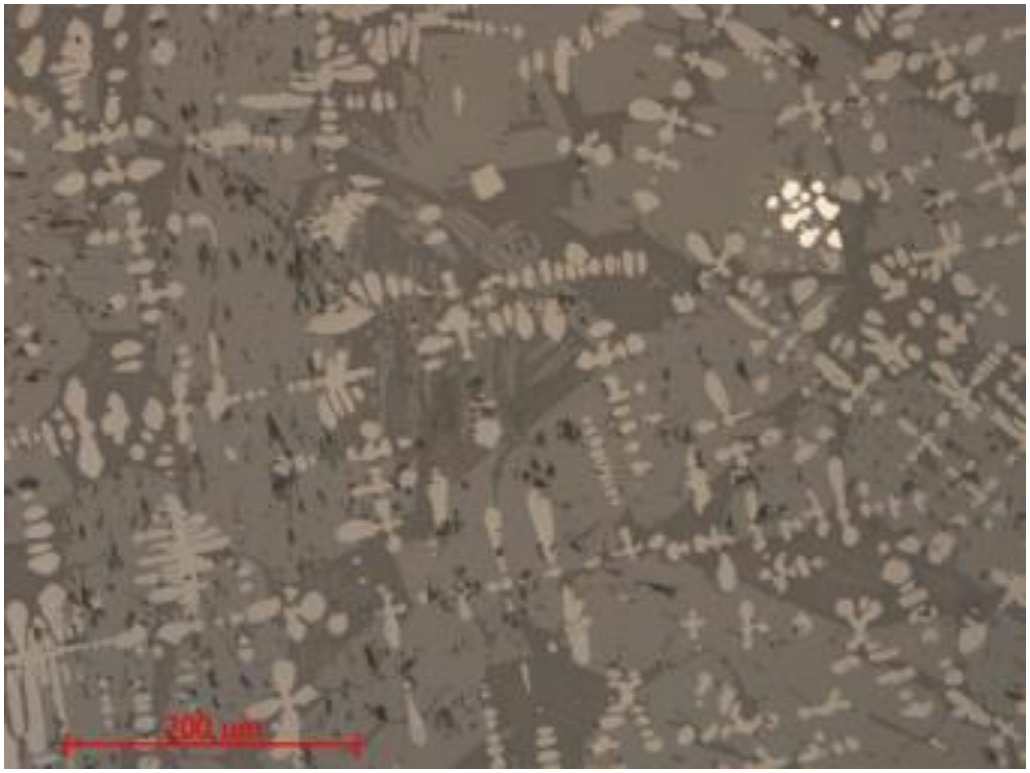

Figure S43. Detail of F396 with olivine crystals (light grey), a glass phase (darker grey) and wüstite (light). In the upper right corner there is also metallic iron (white). Micrograph (The Archaeologists, National Historical Museums, Uppsala, Sweden).

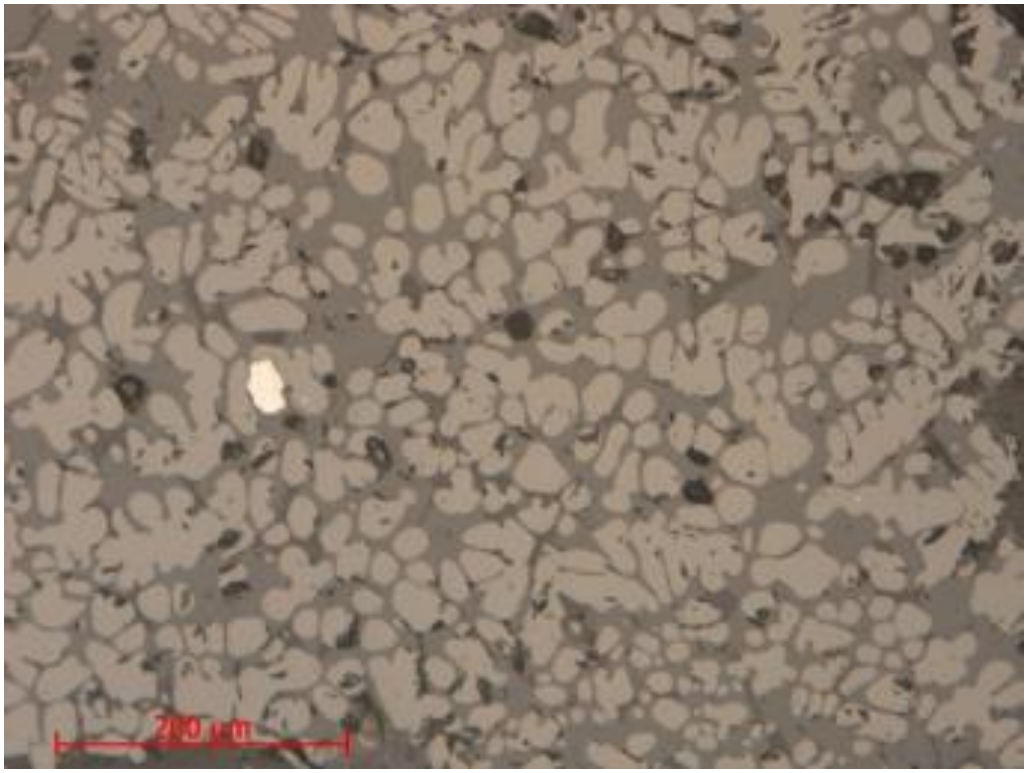

Figure S44. Detail of F756 with dominance of wüstite (light) and olivine crystals (light grey) and a glass phase (darker grey) in a smaller quantity. Micrograph (The Archaeologists, National Historical Museums, Uppsala, Sweden).

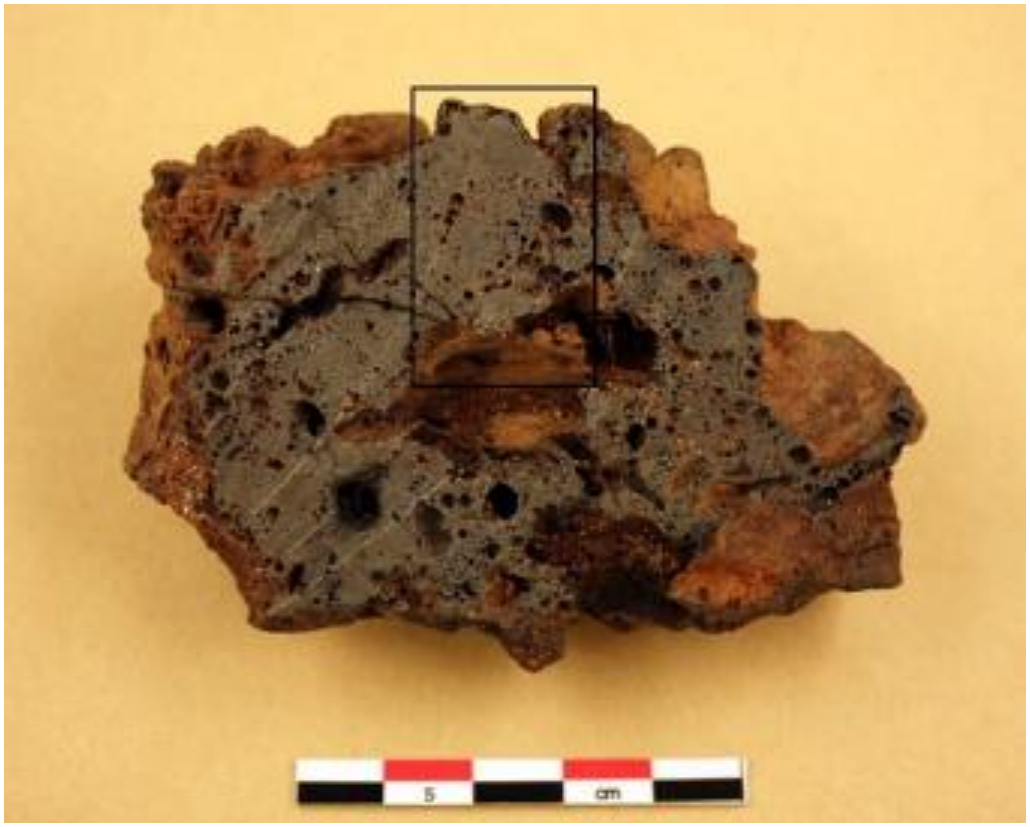

Figure S45. Bottom slag F757 in cross section with central charcoal imprint. The slag within the box has been examined in the microscope (The Archaeologists, National Historical Museums, Uppsala, Sweden).

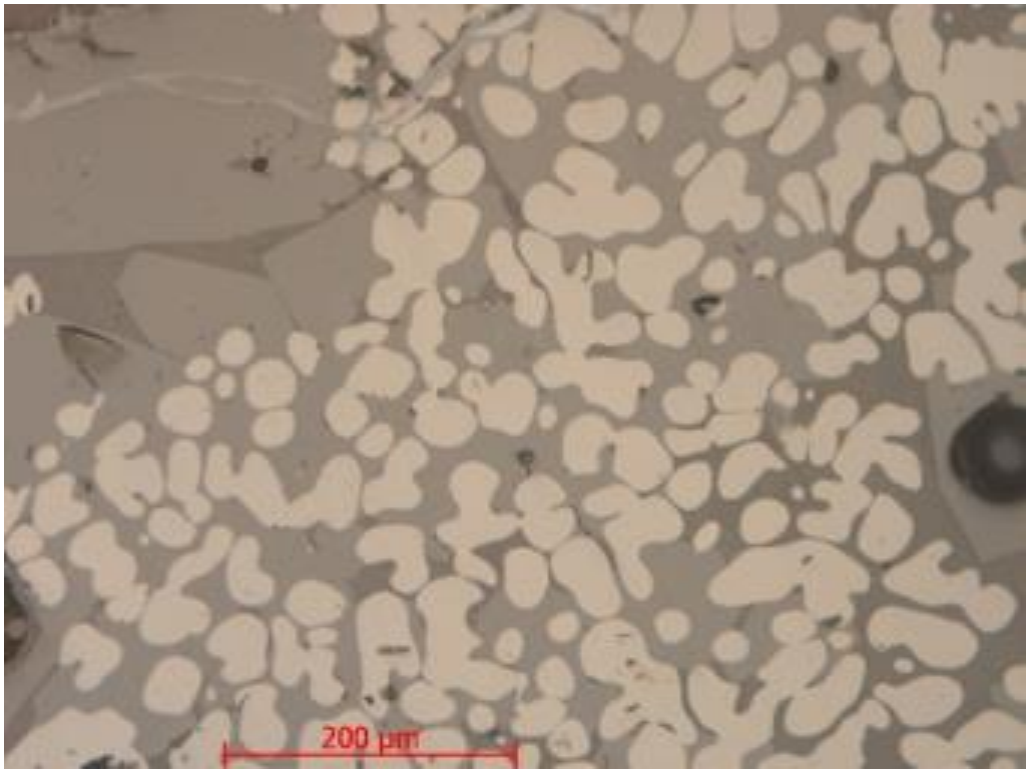

Figure S46. Detail of F757 with wüstite, olivine and glass in somewhat varying proportions. Micrograph (The Archaeologists, National Historical Museums, Uppsala, Sweden).

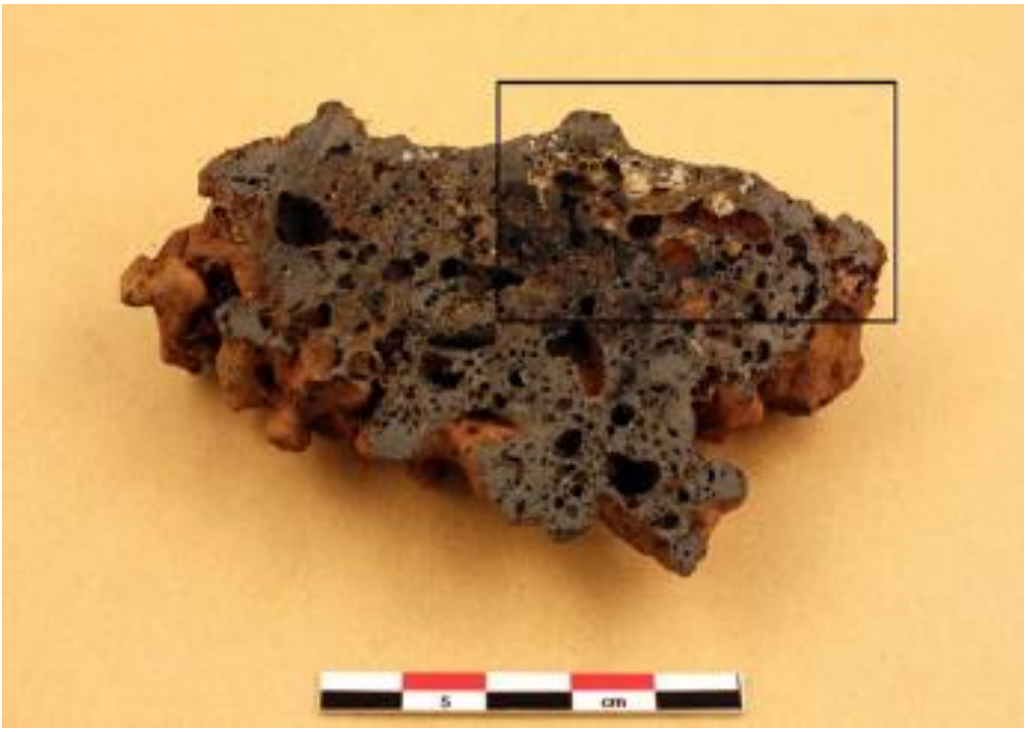

Figure S47. Bottom slag F931 in cross section. The slag is rather porous and at the top there is a concentration of metallic iron. This part, in the square, has been examined in the microscope (The Archaeologists, National Historical Museums, Uppsala, Sweden).

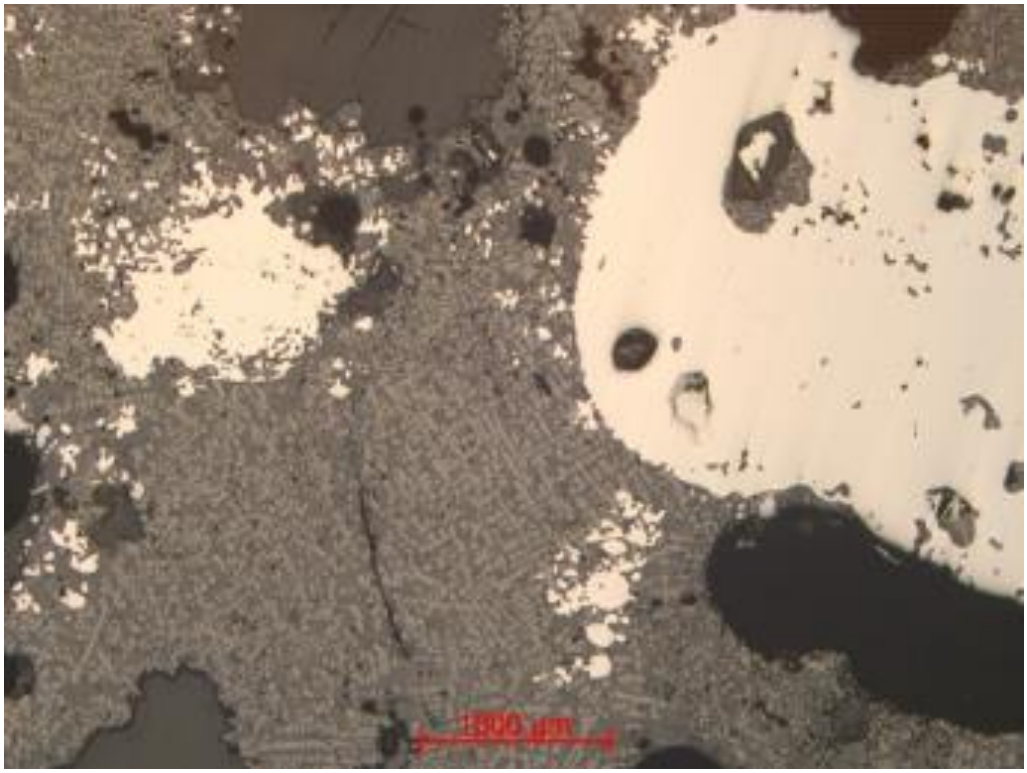

Figure S48. Detail from slag F931 with a large concentration of metallic iron (white) to the right and some smaller ones to the left. Micrograph (The Archaeologists, National Historical Museums, Uppsala, Sweden).

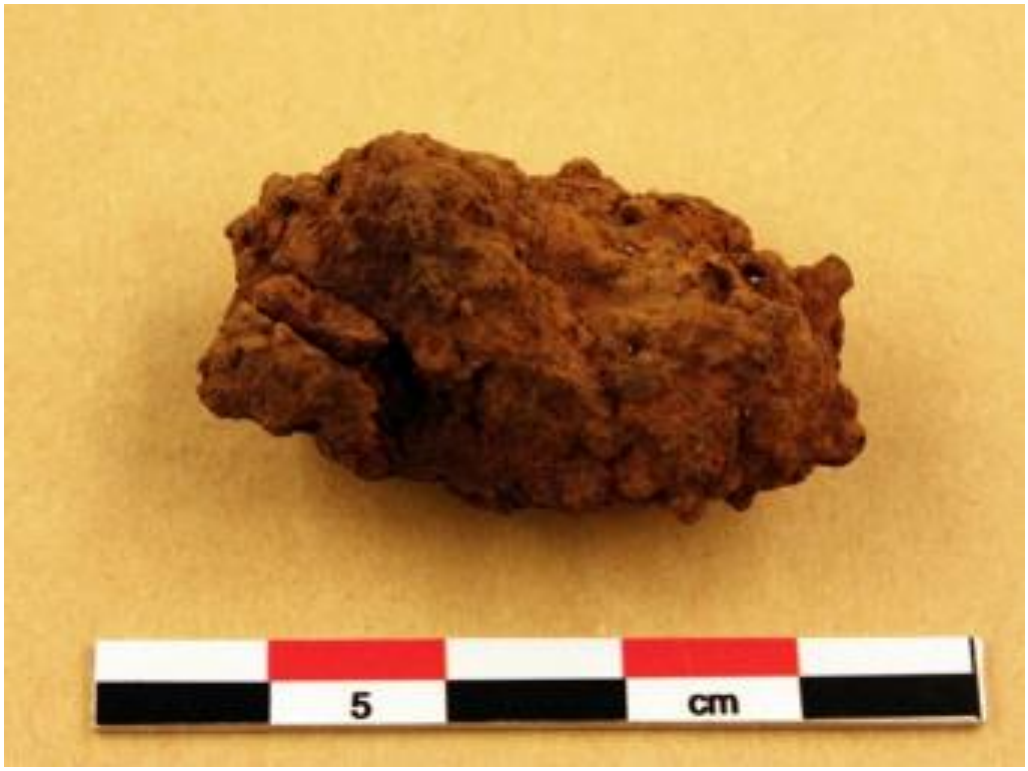

Figure S49. The irregular iron lump F161 (The Archaeologists, National Historical Museums, Uppsala, Sweden).

Figure S50. Iron lump F161 in cross section. Concentration of metallic iron with cavities and corroded outer edges (The Archaeologists, National Historical Museums, Uppsala, Sweden).

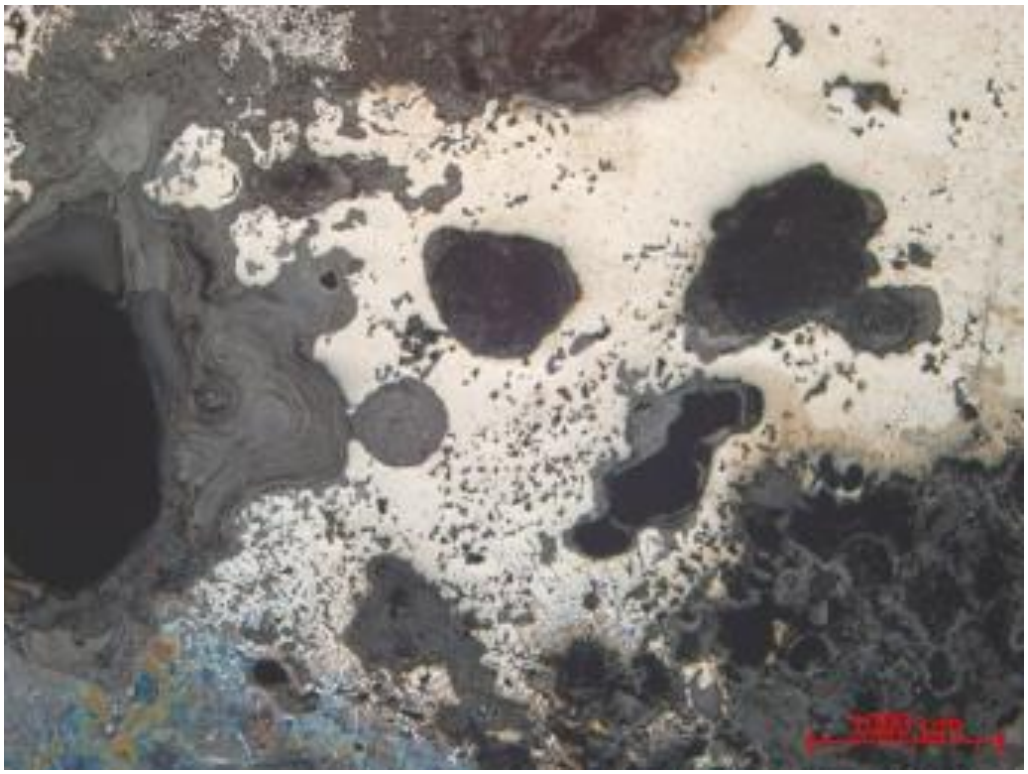

Figure S51. F161. The metal is heterogeneous and varies in composition from carbon-free iron, at top, to high carbon steel at the bottom of the picture. Micrograph of etched sample (The Archaeologists, National Historical Museums, Uppsala, Sweden).

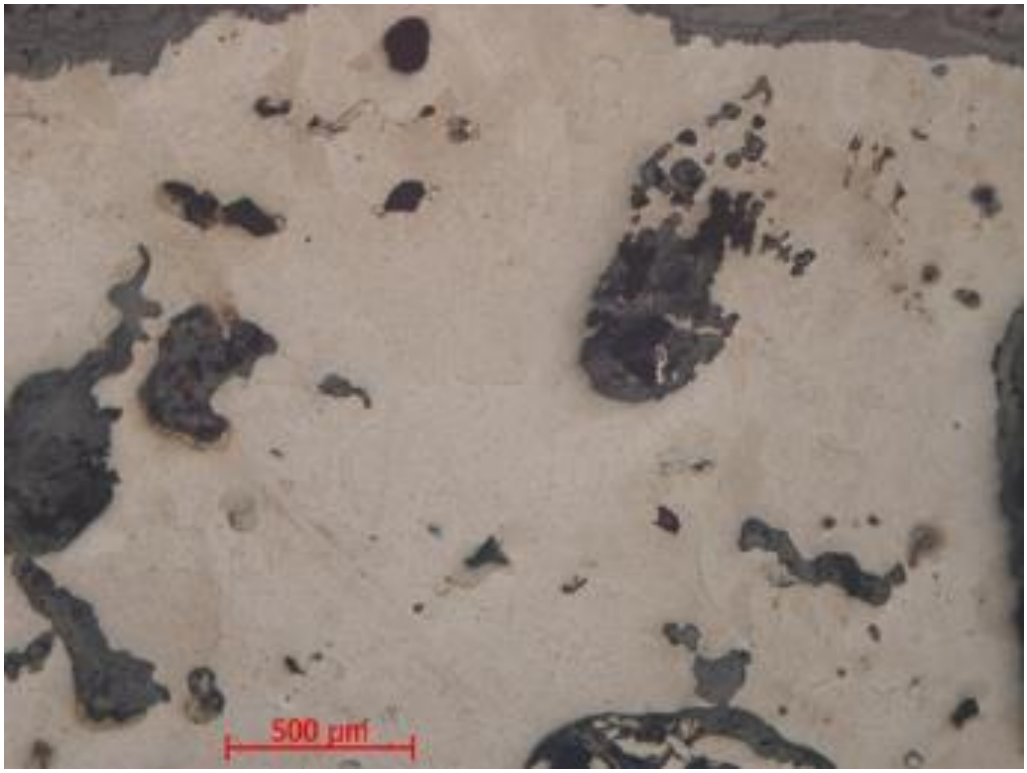

Figure S52. F256. The iron is homogeneous ferrite, i.e., carbon-free (the light areas with diffuse fields). The grey areas are slag and corroded areas. Micrograph of etched sample (The Archaeologists, National Historical Museums, Uppsala, Sweden).

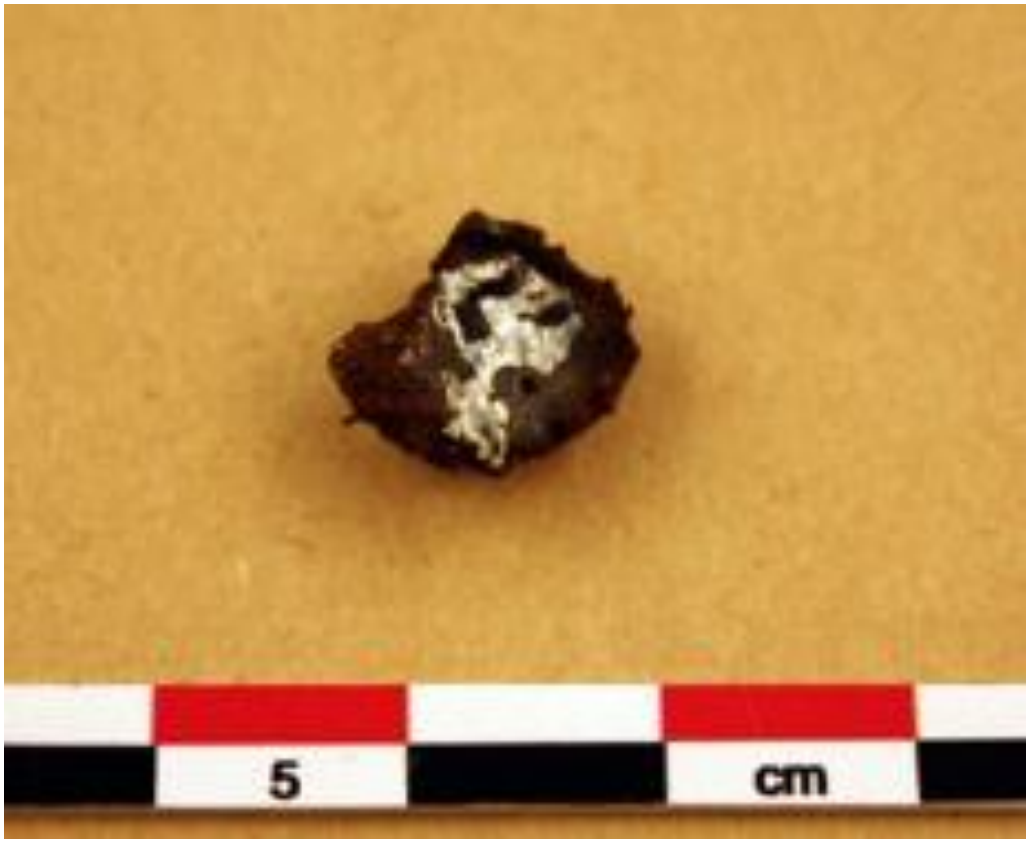

Figure S53. F629. Concentration of metallic iron with cavities and corroded outer edges (The Archaeologists, National Historical Museums, Uppsala, Sweden).

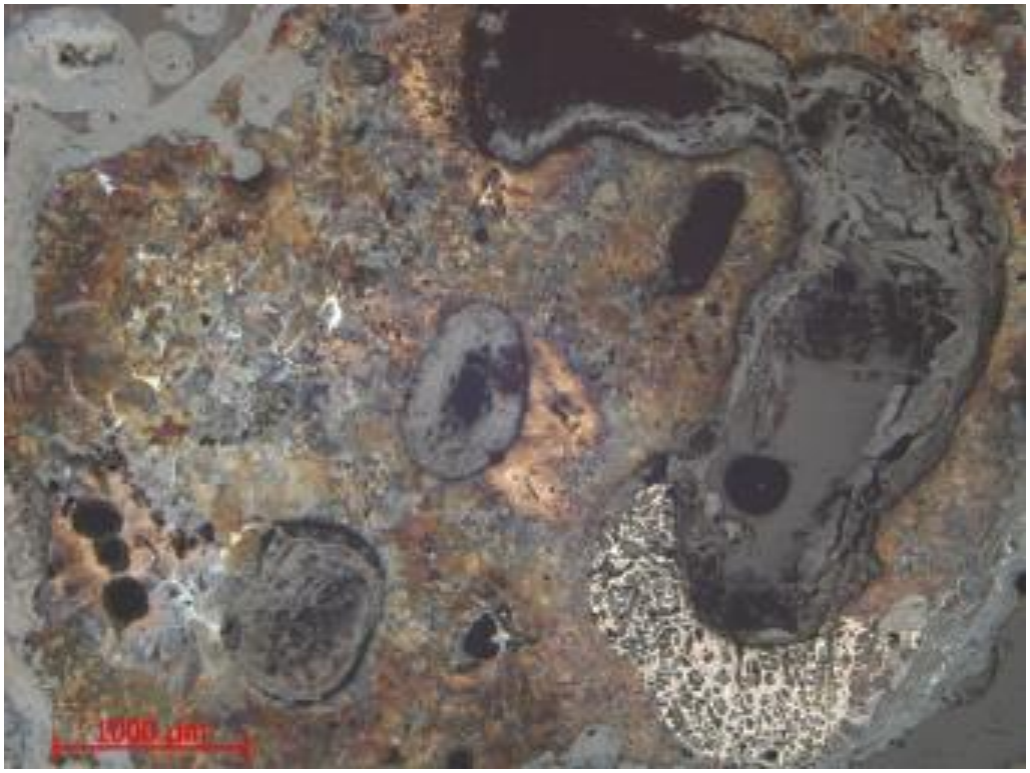

Figure S54. F629. The find consists of steel with a consistently high carbon content (blue-brown speckled areas). Micrograph of etched sample (The Archaeologists, National Historical Museums, Uppsala, Sweden).

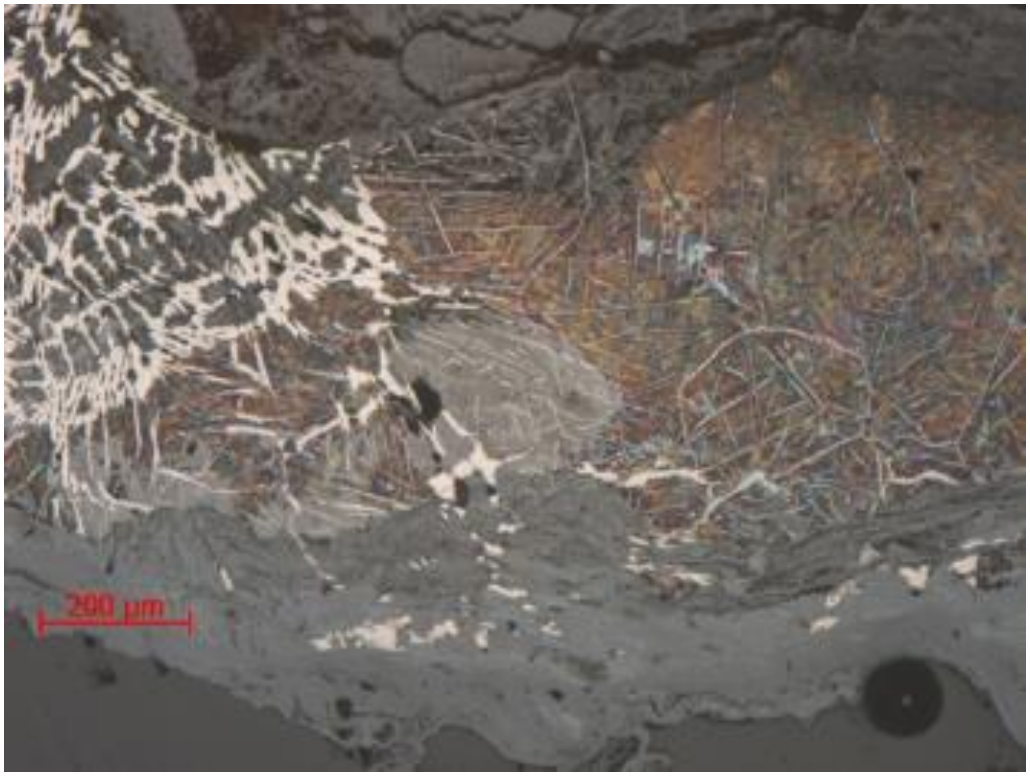

Figure S55. F256. Detail from the above. To the right pearlite with cementite in both grains and grain boundaries. To the left ledeburite. Micrograph of etched sample (The Archaeologists, National Historical Museums, Uppsala, Sweden).

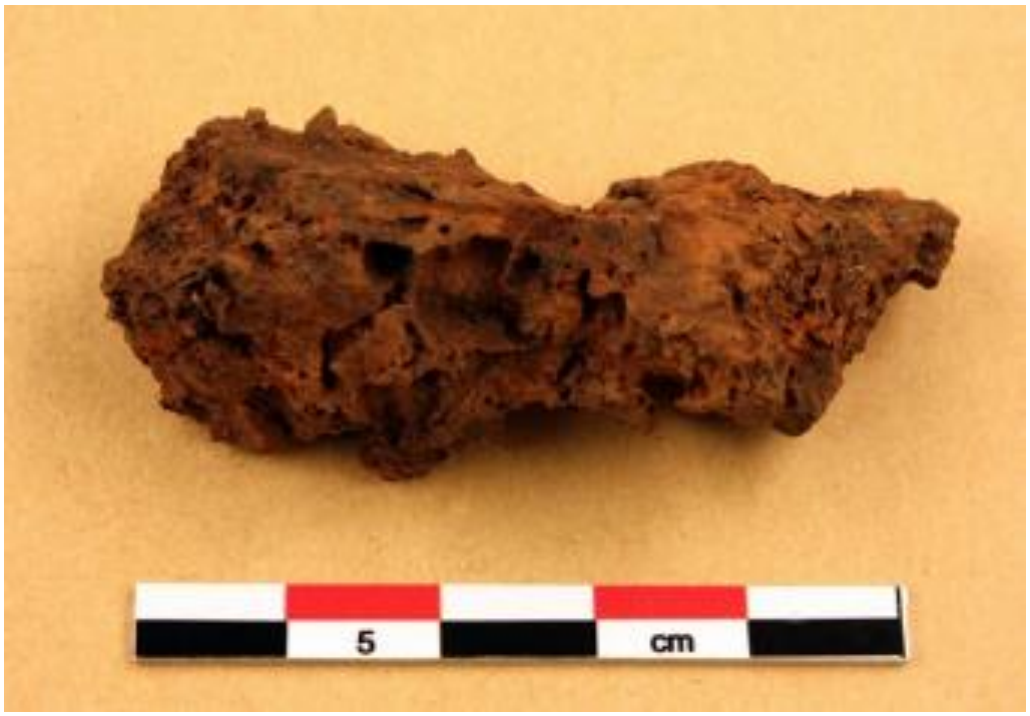

Figure S56. The irregular lump F759 (The Archaeologists, National Historical Museums, Uppsala, Sweden).

Figure S57. F759 in cross section. Concentration of metallic iron which is rather dense (The Archaeologists, National Historical Museums, Uppsala, Sweden).

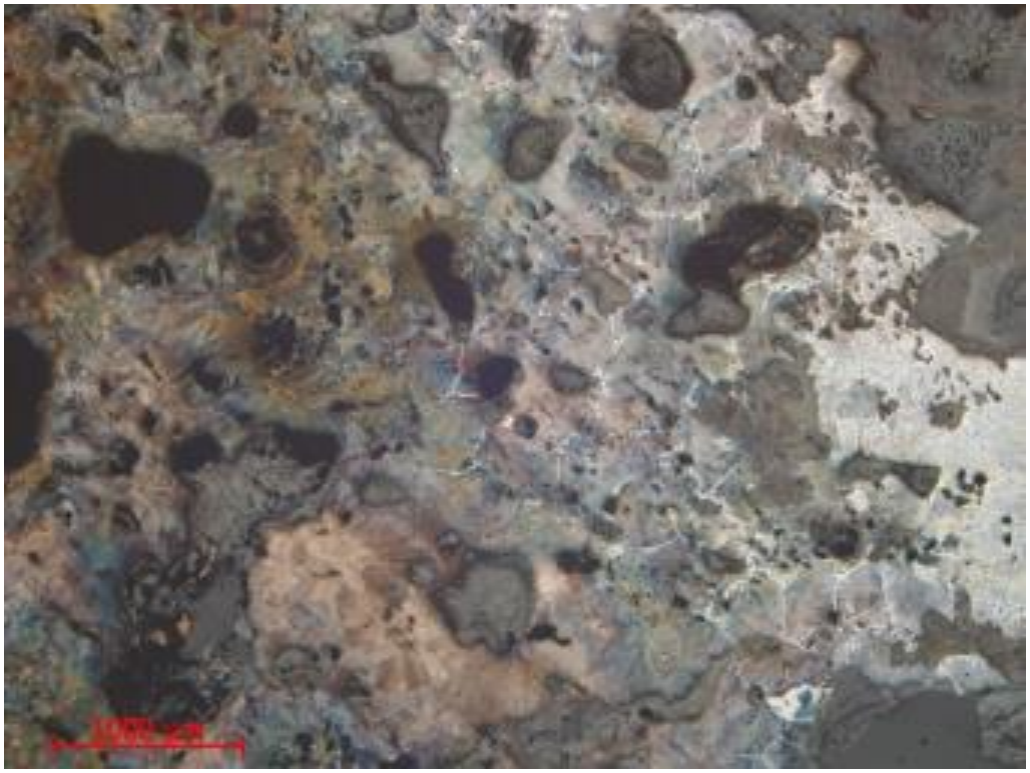

Figure S58. F759. The metal is dominated by steel with high carbon content, to the left in the picture, with locally lower carbon content as in the right-hand part. Micrograph of etched sample (The Archaeologists, National Historical Museums, Uppsala, Sweden).

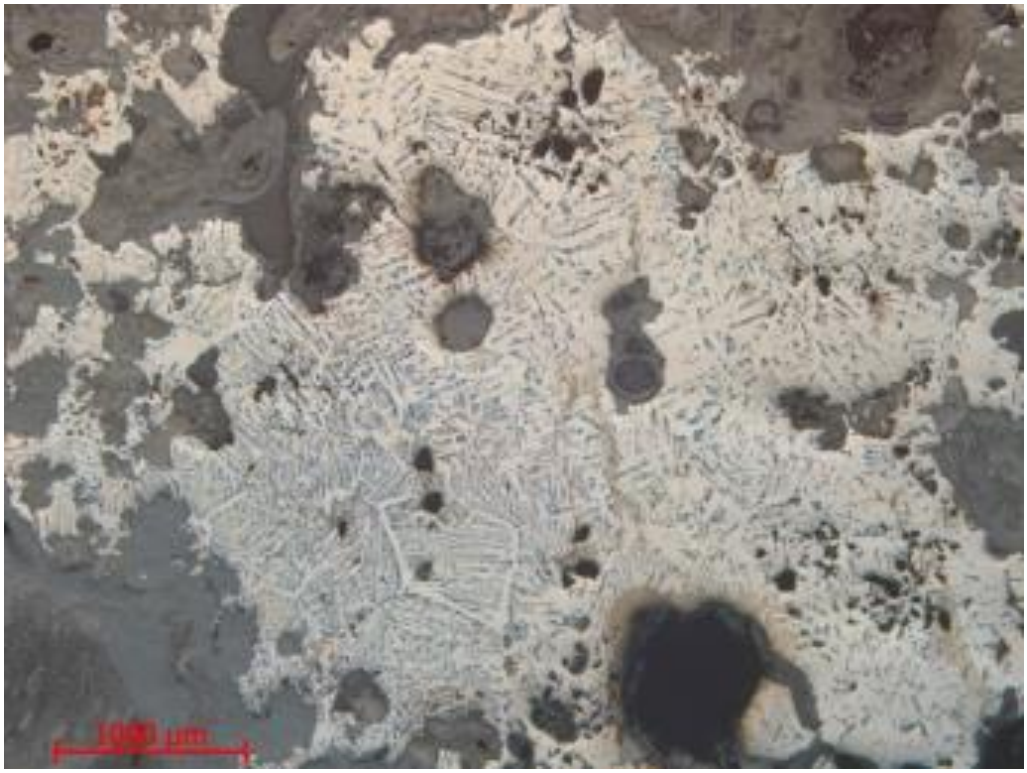

Figure S59. F833 with a coarse-grained texture with low carbon content; ferrite with a little pearlite. Micrograph of etched sample (The Archaeologists, National Historical Museums, Uppsala, Sweden).

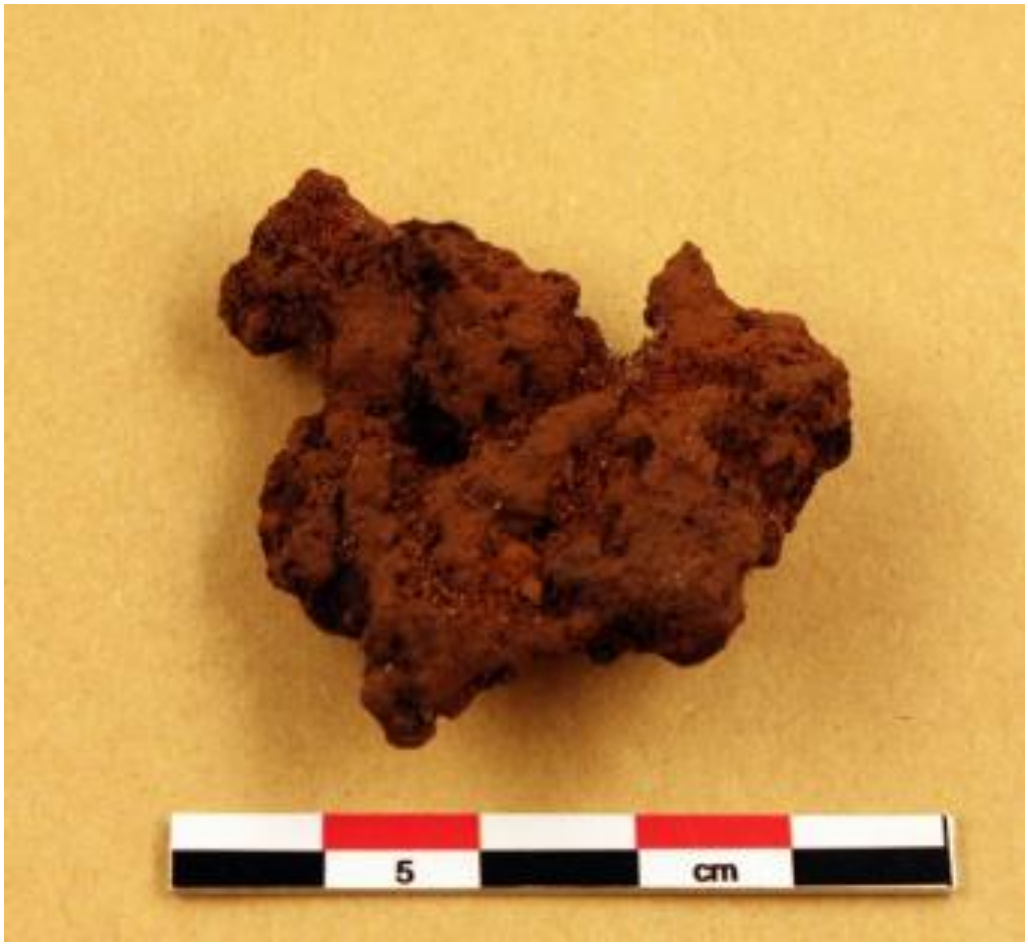

Figure S60. The iron lump Id 242 (The Archaeologists, National Historical Museums, Uppsala, Sweden).

Figure S61. Id 242, in cross section. Concentration of metallic iron (The Archaeologists, National Historical Museums, Uppsala, Sweden).

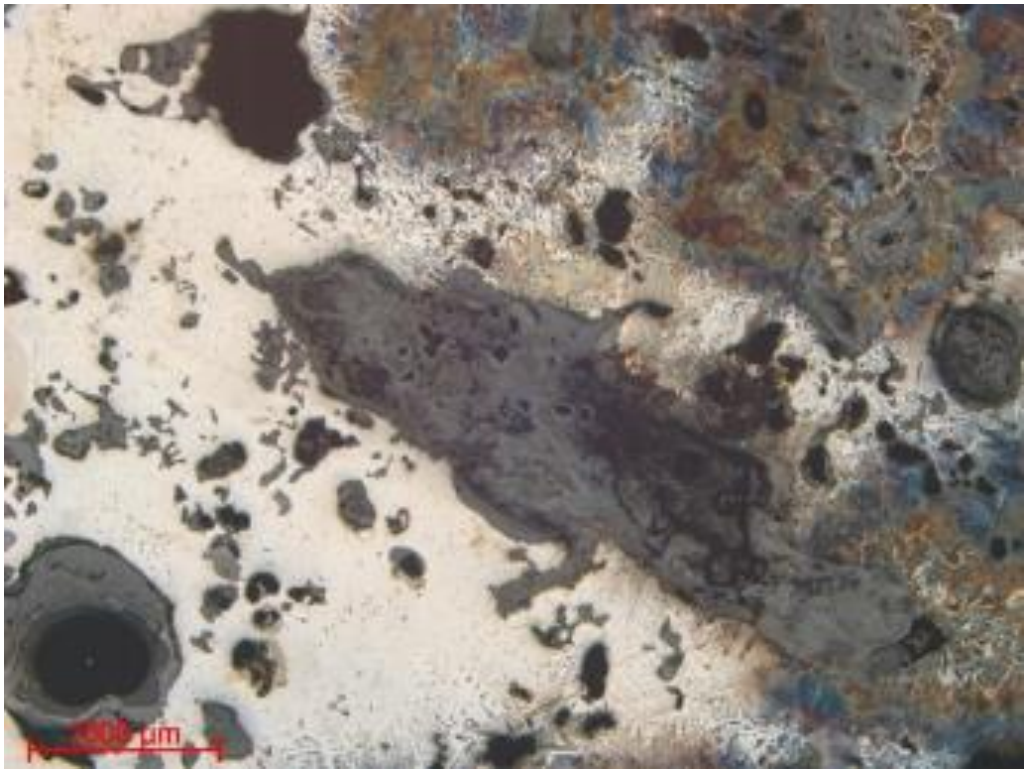

Figure S62. Id 242. To the left the dominant low-carbon ferrite is seen and to the right the less common part with higher carbon content in the steel. Micrograph of etched sample (The Archaeologists, National Historical Museums, Uppsala, Sweden).

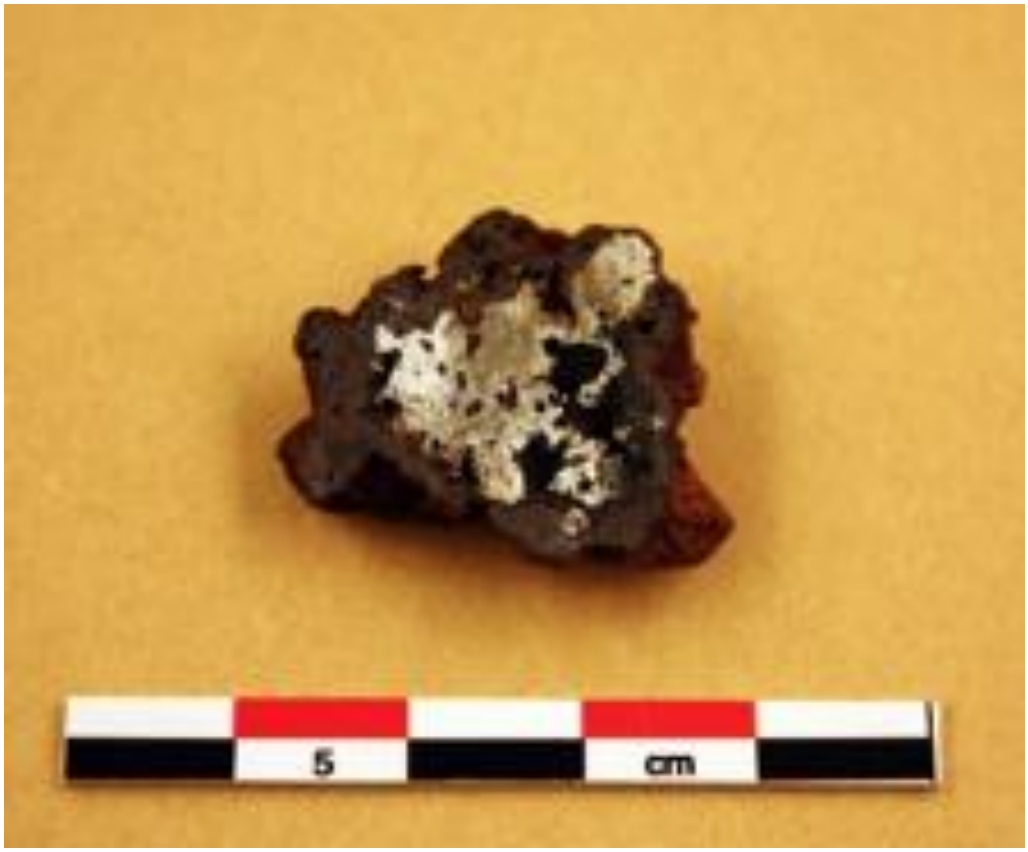

Figure S63. Id 243. Concentration of metallic iron with slag inclusions as well as cavities and corroded areas (The Archaeologists, National Historical Museums, Uppsala, Sweden).

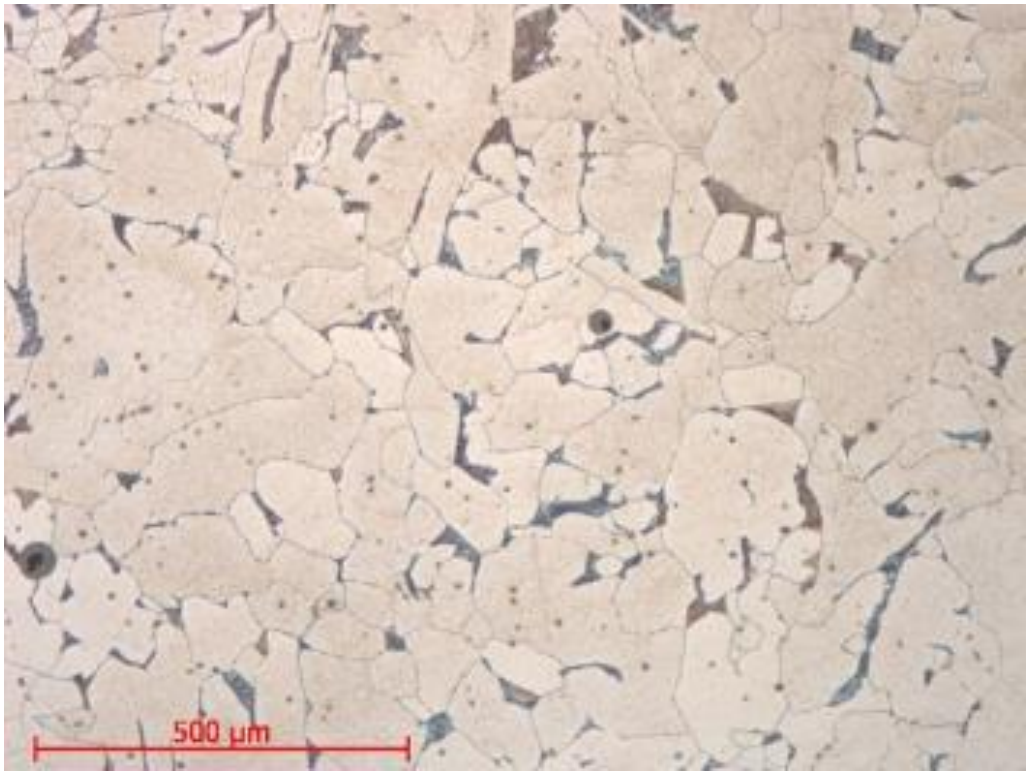

Figure S64. Id 243. The sample is dominated by ferrite, i.e., carbon-free iron. Locally there is a somewhat elevated carbon content with a little dark pearlite in the grain boundaries, which is seen in the micrograph of etched sample (The Archaeologists, National Historical Museums, Uppsala, Sweden).

Figure S65. Photo of F466 with clumps of finer-grained (clayey?) material (The Archaeologists, National Historical Museums, Uppsala, Sweden).

Figure S66. Photo of F138 with feature of coarser sand grains (The Archaeologists, National Historical Museums, Uppsala, Sweden).

Figure S67. Photo of the inside of F105 with shaped blowing hole (The Archaeologists, National Historical Museums, Uppsala, Sweden).

Figure S68. Photo of the inside of F620 with shaped blowing hole (The Archaeologists, National Historical Museums, Uppsala, Sweden).

Figure S69. Photo of F398 which appears to consist of two layers, of which the one furthest back sticks up over the front/inside layer (The Archaeologists, National Historical Museums, Uppsala, Sweden).

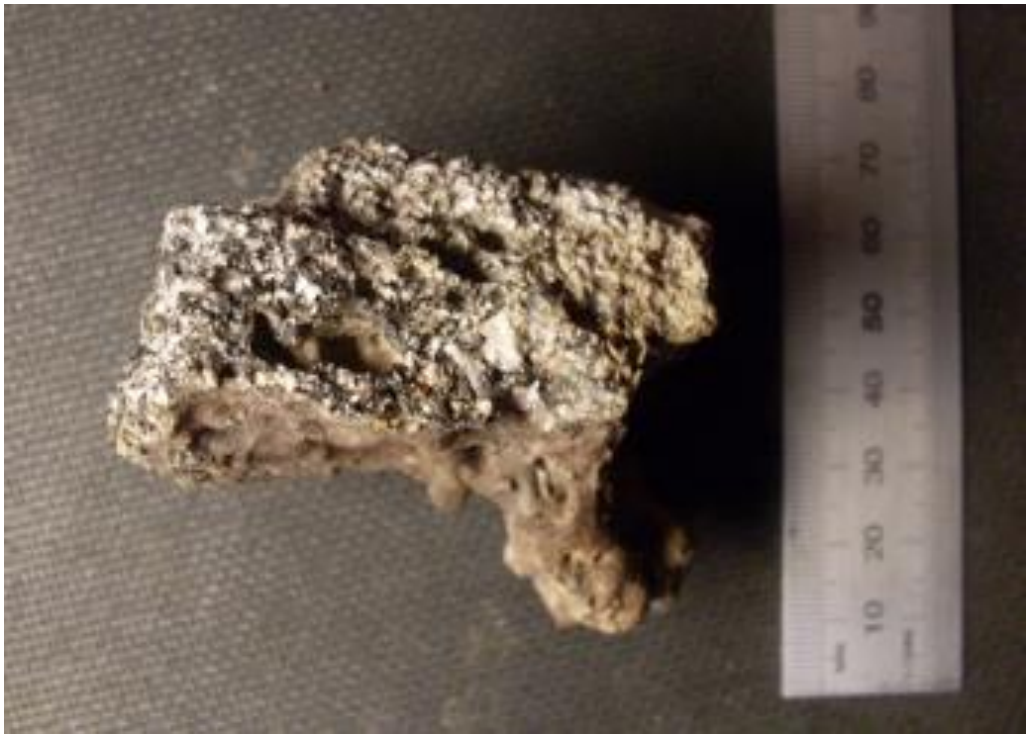

Figure S70. Photo of the profile and fracture on F622, which suggests the occurrence of two layers (The Archaeologists, National Historical Museums, Uppsala, Sweden).

Figure S71. Photo of cross section of F398 (TS 1) (The Archaeologists, National Historical Museums, Uppsala, Sweden).

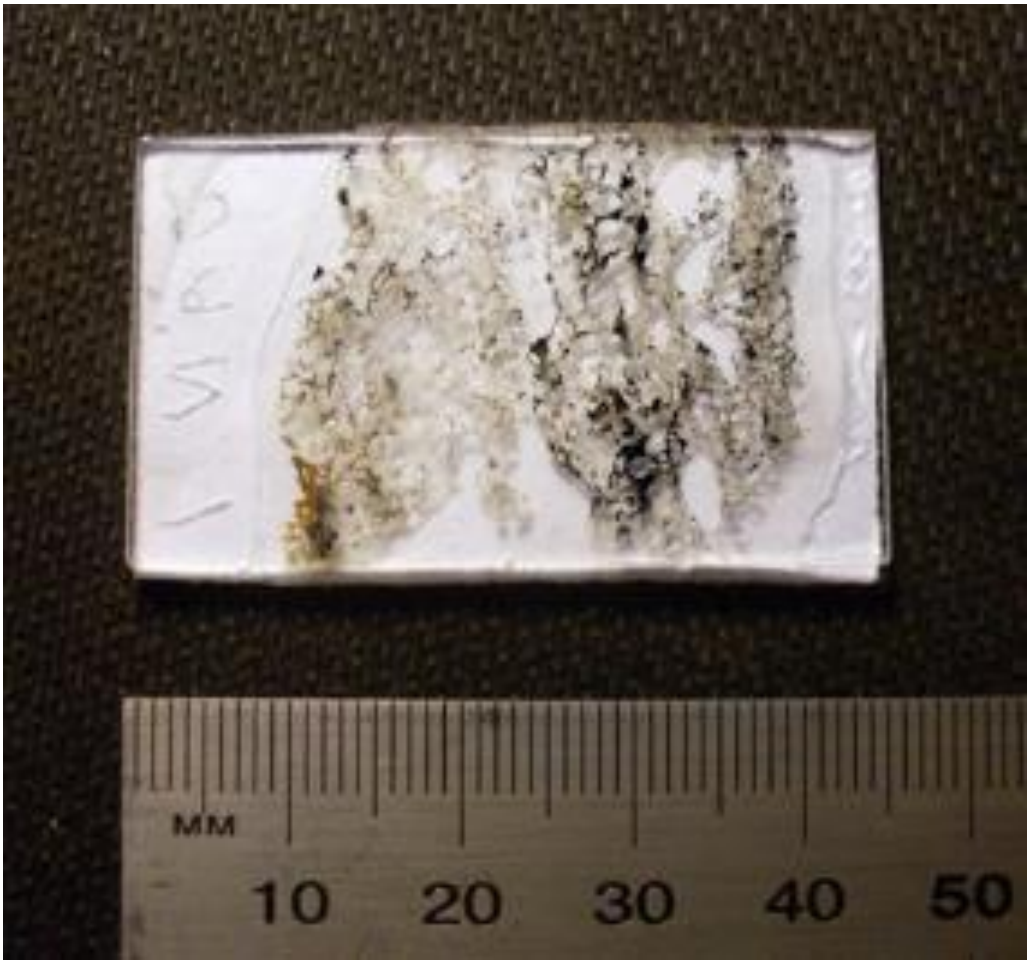

Figure S72. Photo of the TS1 specimen (F398) which indicates the occurrence of vitrified layer with slag inclusions on the "inside" of both layers. The inside of the furnace is to the left (The Archaeologists, National Historical Museums, Uppsala, Sweden).

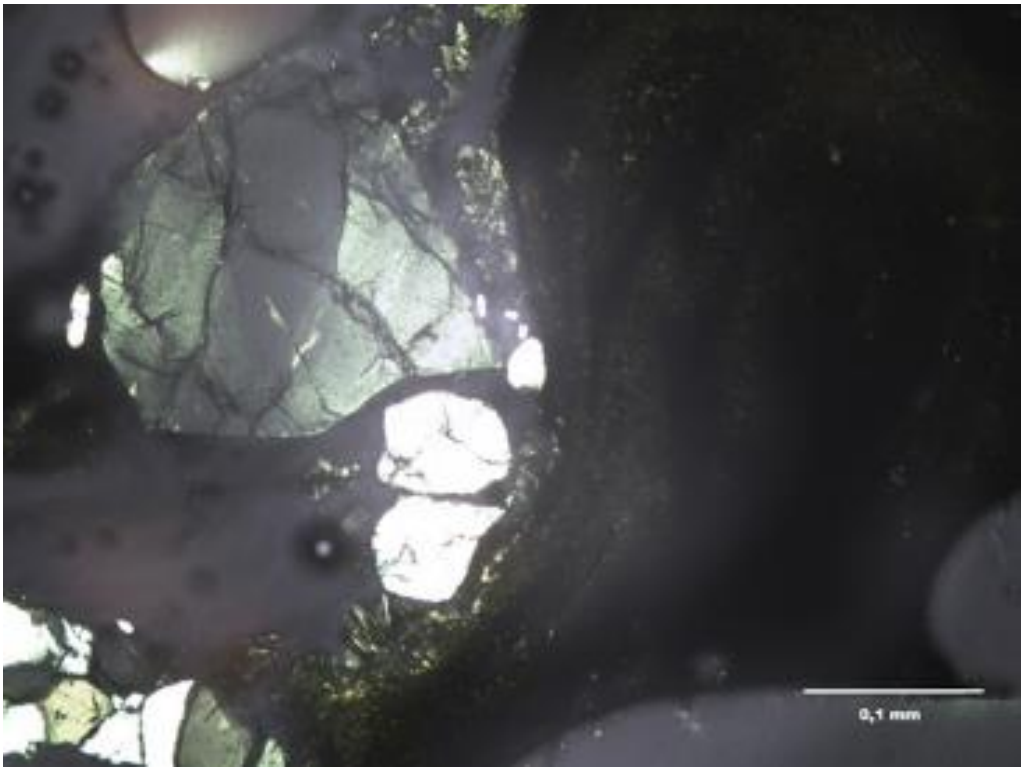

Figure S73. Microscope photo of area with brown-black, granular slag inclusions in outer/primary layer on F398 (The Archaeologists, National Historical Museums, Uppsala, Sweden).

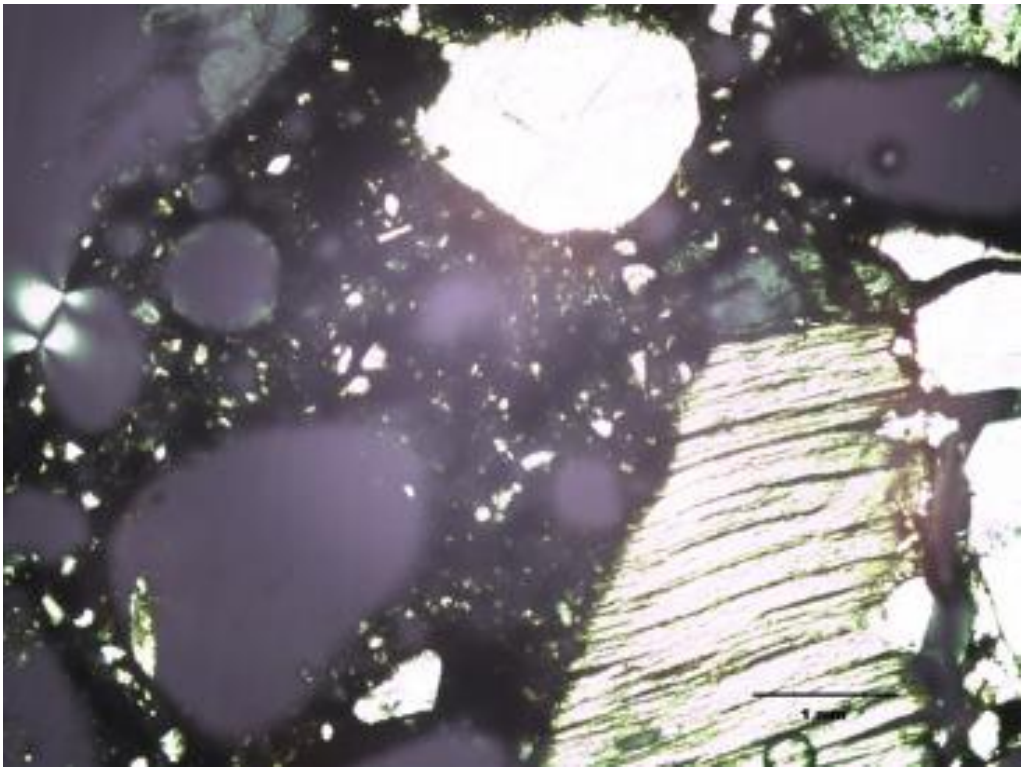

Figure S74. Microscope photo of the material in outer/primary layer on F398 (The Archaeologists, National Historical Museums, Uppsala, Sweden).

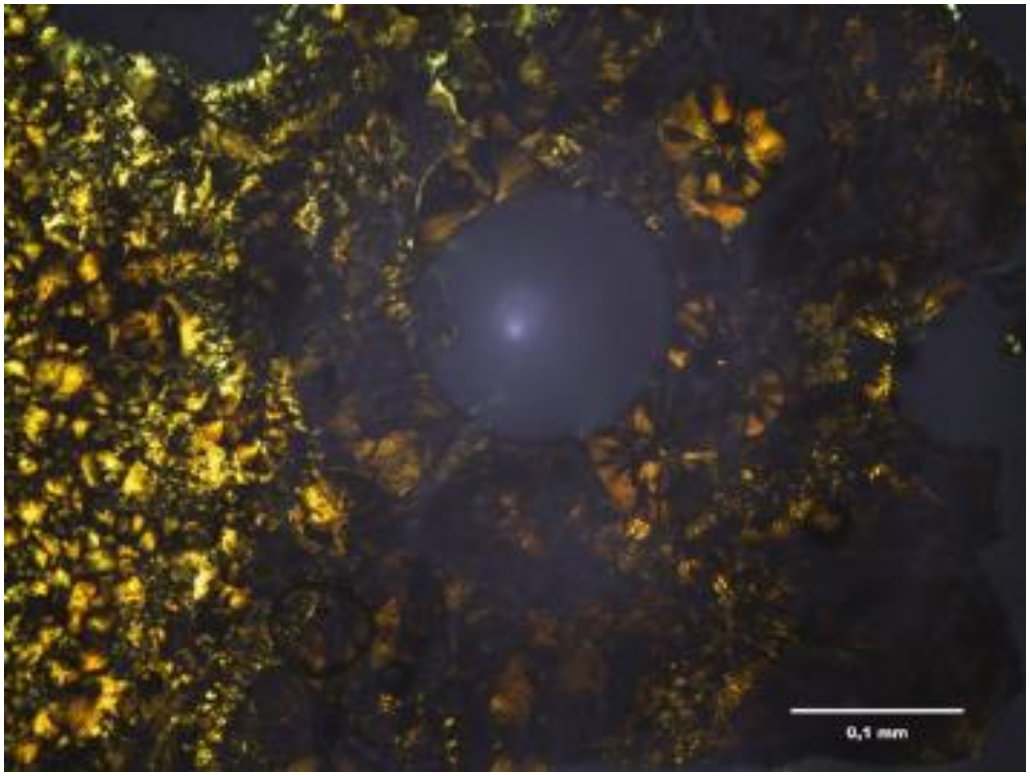

Figure S75. Microscope photo of vitrified area with slag inclusions in inner/later layer on F398 (The Archaeologists, National Historical Museums, Uppsala, Sweden).

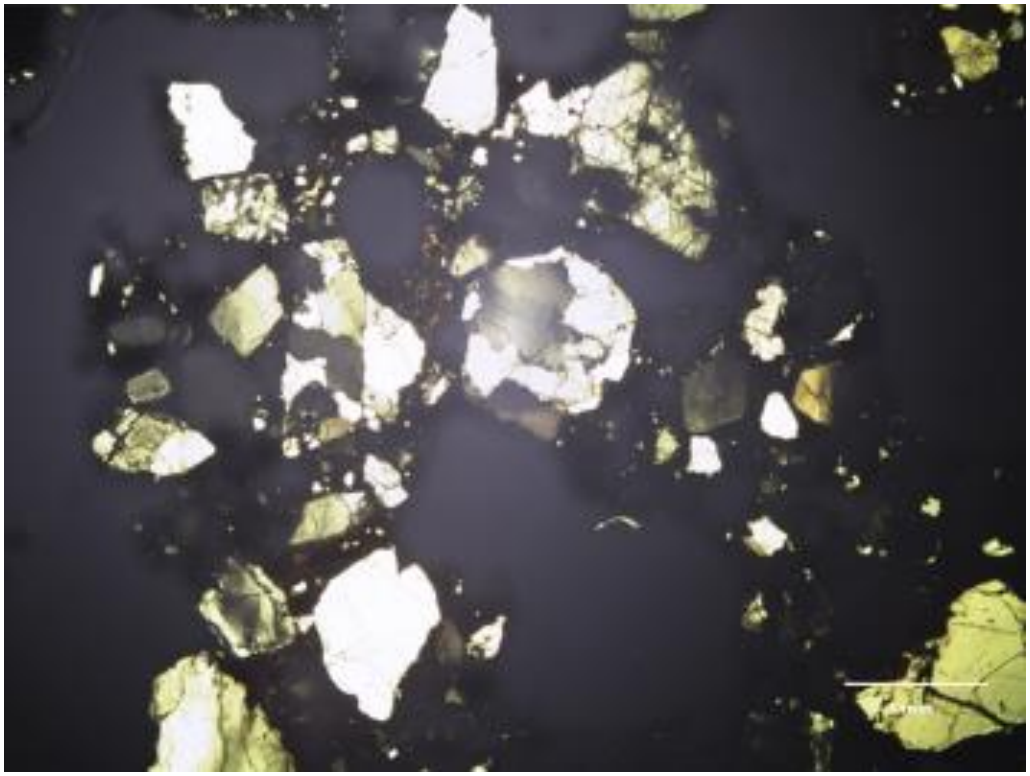

Figure S76. Microscope photo of the material in inner/later layer on F398 (The Archaeologists, National Historical Museums, Uppsala, Sweden).

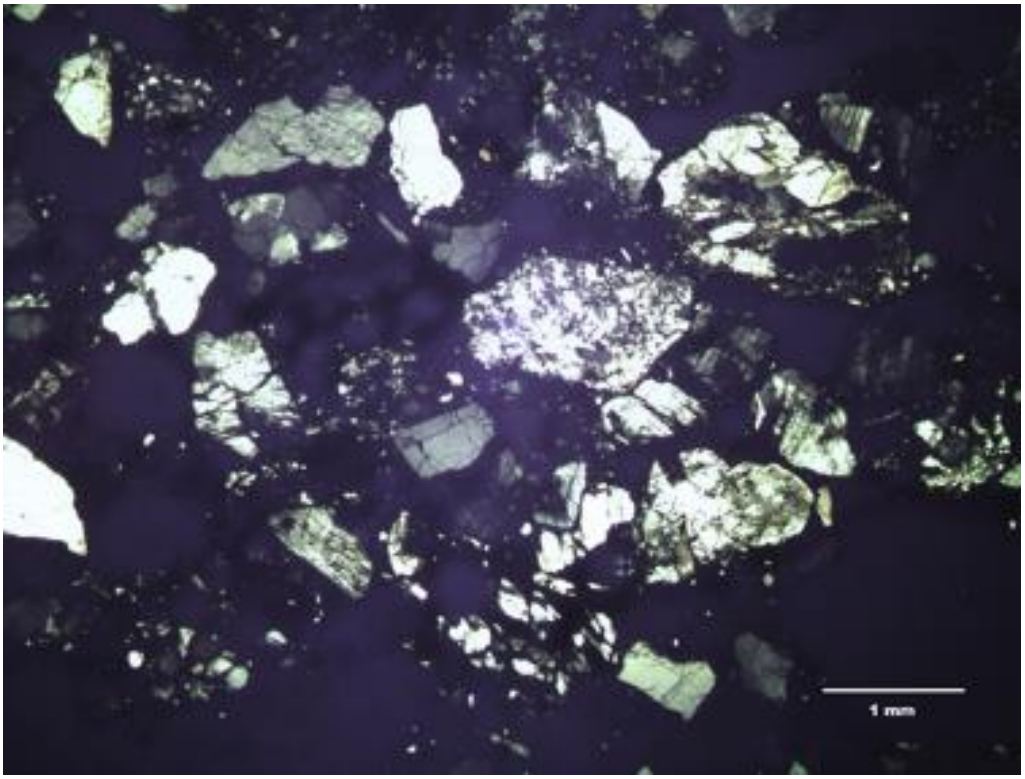

Figure S77. Microscope photo of the material in F620 (TS2) (The Archaeologists, National Historical Museums, Uppsala, Sweden).

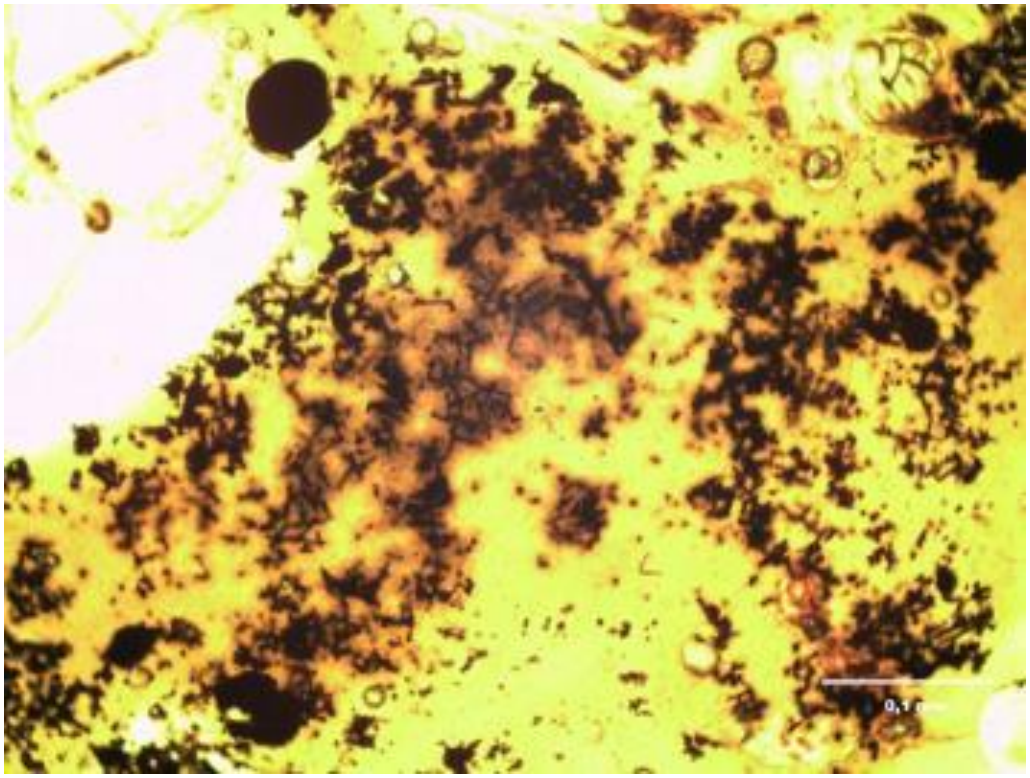

FigureS78. Microscope photo of vitrified area with slag inclusions on the inside of F620 (TS2) (The Archaeologists, National Historical Museums, Uppsala, Sweden).

Figure S79. Slag 1676 from slag heap in furnace area 2. Charcoal imprint, moderately porous, has not flowed (*The Archaeologists, National Historical Museums, Uppsala, Sweden*).

Figure S80. Slag 1809 from slag heap in furnace area 2. Stearin slag, cemented sand below, relatively dense (*The Archaeologists, National Historical Museums, Uppsala, Sweden*).

Figure S81. Slag id 2616 from the furnace chamber in furnace area 2. Small pieces of stearin slag (*The Archaeologists, National Historical Museums, Uppsala, Sweden*).

Figure S82. Slag id 2825 from slag heap in furnace area 2. Stearin slag, cemented sand below, moderately porous (*The Archaeologists, National Historical Museums, Uppsala, Sweden*).

Figure S83. Iron id 2347 from slag heap in furnace area 2 (*The Archaeologists, National Historical Museums, Uppsala, Sweden*).

Figure S84. Iron id 392 from slag heap in furnace area 2 (*The Archaeologists, National Historical Museums, Uppsala, Sweden*).

Figure S85. Ore id 688 (bog-iron ore of cake type?) from ca 2.5m NE of the furnace in area 2 (*The Archaeologists, National Historical Museums, Uppsala, Sweden*).

Figure S86. Slag id 1973 from slag heap in furnace area 3. Low viscosity, charcoal imprint, relatively dense (*The Archaeologists, National Historical Museums, Uppsala, Sweden*).

Figure S87. Slag id 2398 from slag heap in furnace area 3. Low viscosity, charcoal imprint, relatively dense (*The Archaeologists, National Historical Museums, Uppsala, Sweden*).

Figure S88. Slag id 2854 from the furnace chamber in area 3. Stearin slag, charcoal imprint, relatively dense (*The Archaeologists, National Historical Museums, Uppsala, Sweden*).

Figure S89. Slag id 2861 from the furnace chamber in furnace area 3. Scattered charcoal imprint, porous, has flowed (*The Archaeologists, National Historical Museums, Uppsala, Sweden*).

Figure S90. Iron id 1759 from slag heap in furnace area 3 (*The Archaeologists, National Historical Museums, Uppsala, Sweden*).

Figure S91. Iron id 2942 from slag heap in furnace area 3 (*The Archaeologists, National Historical Museums, Uppsala, Sweden*).

Figure S92. Ore id 2382 (coin type) from about 4.5 m NW of the furnace in area 3 (*The Archaeologists, National Historical Museums, Uppsala, Sweden*).

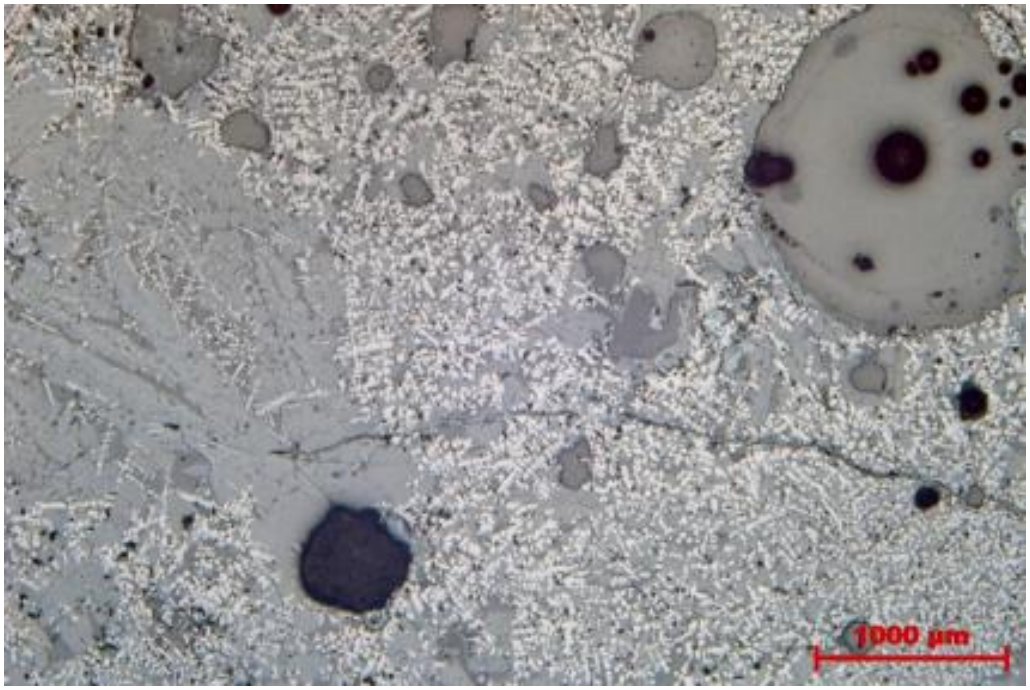

Figure S93. Slag sample id 1676 in low magnification. Several rounded pores are present in the slag, which is dominated by light wüstite and grey olivine. Some areas (flows of slag?) are seen to have only a little of the light wüstite, see left in picture (The Archaeologists, National Historical Museums, Uppsala, Sweden).

Figure S94. Slag id 1676 in higher magnification where the light wüstite is observed to grow dendritic across both the grey olivine and the dark intermediate matrix of glass (The Archaeologists, National Historical Museums, Uppsala, Sweden).

Figure S95. Slag id 1676 with metallic iron, here white, is observed mainly as very small drops at the outer edge of the piece of slag, which here consists of light-grey rust (The Archaeologists, National Historical Museums, Uppsala, Sweden).

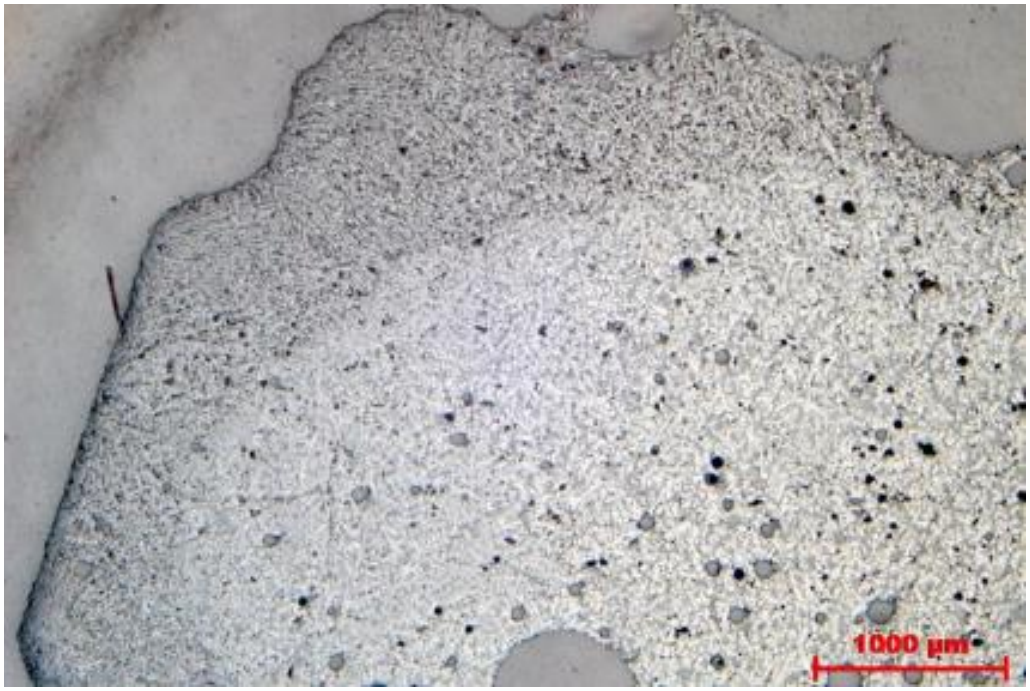

Figure S96. Slag id 1809 in low magnification, clearly showing how the light wüstite dominates (The Archaeologists, National Historical Museums, Uppsala, Sweden).

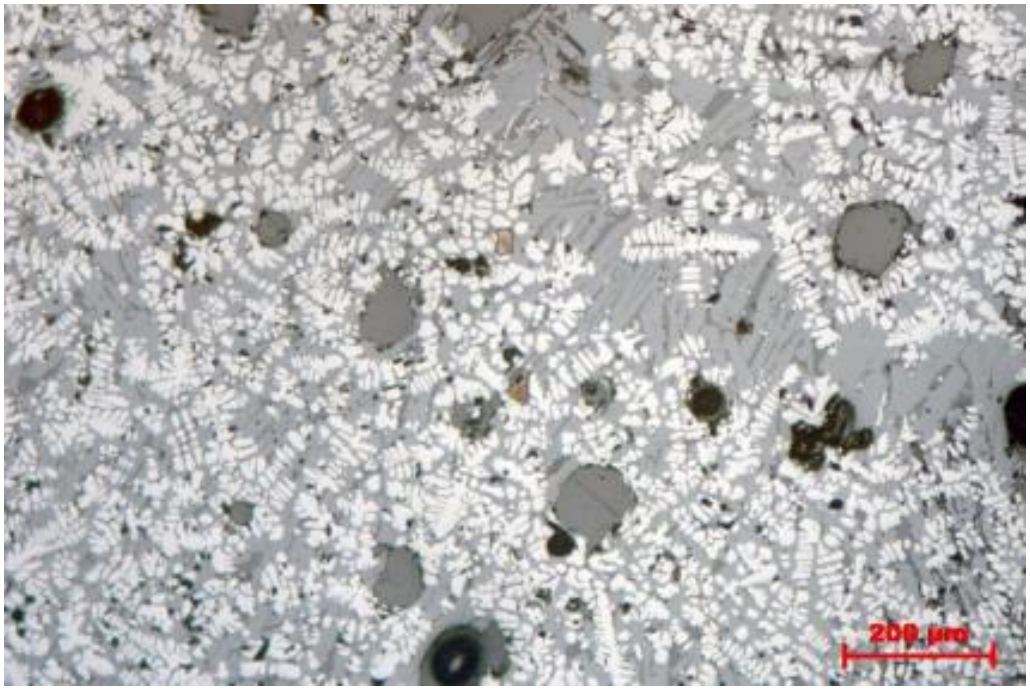

Figure S97. Slag id 1809 in high magnification where the light wüstite is seen to grow dendritic over both grey olivine crystals and the intermediate darker glass phase (The Archaeologists, National Historical Museums, Uppsala, Sweden).

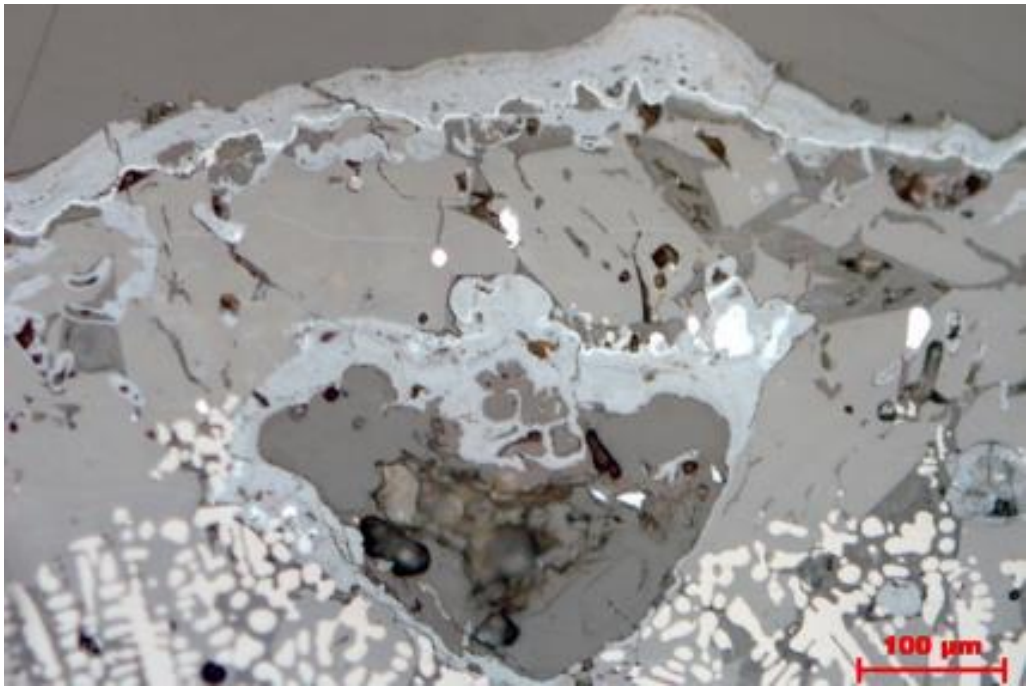

Figure S98. Outer edge of slag id 1809 in very high magnification where scattered white metallic iron drops can be observed. Note how the light wüstite is lacking in areas closest to the surface, which is ultimately covered by light grey rust/iron hydroxide. This may be due to high presence of oxygen at the formation of the slag (The Archaeologists, National Historical Museums, Uppsala, Sweden).

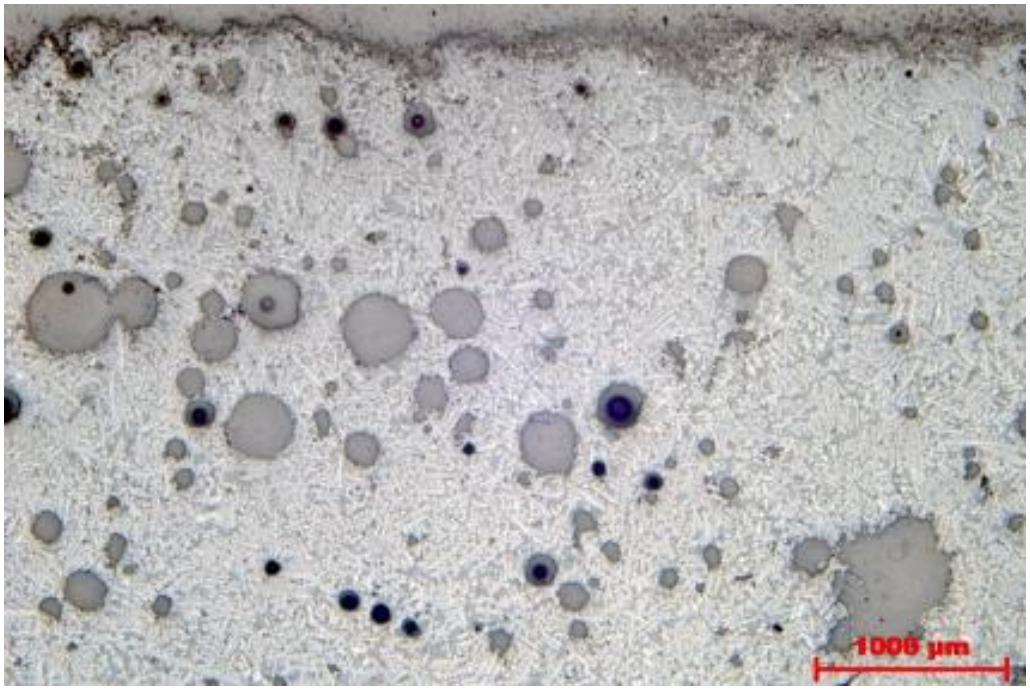

Figure S99. Slag id 2616 is very fine-grained and homogeneous and relatively rich in small pores. Light wüstite dominates (The Archaeologists, National Historical Museums, Uppsala, Sweden).

Figure S100. Slag id 2616 where light wüstite grows dendritic over grey olivine laminae and intermediate dark residual molten mass of glass (The Archaeologists, National Historical Museums, Uppsala, Sweden).

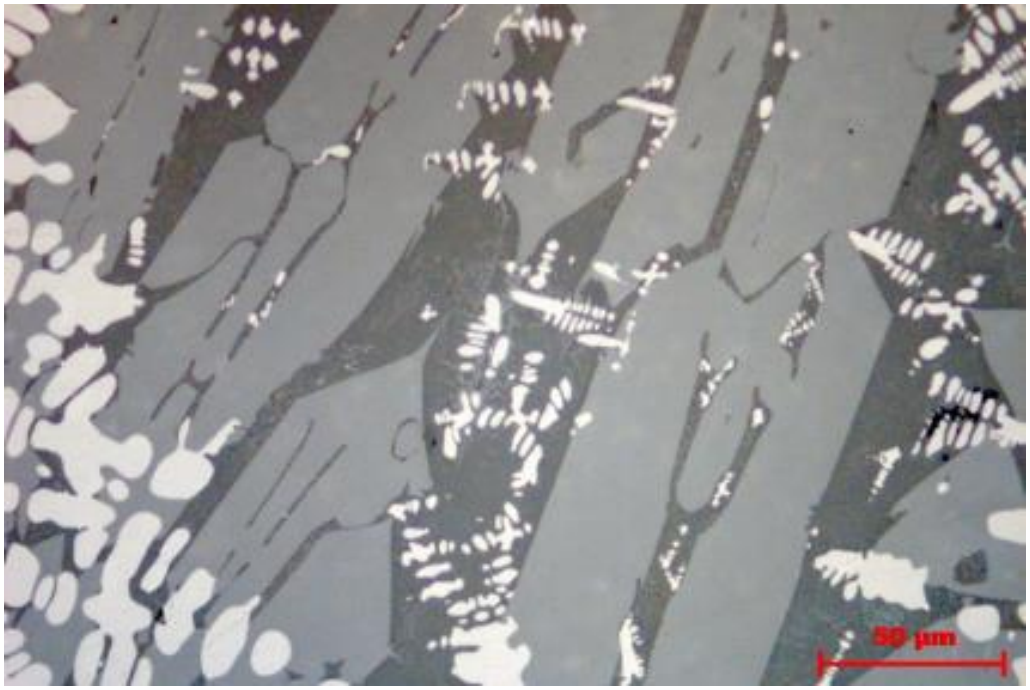

Figure S101. Slag sample id 2616 in very high magnification where the dark residual molten mass of glass is seen to contain microcrystals of lighter olivine (The Archaeologists, National Historical Museums, Uppsala, Sweden).

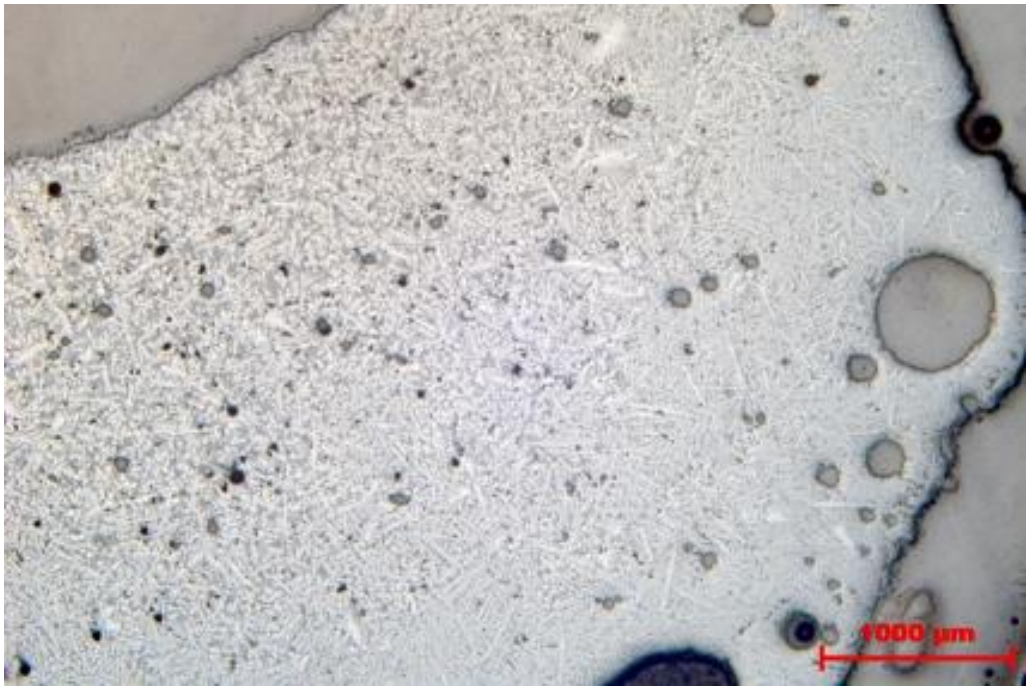

Figure S102. Slag id 2825 is a very fine-grained and homogeneous slag with few pores. It can be seen that the grain size becomes smaller from the upper part of the picture down to the right, due to cooling of the slag. Light wüstite dominates (The Archaeologists, National Historical Museums, Uppsala, Sweden).

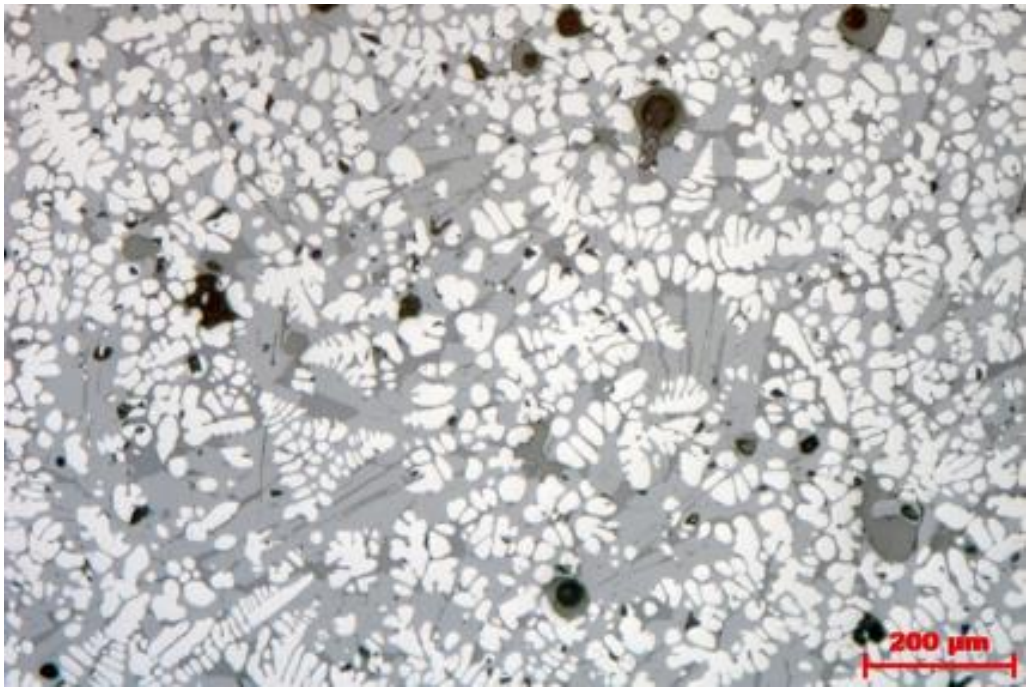

Figure S103. Light wüstite dominates slag id 2825, which grows dendritic over grey olivine crystals and the dark intermediate residual melt of glass (The Archaeologists, National Historical Museums, Uppsala, Sweden).

Figure S104. Slag id 2825 in high magnification. Sparse metallic iron is perceived as very small white drops, mainly close to the surface of the slag. The presence of light wüstite decreases next to the surface of the slag, where instead grey olivine crystals and dark glass dominate (The Archaeologists, National Historical Museums, Uppsala, Sweden).

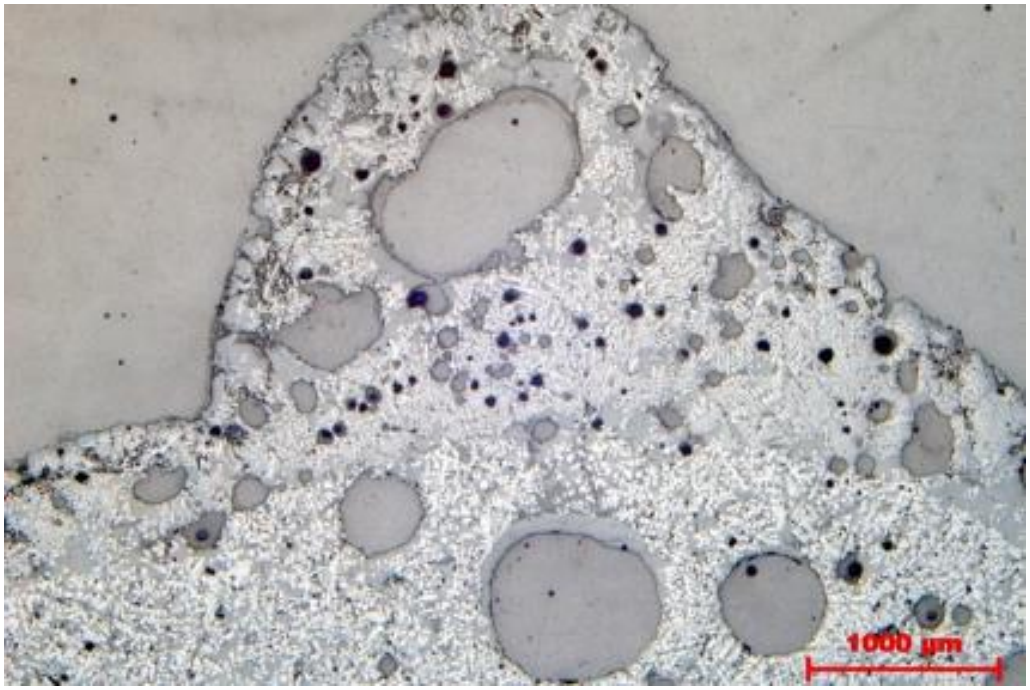

Figure S105. Slag id 1973 is relatively porous and is observed here to consist of two flows with somewhat different composition (The Archaeologists, National Historical Museums, Uppsala, Sweden).

Figure S106. Slag id 1973 in high magnification. It shows how the light wüstite grows dendritic over both the grey olivine laminae and the dark intermediate matrix, which probably consists of glass (The Archaeologists, National Historical Museums, Uppsala, Sweden).

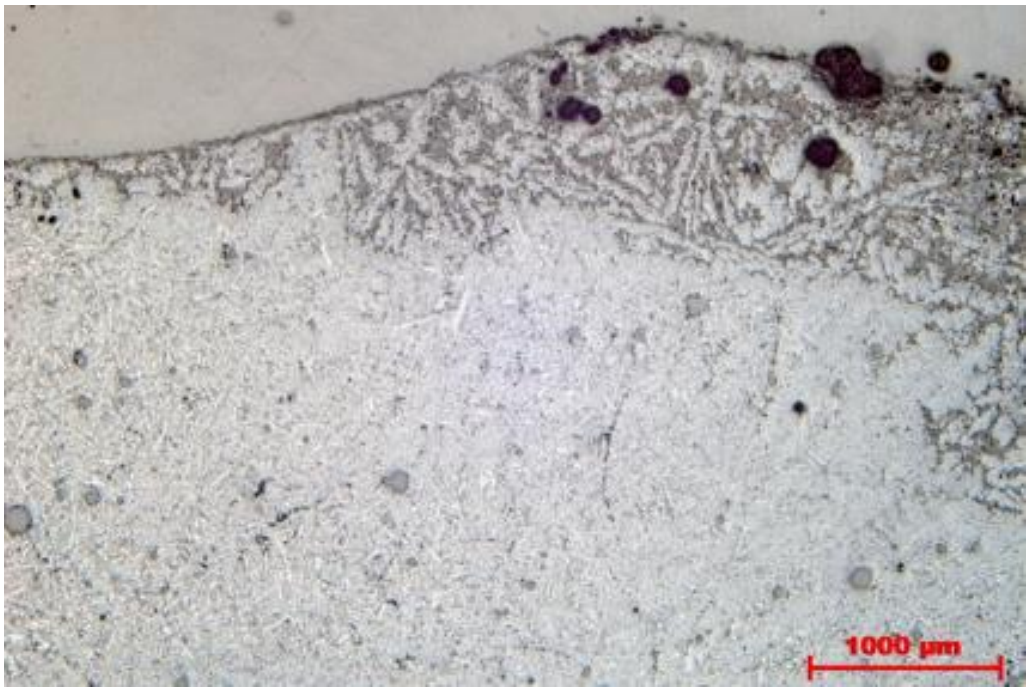

Figure S107. Slag id 2398 in low magnification where the light wüstite dominates, except in certain parts of the outer edge of the slag, which is weathered. The slag has relatively few pores (The Archaeologists, National Historical Museums, Uppsala, Sweden).

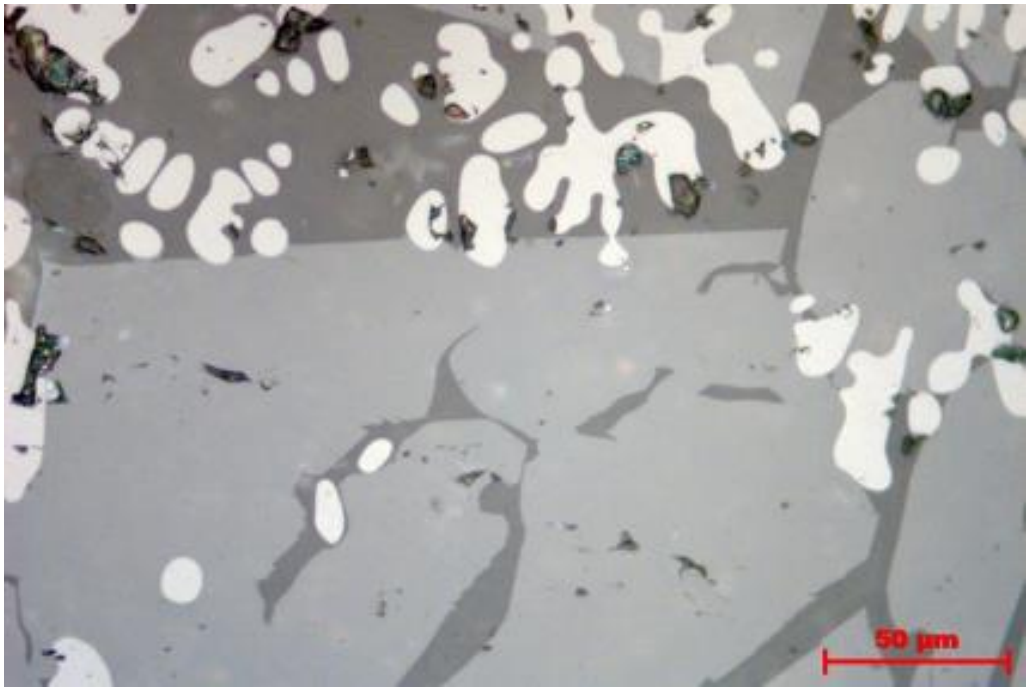

Figure S108. In very high magnification of slag sample id 2398 light, partly dendritic wüstite, grey olivine and dark intermediate residual melt of glass are seen (The Archaeologists, National Historical Museums, Uppsala, Sweden).

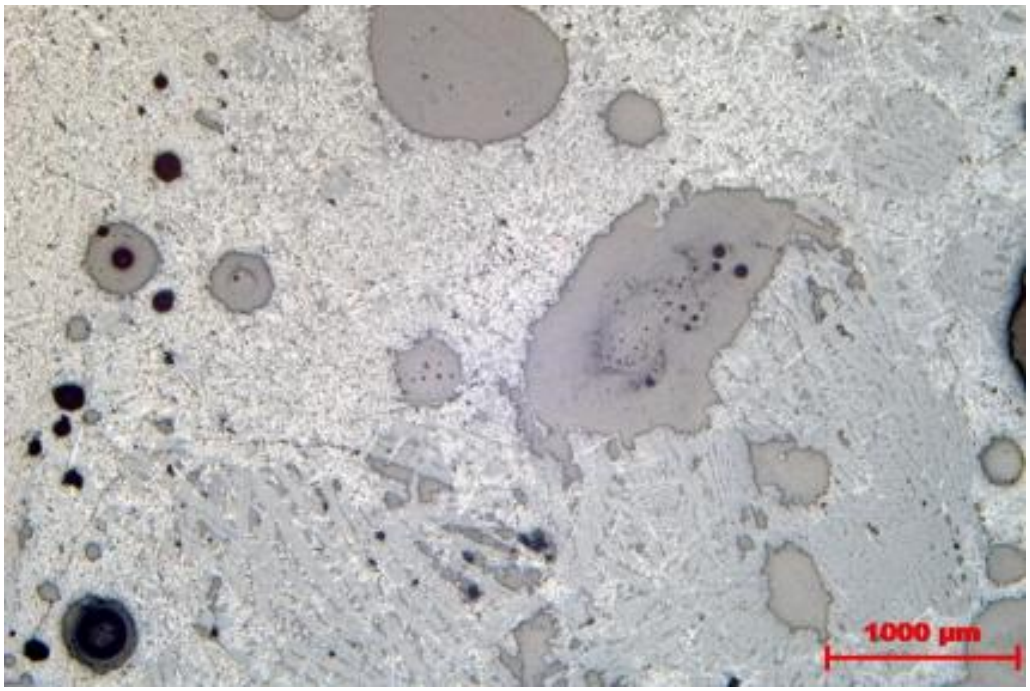

Figure S109. Id 2854. The fine-grained and porous slag is usually dominated by light wüstite (upper left half of the picture), but darker areas/flows with smaller quantity of wüstite can also be seen (lower right portion) (The Archaeologists, National Historical Museums, Uppsala, Sweden).

Figure S110. Id 2854. In higher magnification the dendritic light wüstite is seen to grow over both grey olivine and dark glass (The Archaeologists, National Historical Museums, Uppsala, Sweden).

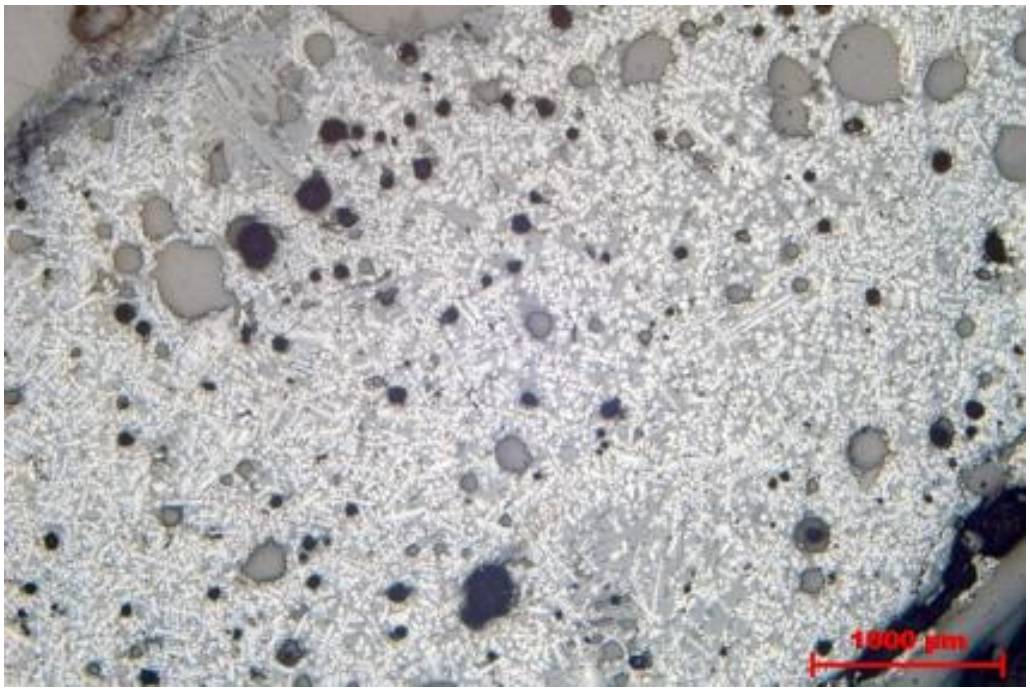

Figure S111. Id 2861. In low magnification it is seen how the light wüstite dominates the slag with small pores (The Archaeologists, National Historical Museums, Uppsala, Sweden).

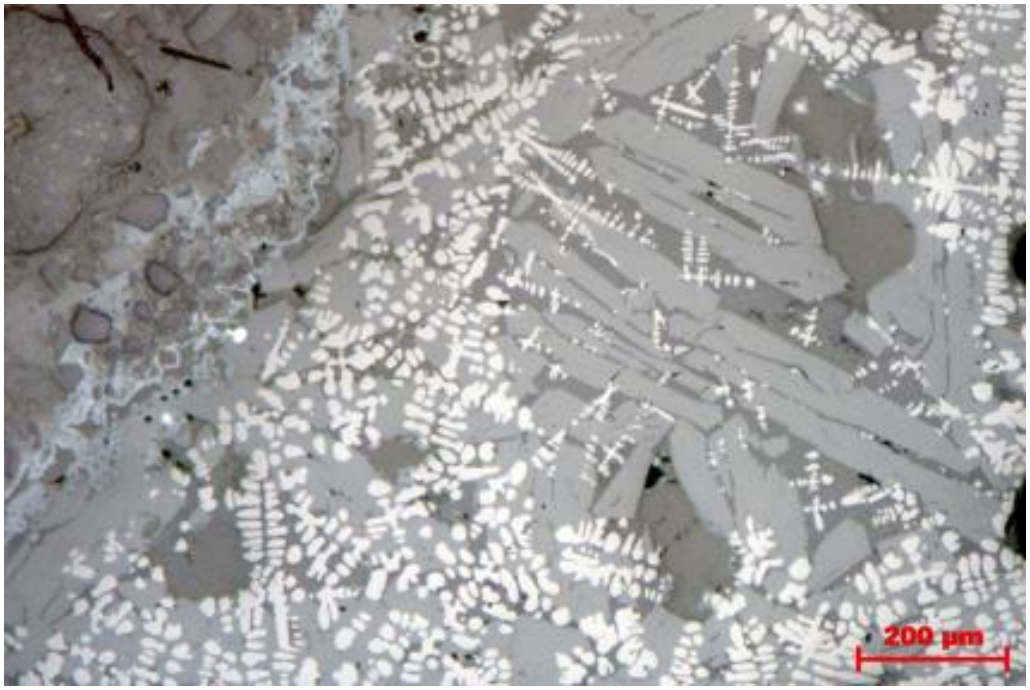

Figure S112. Id 2861. In higher magnification it is observed how the light wüstite grows dendritic over both grey olivine laminae and dark glass. Very small white iron drops can be perceived near the surface of the slag (left in the picture) (The Archaeologists, National Historical Museums, Uppsala, Sweden).

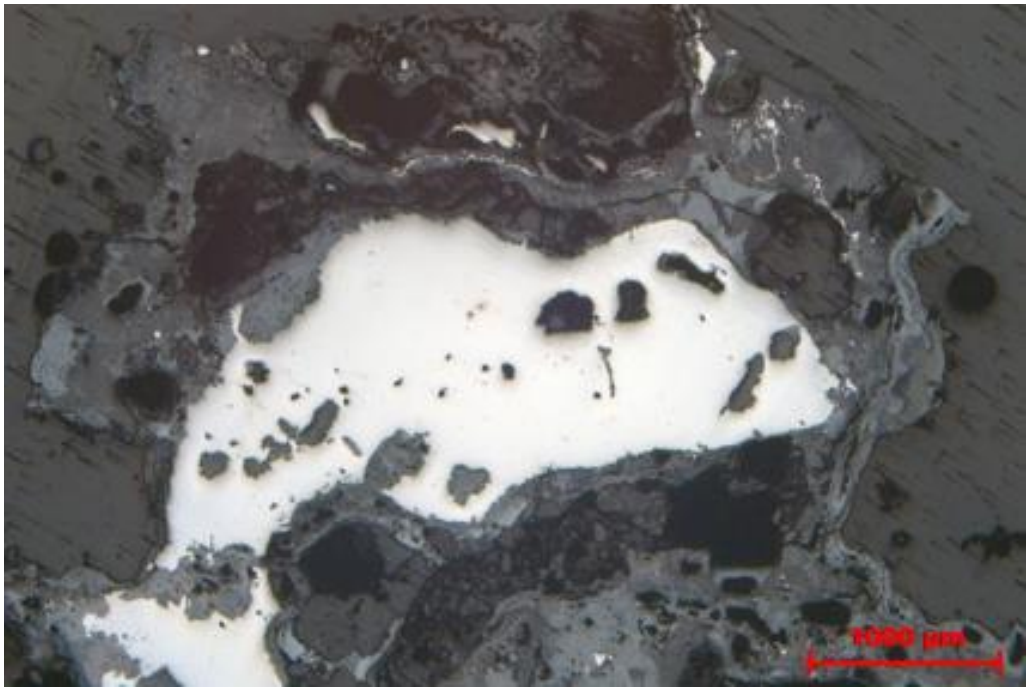

Figure S113. The polished iron sample id 2347 from furnace area 2 is seen to be corroded and with few slag inclusions, which are only seen as scattered irregular inclusions (The Archaeologists, National Historical Museums, Uppsala, Sweden).

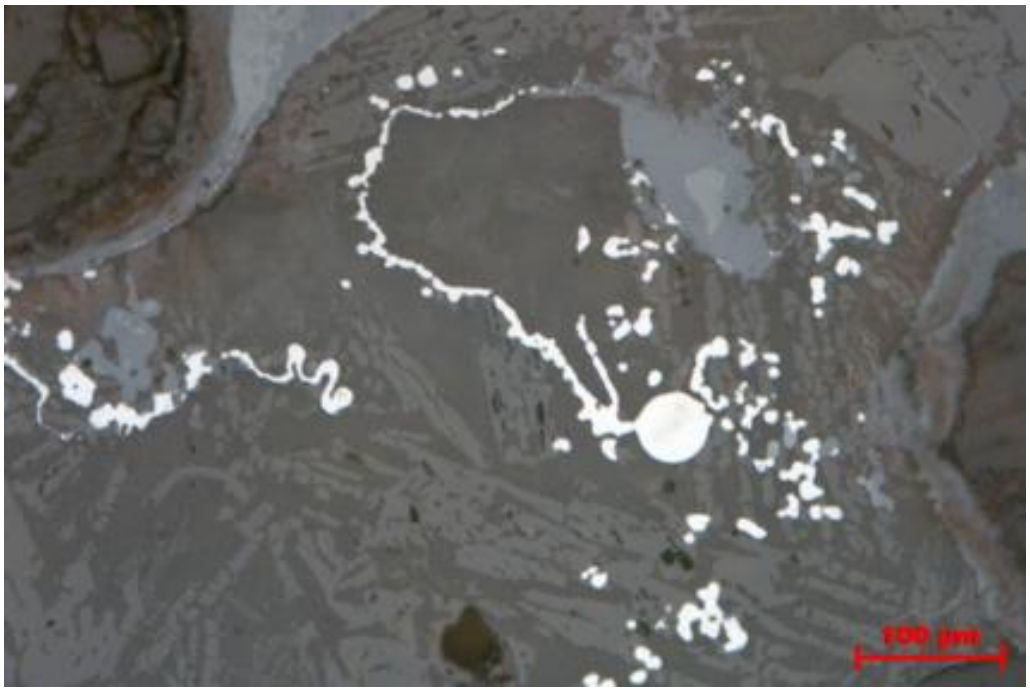

Figure S114. Iron sample id 2347 in high magnification. In the slag located outside the main piece of iron thin strips of metallic iron are seen (The Archaeologists, National Historical Museums, Uppsala, Sweden).

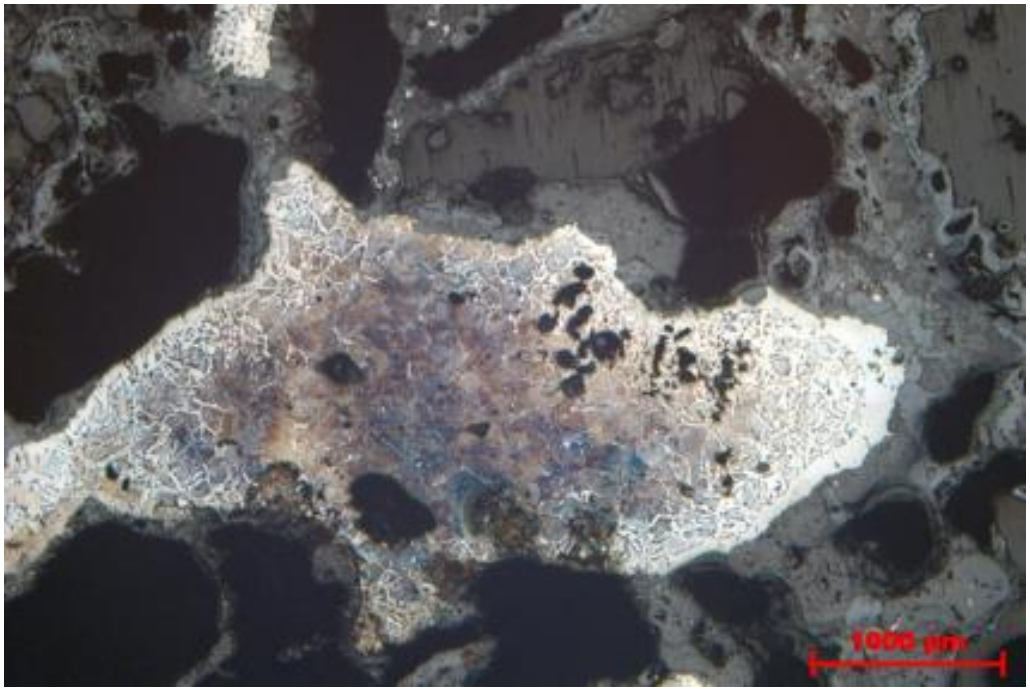

Figure S115. Iron sample id 2347 after etching. The dark pearlite demonstrates a high carbon content, which however is seen to decrease toward the outer edge of the iron (The Archaeologists, National Historical Museums, Uppsala, Sweden).

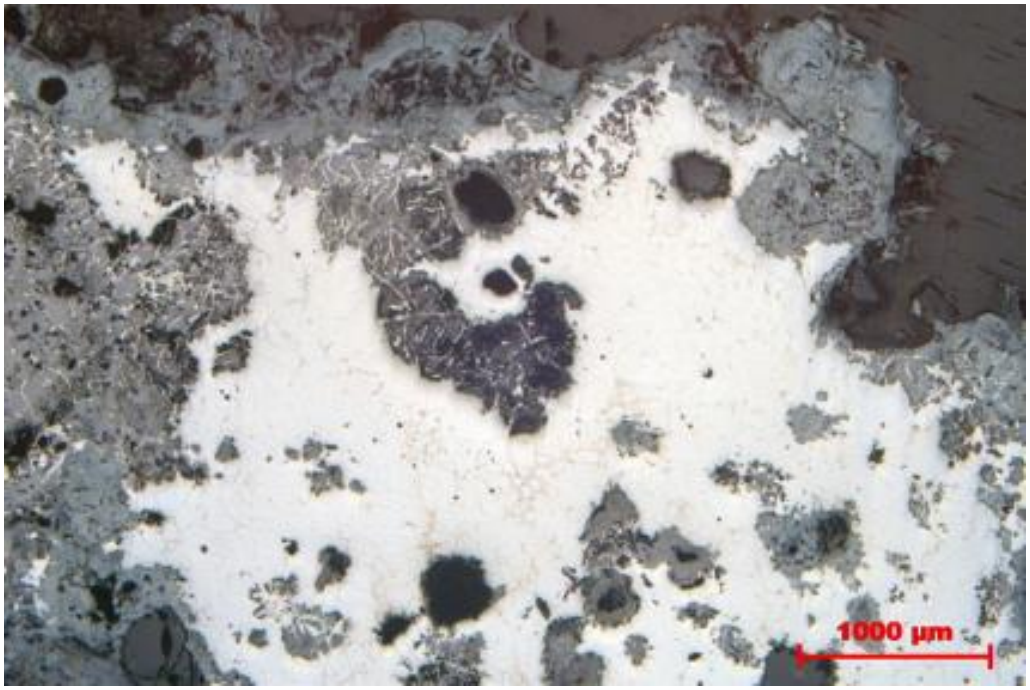

Figure S116. The grey rust has attacked the white iron in sample id 392, where the pale yellow cementite laminae can be faintly perceived (The Archaeologists, National Historical Museums, Uppsala, Sweden).

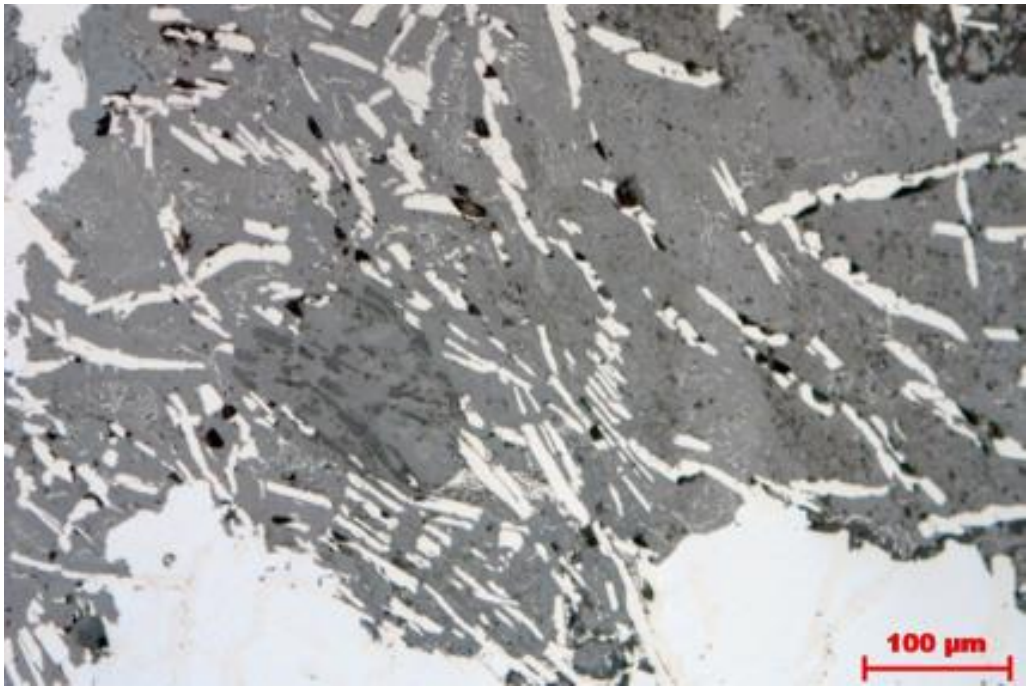

Figure S117. Iron sample id 392 with white iron and surrounding grey rust in high magnification. The pale yellow cementite laminae are seen both in the iron and in the rust (The Archaeologists, National Historical Museums, Uppsala, Sweden).

Figure S118. After etching of iron sample id 392 it appears that the carbon content is high. The sample consists of pearlite and cementite (The Archaeologists, National Historical Museums, Uppsala, Sweden).

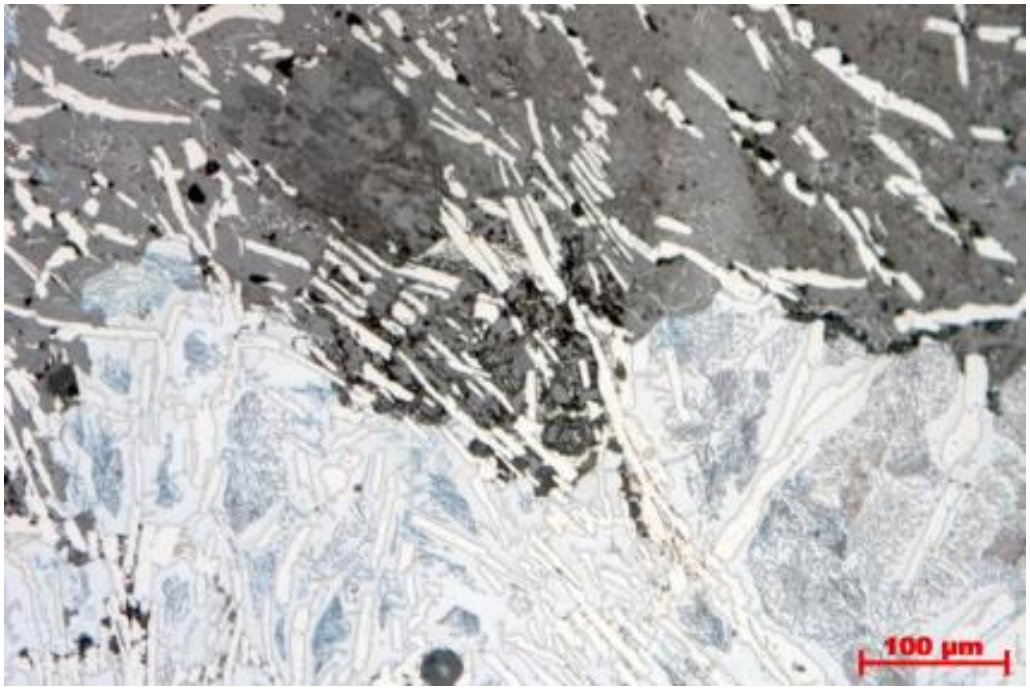

Figure S119. Etched sample id 392 in high magnification where the high carbon content is shown by the brown-blue pearlite texture in the iron and light cementite laminae, which is also preserved in surrounding rust (The Archaeologists, National Historical Museums, Uppsala, Sweden).

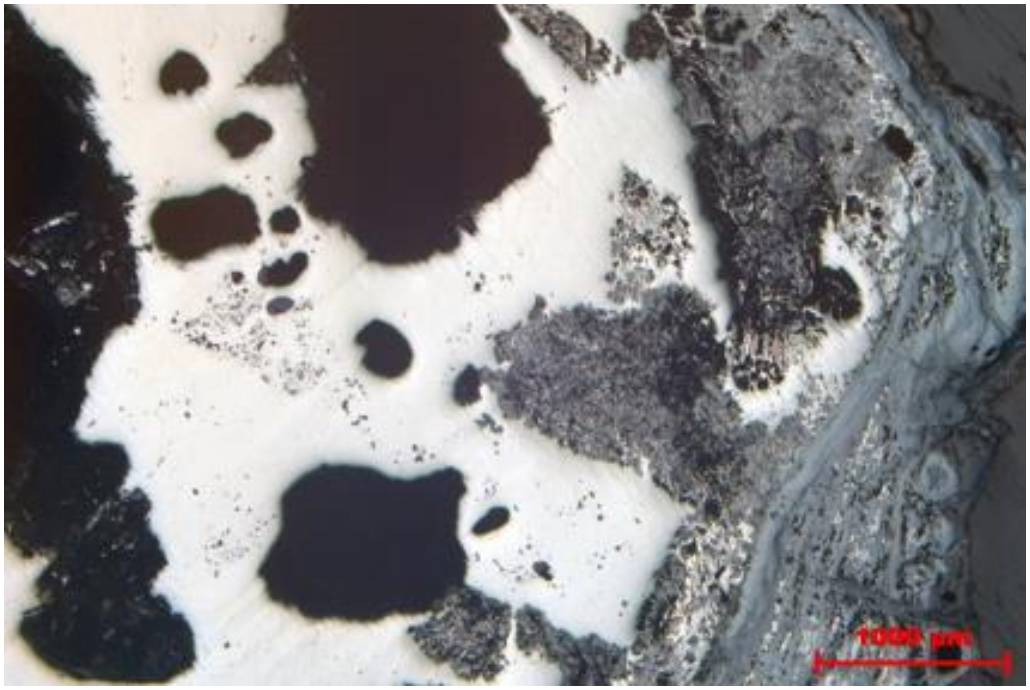

Figure S120. The porous and corroded iron in sample id 1759 before etching (The Archaeologists, National Historical Museums, Uppsala, Sweden).

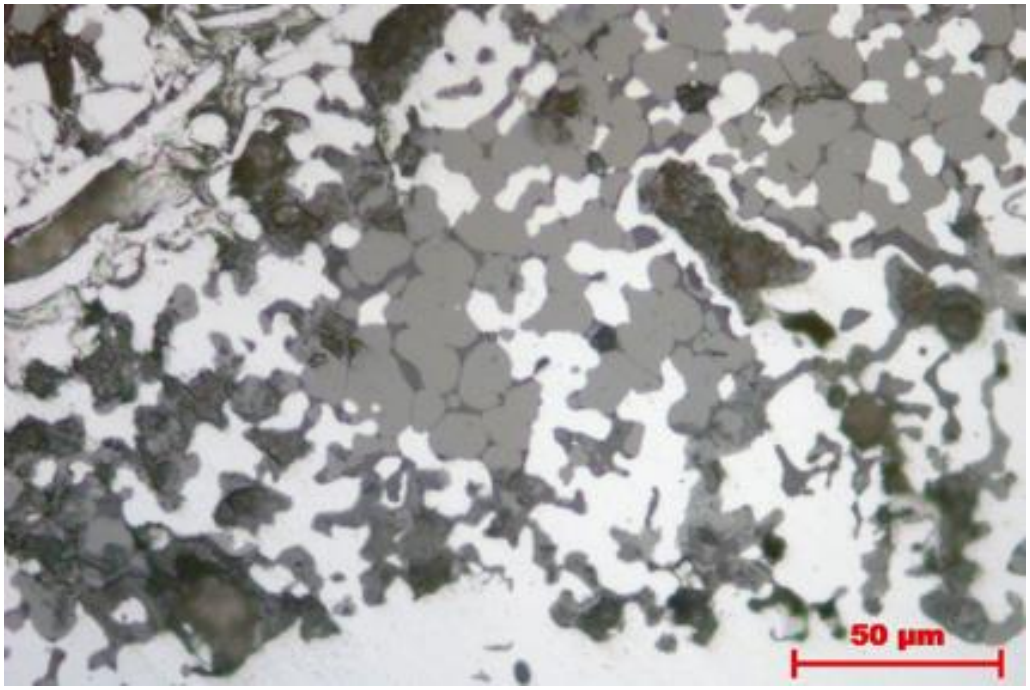

Figure S121. Sample id 1759. In very high magnification the fine-grained slag (in the white iron) is seen to consist of grey drop-shaped wüstite with dark intermediate glass (The Archaeologists, National Historical Museums, Uppsala, Sweden).

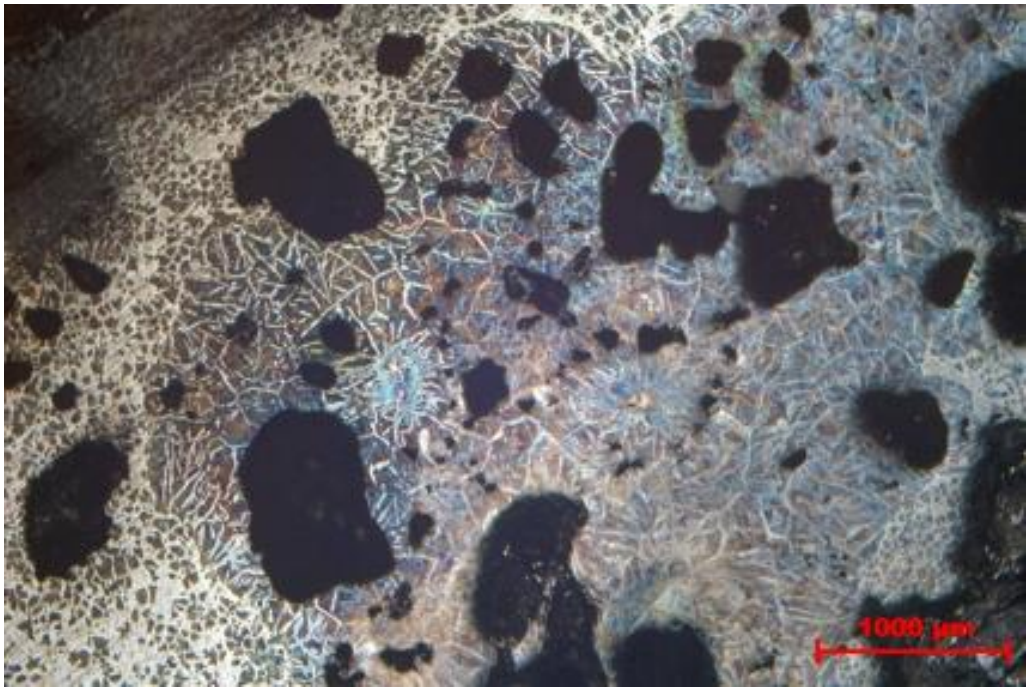

Figure S122. Id 1759. After etching of the sample the dark (brown-blue) texture with pearlite emerges, which demonstrates the presence of carbon in the iron (The Archaeologists, National Historical Museums, Uppsala, Sweden).

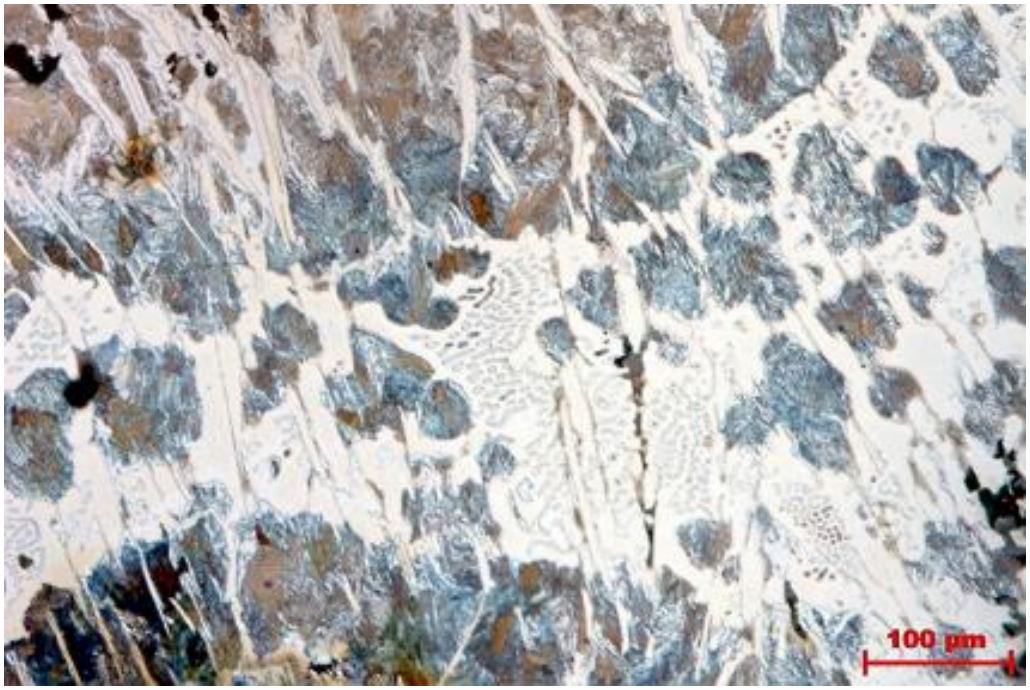

Figure S123. Id 1759. In high magnification it is seen that the iron, besides dark pearlite, also consists of light cementite, which in this picture partly appears with a ledeburite-like texture (The Archaeologists, National Historical Museums, Uppsala, Sweden).

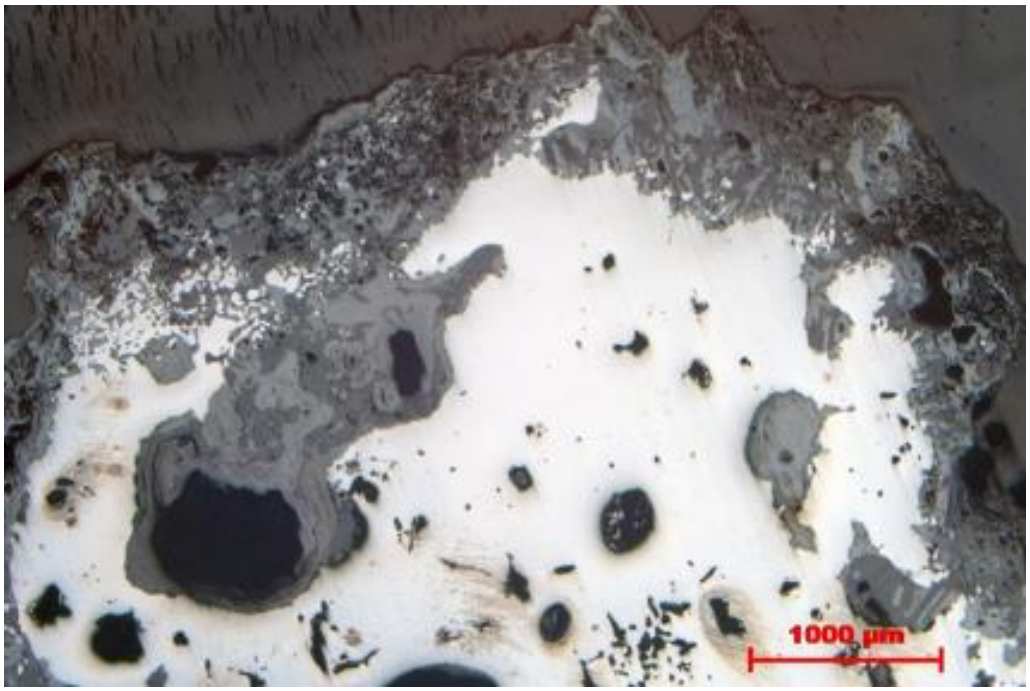

Figure S124. The polished iron sample id 2942 is both porous and corroded, but relatively lacking in slag inclusions (The Archaeologists, National Historical Museums, Uppsala, Sweden).

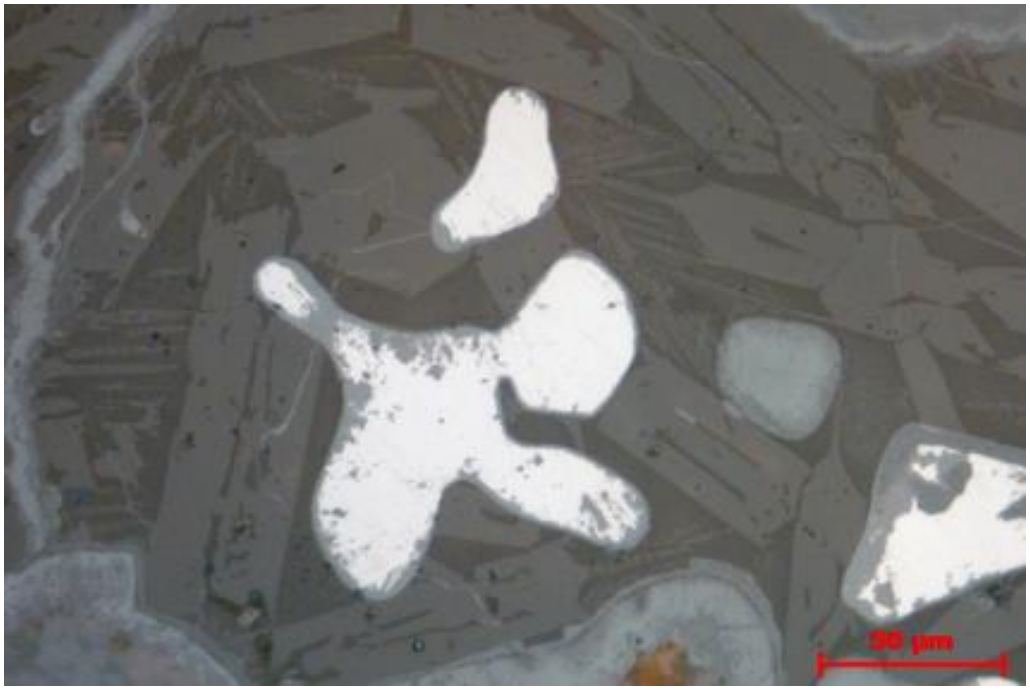

Figure S125. Id 2942. In very high magnification it is seen that (the few) slag inclusions consist of grey olivine with a darker intermediate matrix of glass. Here wüstite is also observed, which is almost completely reduced to white metallic iron (The Archaeologists, National Historical Museums, Uppsala, Sweden).

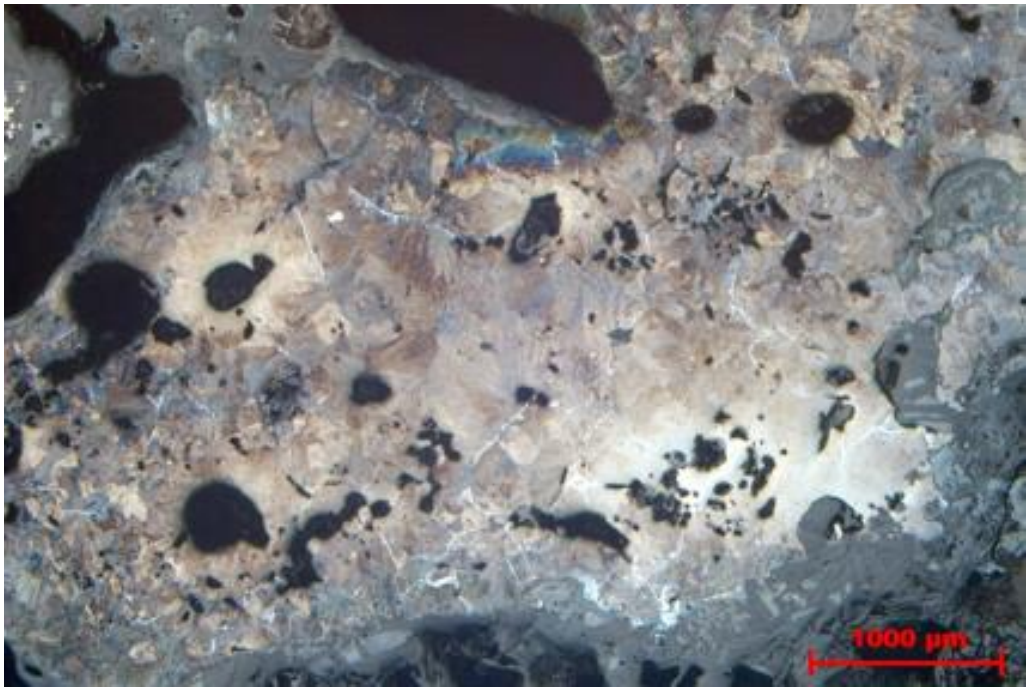

Figure S126. Id 2942. The etched iron sample is completely dominated by brownish pearlite (The Archaeologists, National Historical Museums, Uppsala, Sweden).

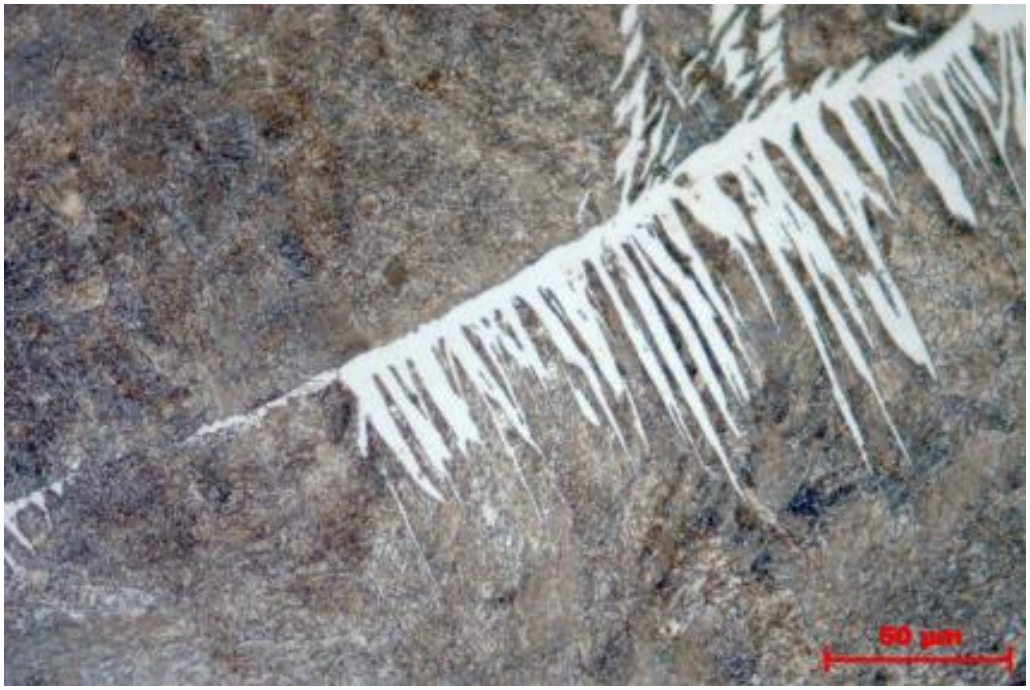

Figure S127. Id 2942. In very high magnification here the brown pearlite texture is seen with a grain boundary of carbon-free iron, ferrite, which shows feather texture (The Archaeologists, National Historical Museums, Uppsala, Sweden).

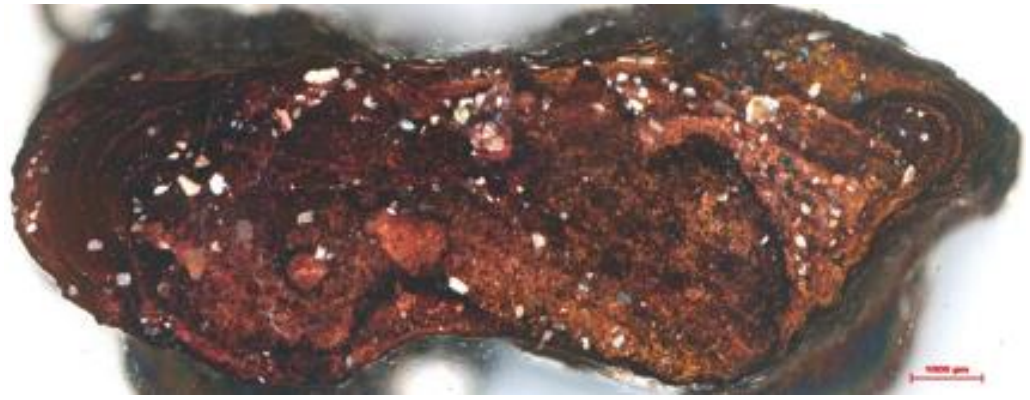

Figure S128. Id 2382. The entire cross section of the divided "coin" where, in part, light sand grains can be observed in the red limonite (The Archaeologists, National Historical Museums, Uppsala, Sweden).

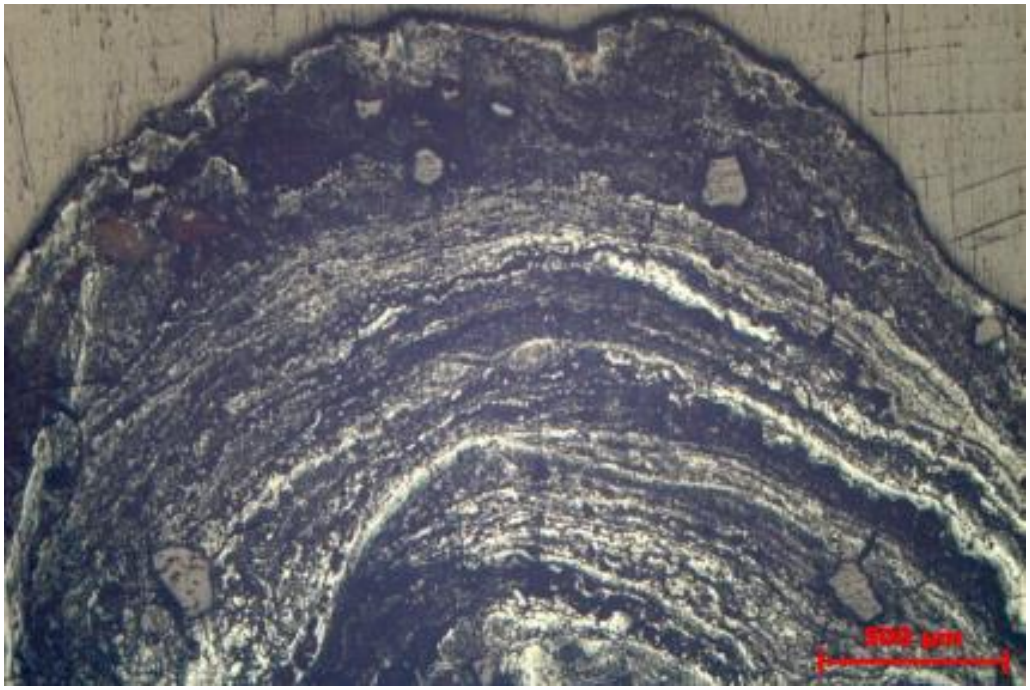

Figure S129. Id 2382. The one end of the ore sample where the concentric growth layers appear. A number of incorporated sand grains can also be seen (The Archaeologists, National Historical Museums, Uppsala, Sweden).

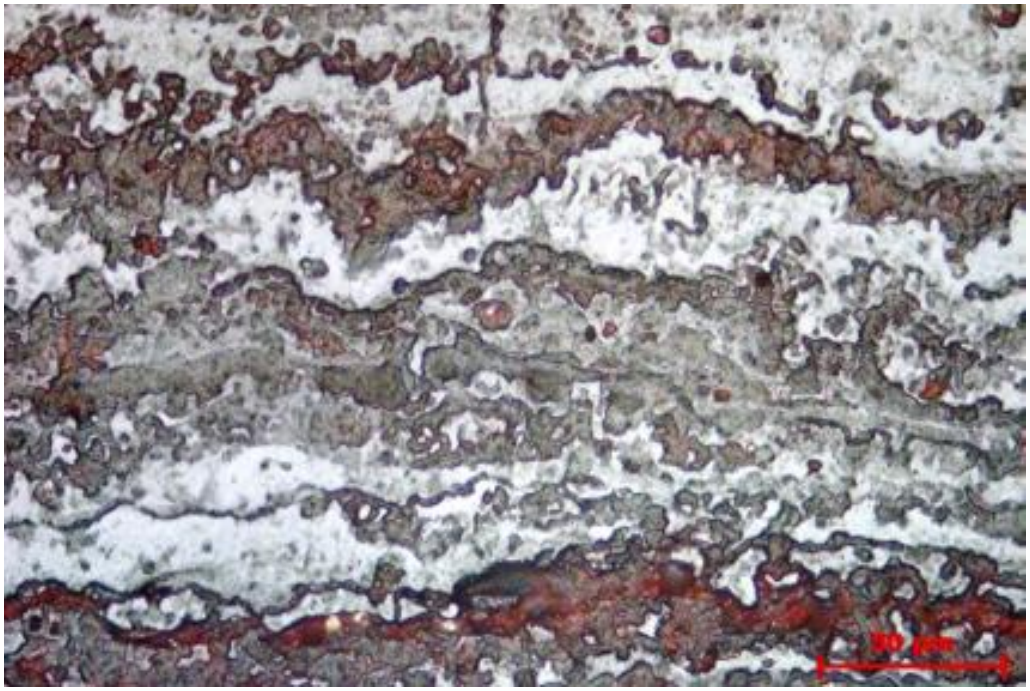

Figure S130. Id 2382. In very high magnification the clear compositional variations can be seen which built up the entire ore (The Archaeologists, National Historical Museums, Uppsala, Sweden).

Figure S131. Photo of stone frame fragment (top) with slag sintered on (vesicular) id 2970 (The Archaeologists, National Historical Museums, Uppsala, Sweden).

Figure S132. Photos of the clay samples' condition after 200 and 500°C (below) compared with the two furnace wall fragments to the left (A. Lindahl).

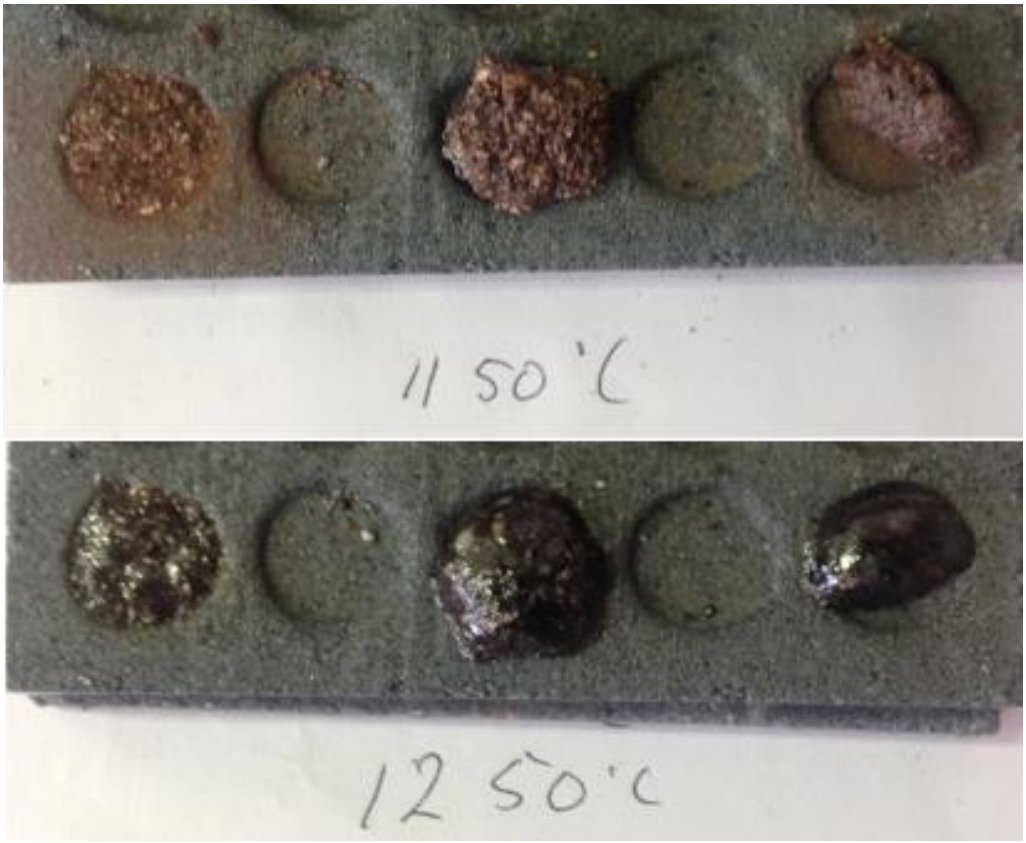

Figure S133. From left to right powder from clay samples I-III; Id 2854 and Id 1649 at 1150 and 1250°C respectively (A. Lindahl).

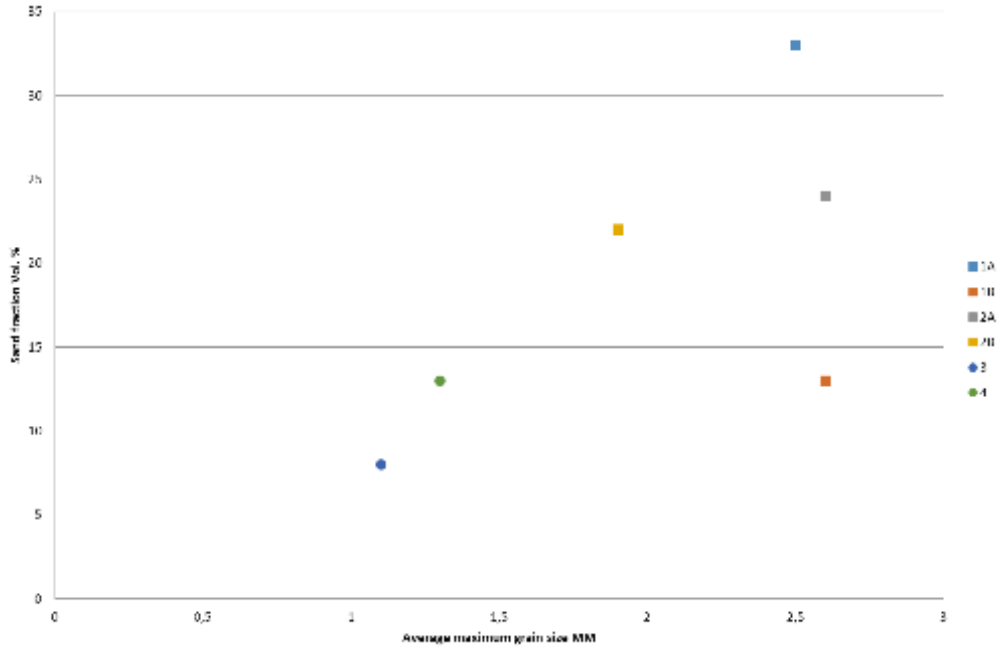

Figure S134. Diagram of percentage and average maximal grain size for the five or six different layers in the furnace wall fragments from furnace area 2 and 3 (Ts 1–4).

Figure S135. Photos of thin section samples 3 (top) and 4 (bottom) with clear temperature gradients from the inside at the bottom of both samples (furnace area 3). Total thickness 15 and 20mm respectively (The Archaeologists, National Historical Museums, Uppsala, Sweden).

Figure S136. The cross-section in fragment id 2270 with indication of two repairs. The fragment is 40mm thick (The Archaeologists, National Historical Museums, Uppsala, Sweden).

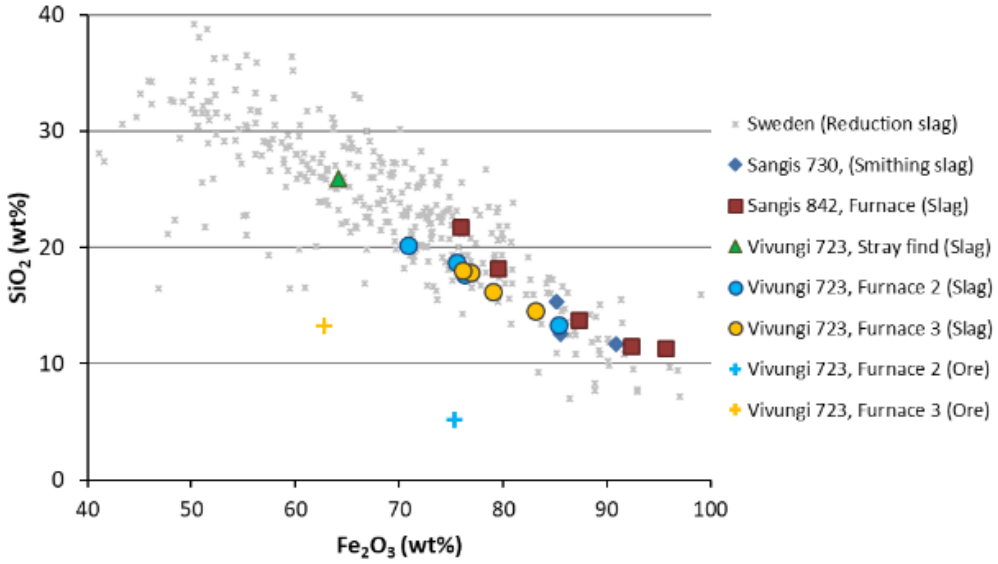

Figure S137. The content of silicon (as SiO_2) and iron (as Fe_2O_3) in the analysed slags from Sangis and Vivungi. The analysed ores are also shown. As a reference all analysed reduction slags from Sweden in GALs database are shown (The Archaeologists, National Historical Museums, Uppsala, Sweden).

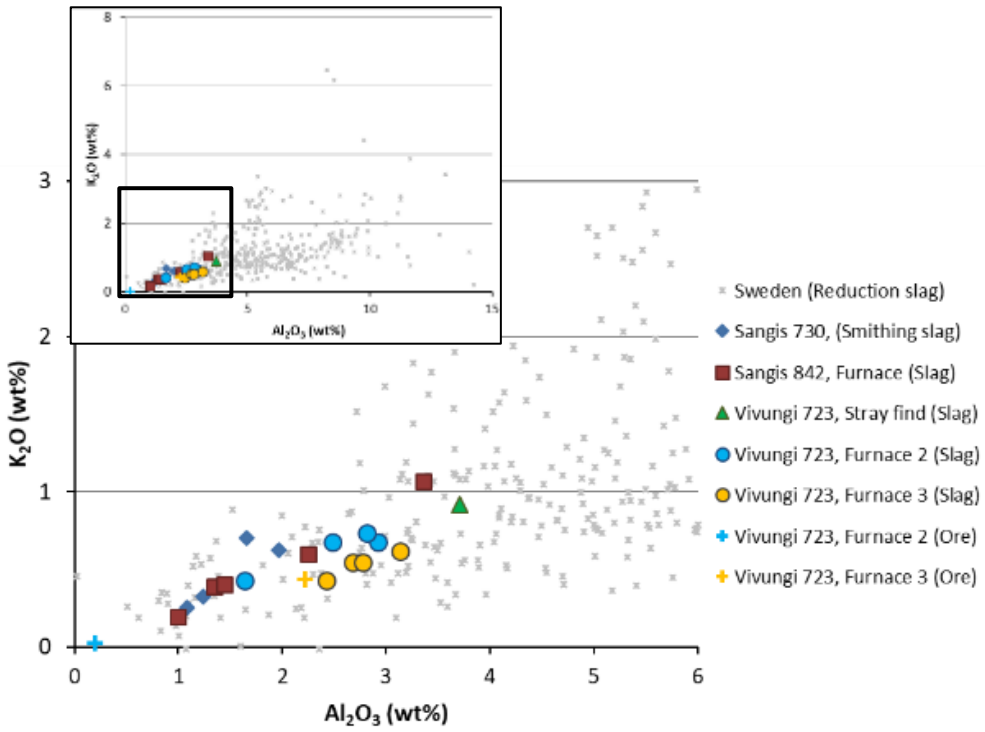

Figure S138. The content of potassium (as K_2O) and aluminum (as Al_2O_3) in the analysed slags from Sangis and Vivungi. The analysed ores are also shown. As a reference analysed reduction slags from Sweden with great variation are shown. The box in the upper diagram is enlarged to better distinguish the relevant slags and ores (The Archaeologists, National Historical Museums, Uppsala, Sweden).

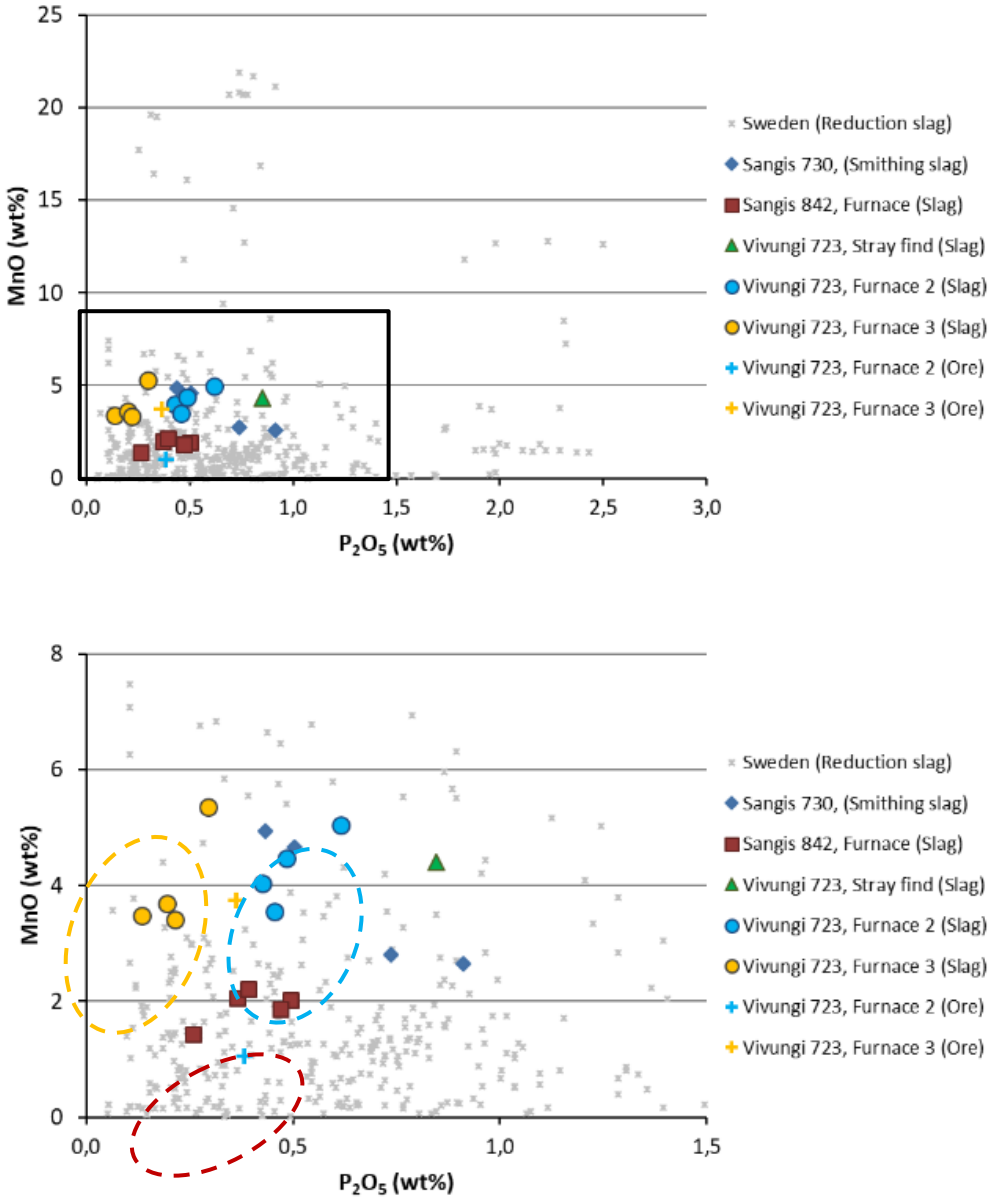

Figure S139. The content of manganese (as MnO) and phosphorus (as P_2O_5) in the analysed slags and ores from Sangis and Vivungi. As a reference analysed reduction slags from Sweden with great variation are shown. The box in the upper diagram is enlarged to better distinguish the relevant slags and ores. The slags from both furnace areas in Vivungi have similar variation in manganese content, but those from area 2 have higher phosphorus content than those from area 3. The reduction slags from Sangis 842 have consistently lower manganese content than those from Vivungi, but overlapping phosphorus content. The outlined areas schematically show these three groups (The Archaeologists, National Historical Museums, Uppsala, Sweden).

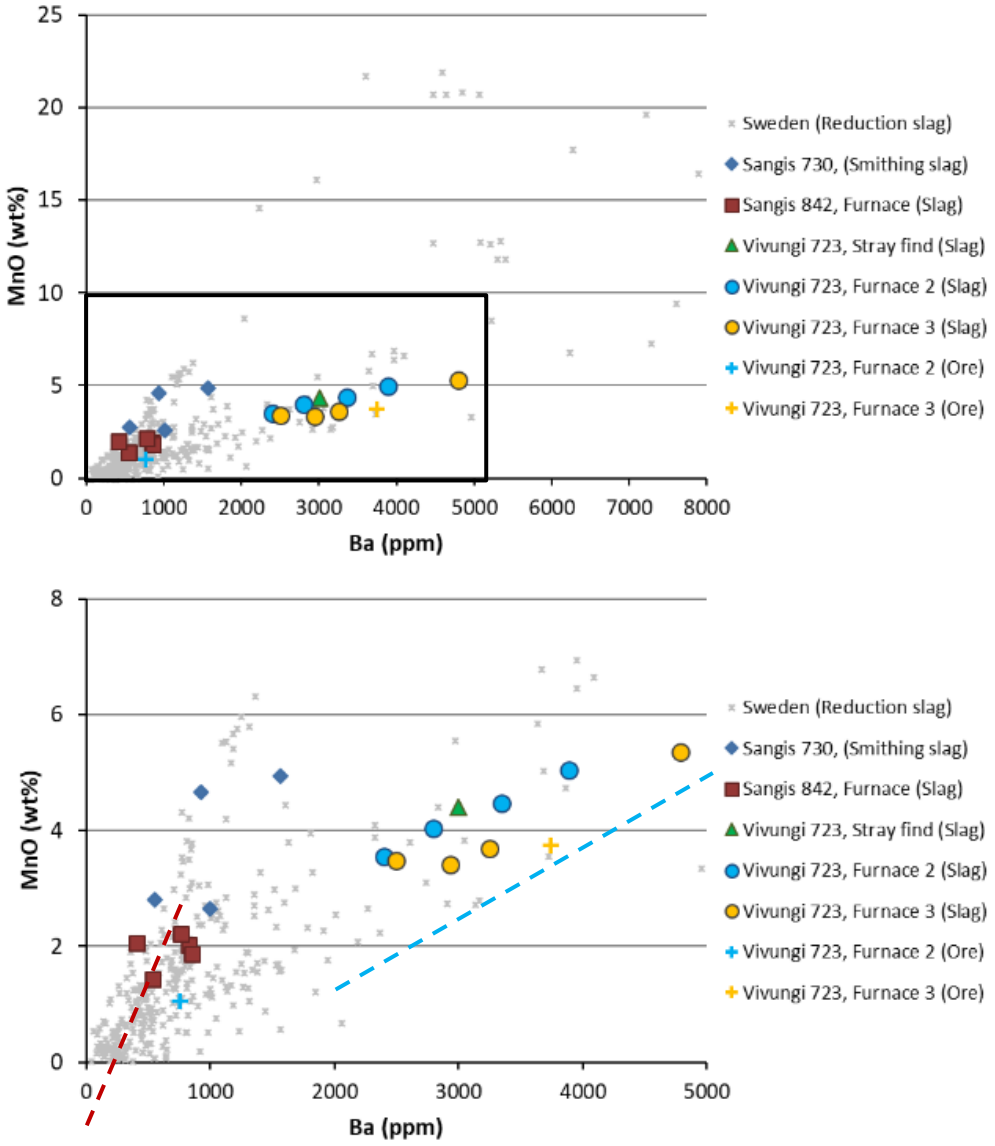

Figure S140. The content of manganese (as MnO) and barium (as Ba) in the analysed slags and ores from Sangis and Vivungi. As a reference analysed reduction slags from Sweden with great variation, but mostly lower amounts, are shown. The box in the upper diagram is enlarged to better distinguish the relevant slags and ores. The slags from the two furnace areas in Vivungi have similar variation in manganese and barium content, where the blue dashed line schematically shows the trend. The reduction slags from Sangis 842 have consistently lower manganese and barium content than those from Vivungi which is shown schematically with the red dashed line with considerably steeper slope. In the combined Swedish reference material corresponding trends can also be detected (The Archaeologists, National Historical Museums, Uppsala, Sweden).

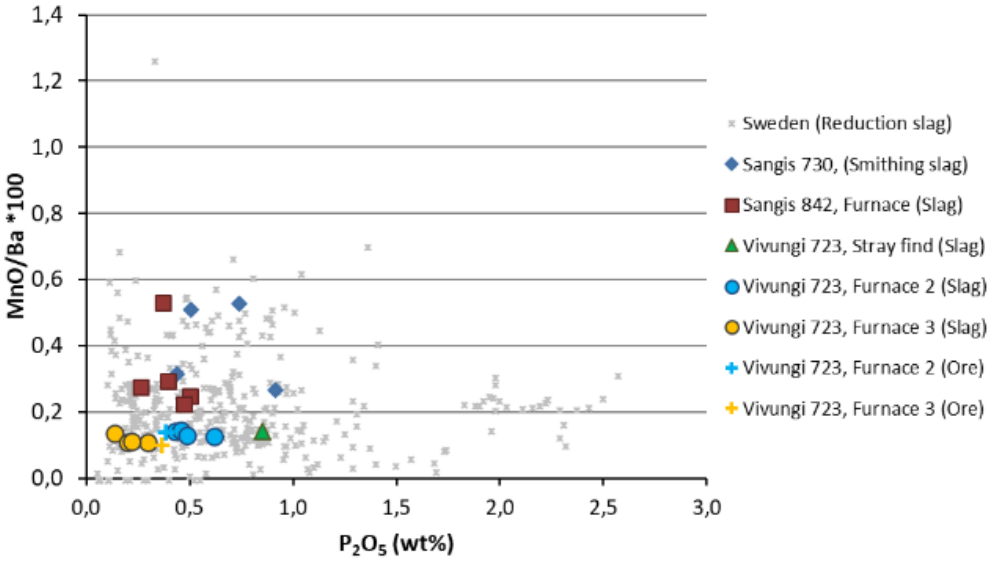

Figure S141. The ratio between manganese and barium compared with phosphorus (as P_2O_5) in the analysed slags and ores from Sangis and Vivungi. As a reference analysed reduction slags from Sweden are shown. The slags from the two furnace areas in Vivungi have similar ratio between manganese and barium content, and varying phosphorus content. The two ores from Vivungi are within the same range. The slags from Sangis 842 and Sangis 730 have consistently higher ratio between manganese and barium content (cf. previous figure) (The Archaeologists, National Historical Museums, Uppsala, Sweden).

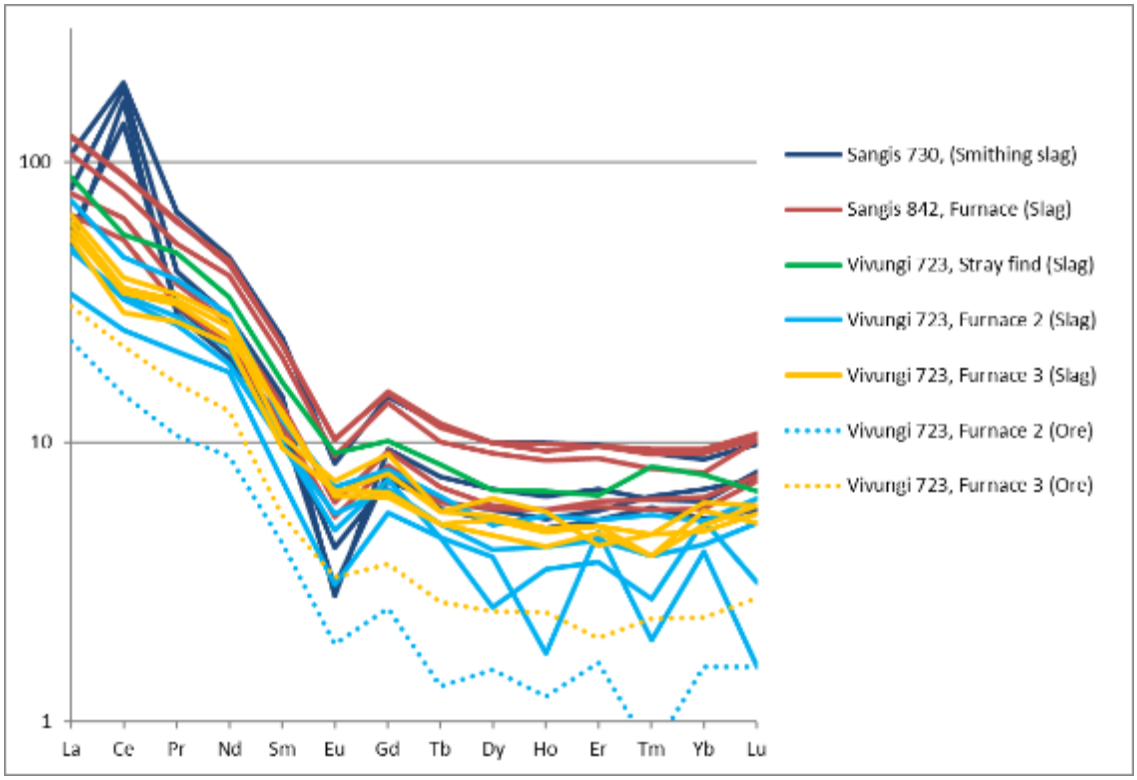
100
10
1
La Ce Pr Nd Sm Eu Gd Tb Dy Ho Er Tm Yb Lu
Sangis 730, (Smithing slag)
Sangis 842, Furnace (Slag)
Vivungi 723, Stray find (Slag)
Vivungi 723, Furnace 2 (Slag)
Vivungi 723, Furnace 3 (Slag)
Vivungi 723, Furnace 2 (Ore)
Vivungi 723, Furnace 3 (Ore)

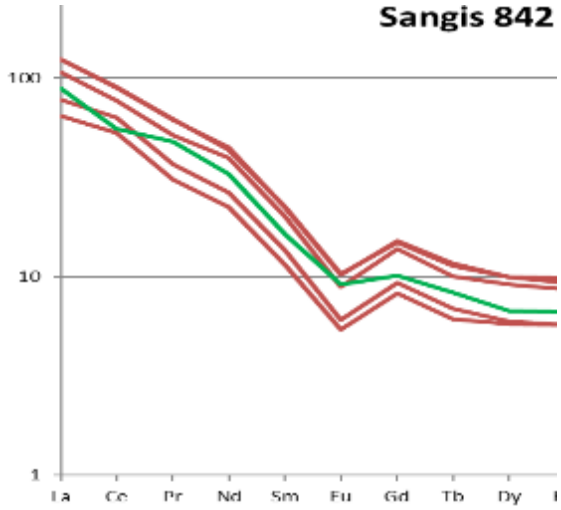
Sangis 842
100
10
1
La Ce Pr Nd Sm Eu Gd Tb Dy

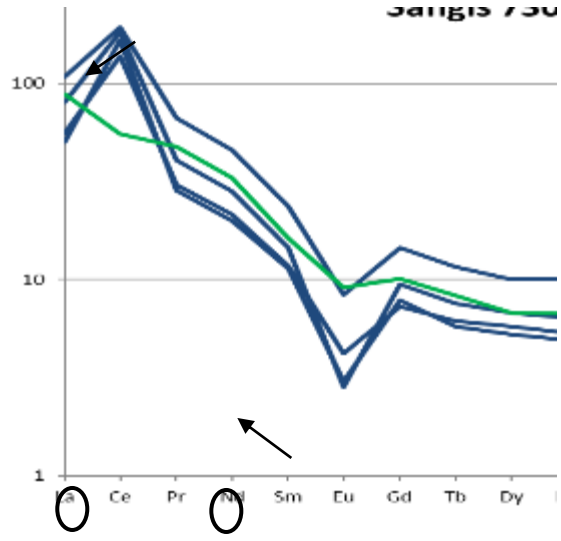
100
10
1
Ce Pr Nd Sm Eu Gd Tb Dy

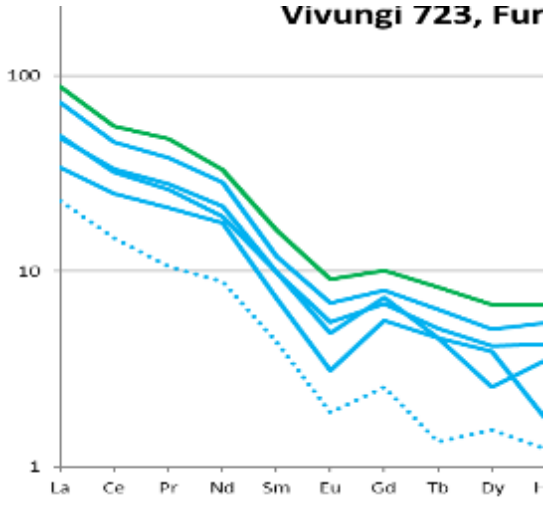
Vivungi 723, Fur
100
10
1
La Ce Pr Nd Sm Eu Gd Tb Dy

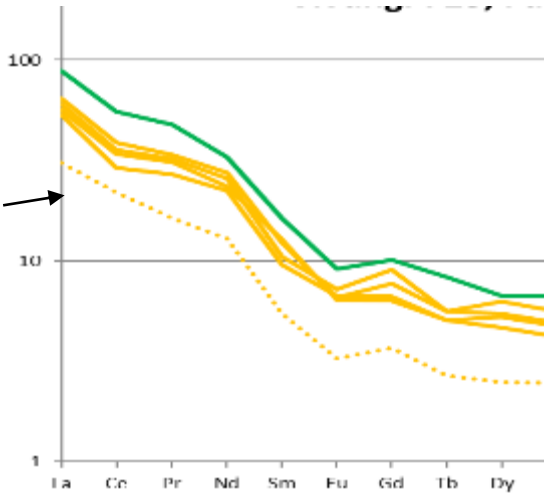
100
10
1
La Ce Pr Nd Sm Eu Gd Tb Dy

Figure S142. Rare earth elements (REE) in the analysed slags and ores from Sangis and Vivungi. The ores have consistently lower content (and close to detection limits) than the slags. In the upper diagram all samples are shown. To better be able to distinguish the respective site, a division has been made into four diagrams. In each one the slag from Vivungi 723, which is a stray find, is shown as reference line. Slags from Sangis 730 and 842 (the diagram in the middle) have higher content than those from Vivungi, but also differ from each other; those from Sangis 730 have a stronger peak for cerium (Ce), i.e., a positive cerium anomaly and a stronger trough for europium (Eu), i.e., negative europium anomaly (see the two arrows). The slags from Vivungi (the two lower diagrams) have lower total content of REE, with a somewhat larger variation in the slags from area 2 (to the left). The slags from furnace area 3 are mutually more similar and demonstrate a weak cerium anomaly (the arrow in the diagram). The values are chondrite normalized and the y-axis is logarithmic (The Archaeologists, National Historical Museums, Uppsala, Sweden).

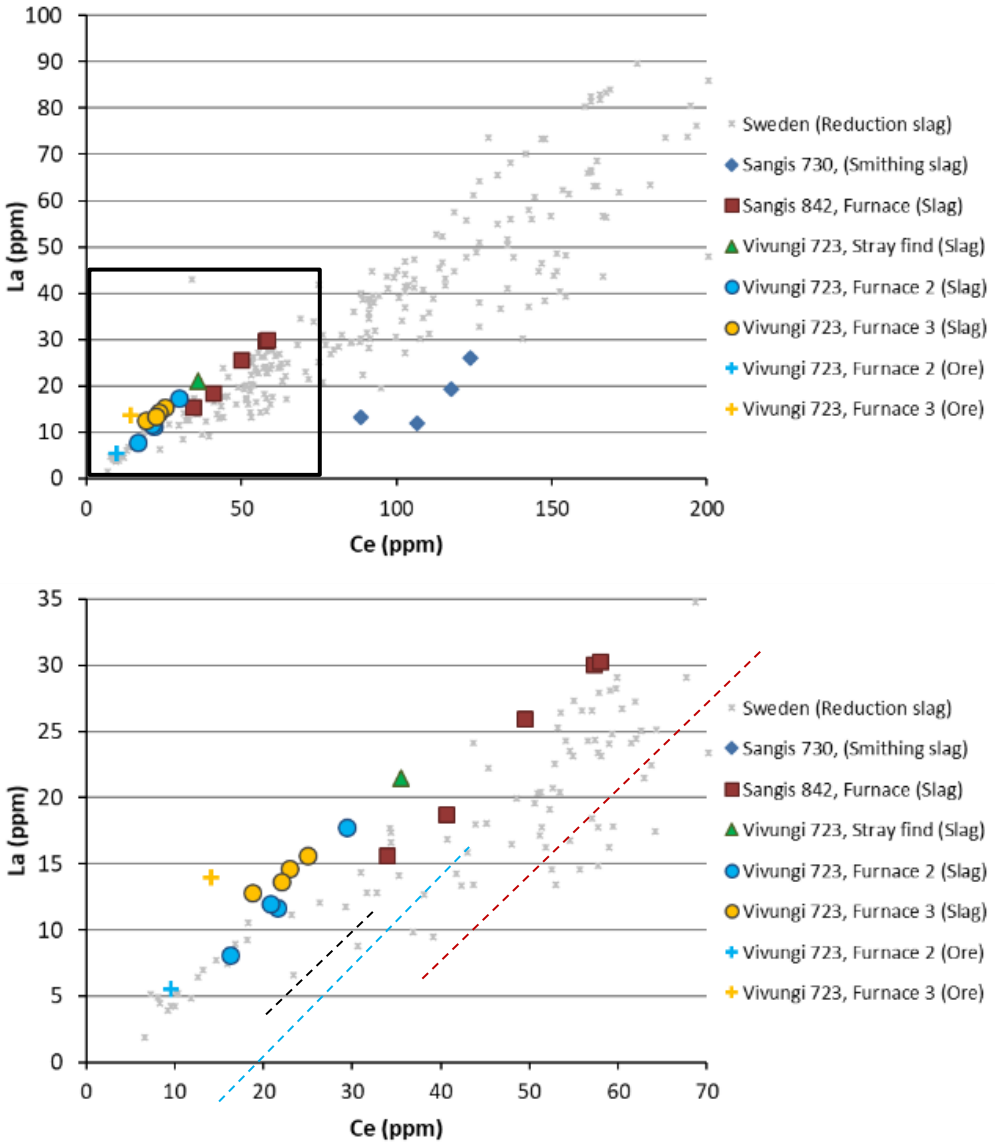

Figure S143. Selection of the rare earth elements lanthanum (La) and cerium (Ce) to additionally show the various cerium anomalies illustrated in the previous figure. As a reference analysed reduction slags from Sweden are shown. The box in the upper diagram is enlarged to better distinguish the relevant slags and ores. Within each site there is a linear relationship between La and Ce (schematically shown with dashed lines). These lines are displaced and show various relationships (The Archaeologists, National Historical Museums, Uppsala, Sweden).

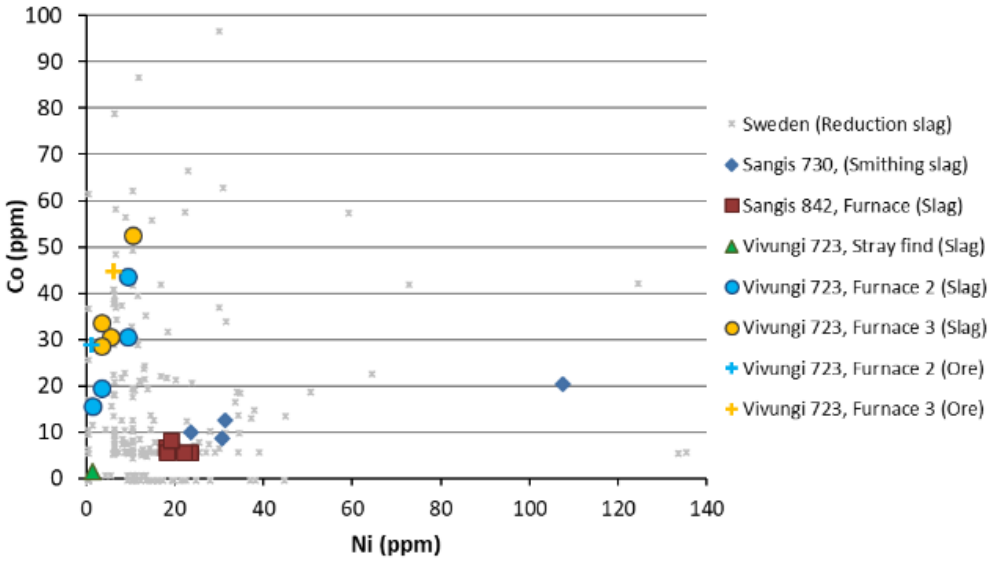

Figure S144. The content of cobalt (Co) and nickel (Ni) in the analysed slags and ores from Sangis and Vivungi. As a reference analysed reduction slags from Sweden are shown. The slags from the two furnace areas in Vivungi have similar variation with higher cobalt content and lower nickel content than in the slags from Sangis 730 and 842. The stray find from Vivungi deviates, however (The Archaeologists, National Historical Museums, Uppsala, Sweden).

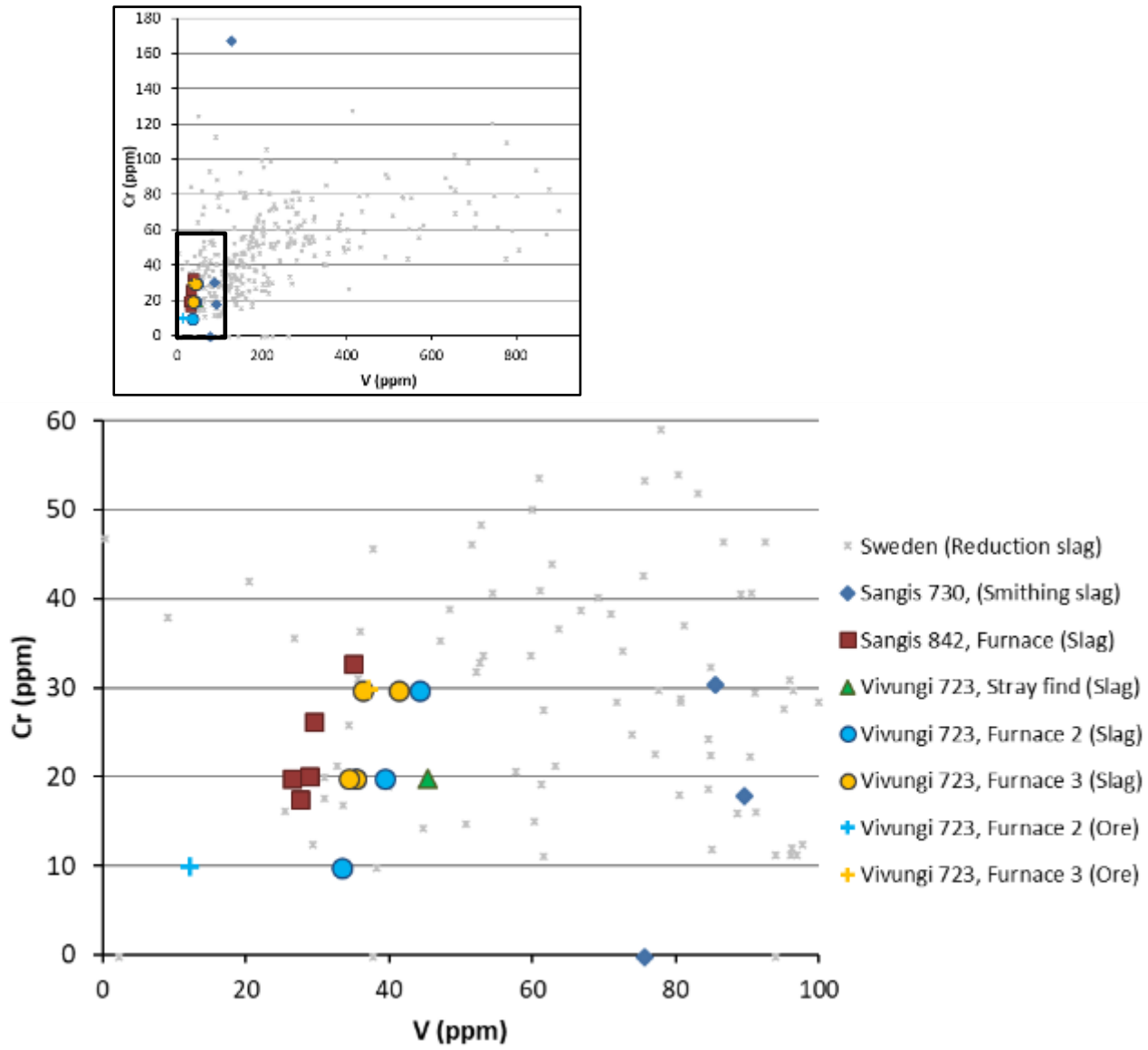

Figure S145. The content of chromium (Cr) and vanadium (V) in the analysed slags and ores from Sangis and Vivungi. As a reference analysed reduction slags from Sweden are shown. The box in the upper diagram is enlarged to better distinguish the relevant slags and ores. Slags from all sites demonstrate similar variation in chromium content. The vanadium content is consistently low; generally somewhat lower in the slags from Sangis 842 than in the slags from Vivungi. The very highest vanadium content is in the slags from Sangis 730 (The Archaeologists, National Historical Museums, Uppsala, Sweden).

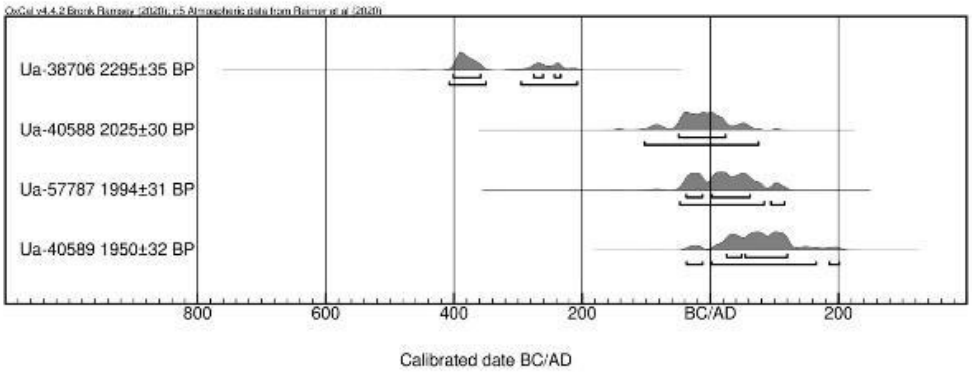

Figure S146. Calibration graphs of radiocarbon dates of iron production remains from the Sangis 842 site (calibrated using OxCal v4.4.2 and the IntCal20 calibration curve; Bronk Ramsey 2020; Reimer et al. *2020). For details about the samples, see Table S5.1. The result show that one of the samples (Ua 38706, charcoal from pine embedded in slag) is older than the other ones, deviating with more than 300 radiocarbon years. Judging from field observations of metallurgical remains, showing one coherent assemblage deposited over a short time, the early phase of sample Ua-38706 does not seem plausible. This is further confirmed by the obtained dating of a reindeer antler showing cutting marks made with a metal blade, which has given a date range to 198–43 cal BC (Ua-40612, 2σ, 94.3%) (Table S5.2). Given the negligible intrinsic age of the antler (Lanting et al 2001) and the consistent dating of the (three remaining) metallurgical samples (Ua-40588, Ua-57787, Ua-40589), this indicate that the dating of the smelting activity at Sangis 842 site is by no means older than 200 BC (The Archaeologists, National Historical Museums, Uppsala, Sweden).*

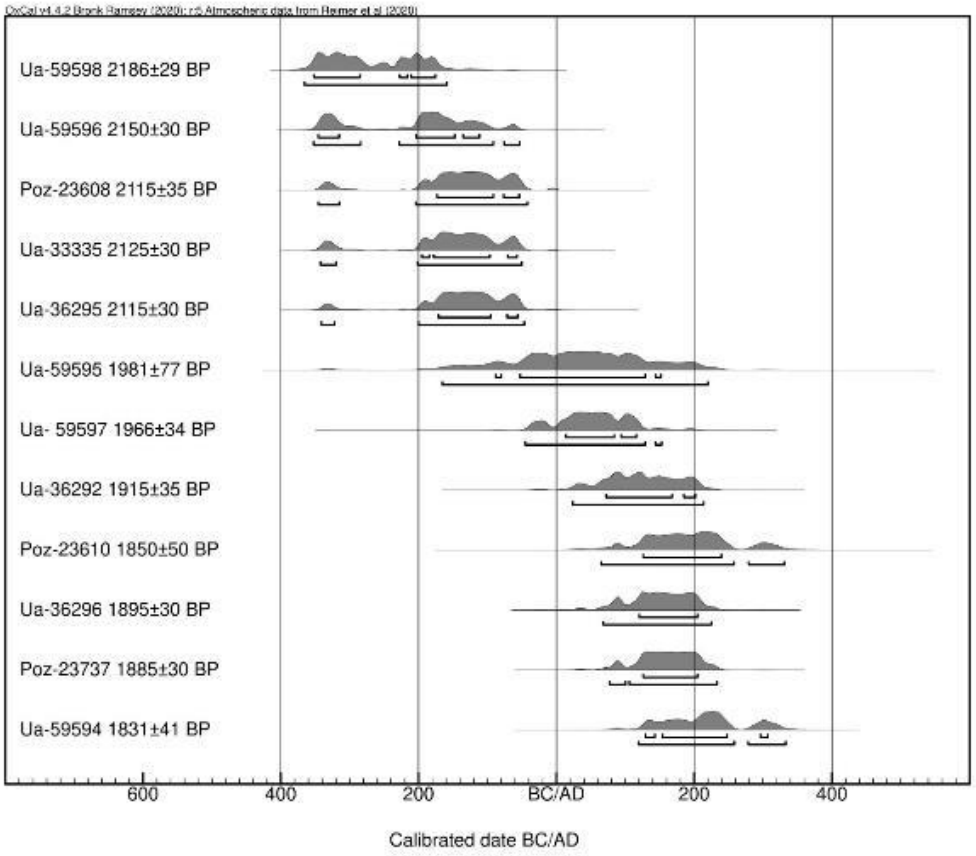

Figure S147. Calibration graphs of radiocarbon dates of smithing remains from the Sangis 730 site (calibrated using OxCal v4.4.2 and the IntCal20 calibration curve; Bronk Ramsey 2020; Reimer et al. *2020). For details about the samples, see Table S5.1. The radiocarbon distribution seems to form two distinct chronological groups: one before 0 BC/AD and one after. Four radiocarbon dated samples have been excluded from the graph (Ua-36293, Ua-36294, Poz-23960 and Poz-23611). Given the elevation above sea level and shoreline displacement of the area (Lindén* et al. *2006), the maximum permitted dating (*terminus post quem*) is 500–400 BC, making these dates highly unlikely (The Archaeologists, National Historical Museums, Uppsala, Sweden).*

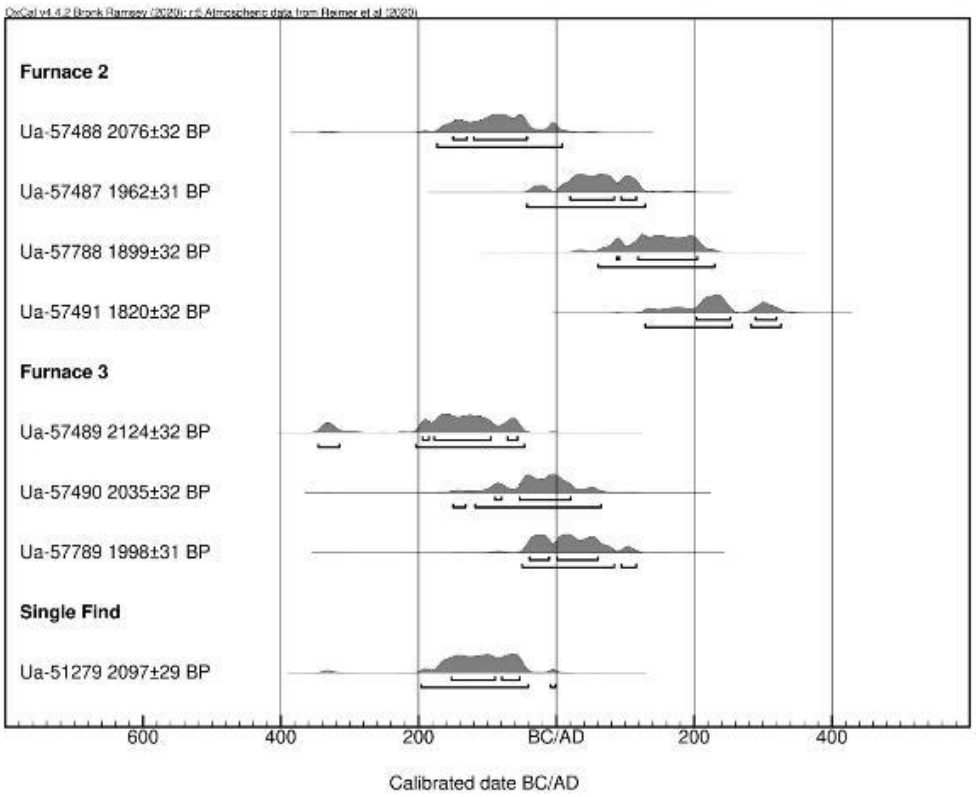

Figure S148. Calibration graphs of radiocarbon dates of iron production remains from the Vivungi 723 site (calibrated using OxCal v4.4.2 and the IntCal20 calibration curve; Bronk Ramsey 2020; Reimer et al. *2020). For details about the samples, see Table S5.1. The radiocarbon distribution indicates that iron production started around 200–100 BC, with a tendency for overlapping dates around 50 BC–AD 50. Sample Ua-57491 from furnace 2 (charcoal from pine taken from the slagheap) show a somewhat younger radiocarbon distribution than the other samples. Archaeologically, however, we see nothing to suggest a younger phase in iron production, even though there are radiocarbon dates of habitation remains (Table S5.2) indicating a younger occupation of the site (The Archaeologists, National Historical Museums, Uppsala, Sweden).*

Table S4. Overview of the distribution of different observed phenomena on the furnace wall fragments from furnace area 2 and 3 at the Vivungi 723 site.

Furnace area & find Id	Thickness of wall etc.	Stone frame fragment	Slag sintered on	Temperature gradient	Repair
Furnace area 2, Id 560 A	10		X		
Furnace area 2, Id 560 B	15		X		
Furnace area 2, Id 592 A	15	X			X?
Furnace area 2, Id 1649 A	9				
Furnace area 2, Id 1649 B	20	X	X		
Furnace area 2, Id 1649 C	11			2 zones	
Furnace area 2, Id 1649 D	23		X	2 zones	
Furnace area 2, Id 1649 E	19		X	2 zones	
Furnace area 2, Id 2270 A	25	X			X?
Furnace area 2, Id 2819 A	10		X		
Furnace area 3, Id 2685 A	15			3 zones	
Furnace area 3, Id 2685 B	12			2 zones	
Furnace area 3, Id 2610 A	15			3 zones	
Furnace area 3, Id 2854 A	20		X (little)	2 zones	

Furnace area 3, Id 1703 A	15		X	3 zones	
Furnace area 3, Id 1745 A	5		X	2 zones	
Furnace area 3, Id 1749 A	8		X	2 zones	
Furnace area 3, Id 2932 A	15		X	3 zones	
Furnace area 3, Id 2952 A	20	X	X	3 zones	
Furnace area 3, Id 2970 A	10	X	X	2 zones	

Table S5.1. Radiocarbon dating of metallurgical remains from Sangis 842, Sangis 730 and Vivungi 723. Processed at the Ångström Laboratory in Uppsala, Sweden and Poznan Radiocarbon Laboratory, Poland. Calibrated using the OxCal v4.4.2 Bronk Ramsey (2020); r:5 IntCal 20 atmospheric curve (Reimer *et al.* 2020).

Lab ID	Site	Context	Material	Radiocarbon age (BP)	Calibrated age (2σ)
Sangis 842					
Ua-38706	Sangis 842	Furnace, slag heap, F13:1	Charcoal embedded in slag, pine	2295±35	408–208 cal BC
Ua-40588	Sangis 842	Furnace, slag heap	Charcoal, birch	2025±30	103 cal BC–cal AD 76
Ua-57787	Sangis 842	Furnace, slag heap, F759	Carbon extracted from iron waste	1994±31	48 cal BC–cal AD 116
Ua-40589	Sangis 842	Furnace, slag pit	Charcoal, birch	1950±32	38 cal BC–cal AD 202
Sangis 730					
Ua-36293	Sangis 730	Smithing hearth A4, F1112	Charcoal embedded in slag, pine	2980±100	1431–930 cal BC
Ua-59598	Sangis 730	Smithing hearth A4, F7045	Carbon extracted from iron waste	2186±29	366–160 cal BC
Ua-33335	Sangis 730	Smithing hearth A4	Charcoal, pine	2125±30	343–51 cal BC
Ua-59595	Sangis 730	Smithing hearth A4, F925	Carbon extracted from iron waste	1981±77	166 cal BC–cal AD 221
Poz-23960	Sangis 730	Structure A27, F2768	Pottery	2740±30	971–813 cal BC

Poz-23611	Sangis 730	Structure A27	Burnt bone	2720±110	1213–549 cal BC
Poz-23733	Sangis 730	Structure A27, F1784	Charcoal, organic residue next to bronze buckle	1990±30	46 cal BC–cal AD 117
Ua- 59597	Sangis 730	Structure A27, F2771	Carbon extracted from steel object	1966±34	46 cal BC–cal AD 154
Ua-36296	Sangis 730	Structure A27, F3010	Carbon extracted from iron waste	1895±30	cal AD 69–226
Poz-23737	Sangis 730	Structure A29	Charcoal, crowberry (small twigs)	1885±30	cal AD 78–234
Poz-23610	Sangis 730	Structure A29	Burnt bone	1850±50	cal AD 66–332
Ua-36294	Sangis 730	Smithing hearth, A45, F3763	Charcoal embedded in slag, pine	2430±75	770–397 cal BC
Poz-23608	Sangis 730	Smithing hearth A45	Burnt bone	2115±35	346–43 cal BC
Ua-59596	Sangis 730	Smithing hearth A53, F1840	Carbon extracted from iron waste	2150±30	353–54 cal BC
Ua-36292	Sangis 730	Smithing hearth A53, F913	Charcoal embedded in slag, pine	1915±35	cal AD 25–215
Ua-36295	Sangis 730	Single find within site, F2684	Carbon extracted from socketed axe	2115±30	342–47 cal BC
Ua-59594	Sangis 730	Single find within site, F878	Carbon extracted from knife	1831±41	cal AD 120–334
Vivungi 723					
Ua-57488	Vivungi 723	Furnace 2, slag pit	Charcoal, pine	2076±32	174 cal BC–cal AD 9
Ua-57487	Vivungi 723	Furnace 2, slag heap	Charcoal, pine (twig/branch)	1962±31	43 cal BC–cal AD 130

Ua-57788	Vivungi 723	Furnace 2, slag heap, id 392	Carbon extracted from iron waste	1899±32	cal AD 62–cal AD 231
Ua-57491	Vivungi 723	Furnace 2, slag heap	Charcoal, pine	1820±32	cal AD 130–cal AD 327
Ua-57489	Vivungi 723	Furnace 3, slag heap	Charcoal, pine	2124±32	346–47 cal BC
Ua-57490	Vivungi 723	Furnace 3, slag pit	Charcoal, pine (twig/branch)	2035±32	151 cal BC–cal AD 66
Ua-57789	Vivungi 723	Furnace 3, slag heap, id 1759	Carbon extracted from iron waste	1998±31	50 cal BC–cal AD 117
Ua-51279	Vivungi 723	Single find within site	Charcoal embedded in slag, birch	2097±29	197–1 cal BC

Table S5.2. Radiocarbon datings of habitation remains from Sangis 842, Sangis 730 and Vivungi 723. Processed at the Ångström Laboratory in Uppsala, Sweden and Poznan Radiocarbon Laboratory, Poland. Calibrated using the OxCal v4.4.2 Bronk Ramsey (2020); r:5 IntCal20 atmospheric curve (Reimer *et al*. 2020).

Lab ID	Site	Context	Material	Radiocarbon age (BP)	Calibrated age (2σ)
Sangis 842					
Ua-38707	Sangis 842	Hearth A2	Charcoal, pine	2147±30	353–53 cal BC
Ua-40612	Sangis 842	Hearth A4	Antler, reindeer	2102±30	337–43 cal BC
Sangis 730					
Poz 23875	Sangis 730	Cultural layer, F2732	Pottery	2410±35	749–397 cal BC
Poz 23738	Sangis 730	Post-hole A47c	Charcoal, pine (branch, 10 years)	2380±30	717–393 cal BC

Ua 33330	Sangis 730	Hearth A3	Charcoal, pine	2295±30	407–210 cal BC
Poz 23612	Sangis 730	Hearth A21	Burnt bone	2295±35	408–208 cal BC
Poz 23734	Sangis 730	Hearth A7	Charcoal, pine (twig)	2230±30	387–200 cal BC
Poz 23736	Sangis 730	Hearth A12	Charcoal, pine (outer 4 year ring)	2230±35	390–197 cal BC
Poz 23729	Sangis 730	Hearth A5:1, F3005	Resin	2205±30	371–176 cal BC
Poz 23615	Sangis 730	Hearth, A15	Burnt bone	2140±40	355–47 cal BC
Poz 23607	Sangis 730	Hearth A46	Burnt bone	2110±30	339–46 cal BC
Poz 23735	Sangis 730	Cooking pit A36	Charcoal, soot	2045±30	154 cal BC–cal AD 58
Poz 23661	Sangis 730	Hearth A28	Burnt bone	2020±40	149 cal BC–cal AD 116
Poz 23877	Sangis 730	Hearth A6, F3546	Pottery	2010±35	96 cal BC–AD 117
Poz 23609	Sangis 730	Hearth A42	Burnt bone	1850±40	cal AD 81–324
Poz 23873	Sangis 730	Cultural layer, F2087	Pottery	1730±35	cal AD 247–408
Ua 33338	Sangis 730	Pit hearth A2	Burnt bone	1310±30	cal AD 656–775
Poz-23616	Sangis 730	Cultural layer A5:2	Burnt bone	1295±30	cal AD 659–775
Poz-23613	Sangis 730	Hearth A20	Burnt bone	1250±40	cal AD 671–880
Vivungi 723					

Ua-57833	Vivungi 723	Furnace area 3	Burnt bone	6310±33	5359–5214 cal BC
Ua-57836	Vivungi 723	Furnace area 3	Burnt bone	5512±34	4446–4268 cal BC
Ua-57835	Vivungi 723	Furnace area 2	Burnt bone	2631±33	894–772 cal BC
Ua-57837	Vivungi 723	Furnace area 2/3, hearth	Burnt bone	516±30	cal AD 1327–1446
Ua-57834	Vivungi 723	Furnace area 2	Burnt bone	331±30	cal AD 1479–1640
Ua-57832	Vivungi 723	Furnace area 2	Unburnt bone	288±31	cal AD 1499–1792

References

BENNERHAG, C. 2008. *Arkeologisk förundersökning. Haparandabanan 2006/2007. Lokal 7, 13, 20 och 39, Nederkalix socken. Inför byggandet av ny järnväg, sträckan Kalix-Haparanda, Norrbottens län* (Rapport 2008: 1). Luleå: Norrbottens museum.

– 2009a. *Arkeologisk slutundersökning. Haparandabanan 2007. Lokal 13, 20 och 39, Nederkalix socken, Norrbottens län* (Rapport 2009: 1). Luleå: Norrbottens museum.

– 2009b. *Arkeologisk förundersökning. En järnframställningsplats från förromersk järnålder. Raä 842, Nederkalix socken, Norrbottens län.* (Rapport 2009: 32). Luleå: Norrbottens museum.

– 2010. *Arkeologisk slutundersökning. Järnframställning vid Jernbacksmyren under förromersk järnålder. Raä 842, Nederkalix socken* (Rapport 2010: 42). Luleå: Norrbottens museum.

– 2018. Arkeologisk forskningsundersökning. *Järnframställning under förromersk järnålder i Vivungi. Raä Jukkasjärvi 723:2-3, Kiruna kommun, Norrbottens län* (Rapport 2018: 2). Luleå: Norrbottens museum.

BRONK RAMSEY, C. 2020. OxCal v4.4. Available at: http://c14.arch.ox.ac.uk/oxcal.html (accessed 2 September 2020).

BUCHWALD, V.F. 1998. Myremalm. *Geologisk Tidsskrift* 1: 1–26.

– 2005. *Iron and steel in ancient times.* Copenhagen: Det Kongelige Danske Videnskabernes Selskab.

BUCHWALD, V.F. & H. WIVEL. 1998. Slag analysis as a method for the characterization and provenancing of ancient iron objects. *Materials Characterization* 40: 73–96. https://doi.org/10.1016/S1044-5803(97)00105-8

DEVOS, W., M. SENN-LUDER, CH. MOOR & CH. SALTER. 2000. Laser ablation inductively coupled plasma mass spectrometry (LA-ICP-MS) for spatially resolved trace analysis of early-medieval archaeological iron finds. *Fresenius Journal of Analytical Chemistry* 366: 873–80. https://doi.org/10.1007/s002160051588

DILLMANN, PH. *et al*. 2017. Circulation of iron products in the North-Alpine area during the end of the first Iron Age (6^{th}–5^{th} c. BC): a combination of chemical and isotopic approaches. *Journal of Archaeological Science* 87: 108–24. https://doi.org/10.1016/j.jas.2017.10.002

GRANDIN, L. 2009. *En järnframställningsplats vid Korsbacken. Granskning av slagger och infodringsmaterial. Norrbotten, Nederkalix socken, Vånafjärden 100:1, fornlämning 842.* Riksantikvarieämbetet (UV GAL, analysrapport 2009: 20). Stockholm: Riksantikvarieämbetet.

– 2016. Smide i Gudbrandsdalen. Varifrån kom järnet? in I.M. Gundersen (ed.) *Gård og utmark i Gudbrandsdalen. Arkeologiske undersøkelser i Fron 2011–2012*: 243–52. Kristiansand: AS and Kulturhistorisk museum.

GRANDIN, L. & A. WILLIM. 2008. *Arkeometallurgiska analyser av slagg och metall från undersökningar längs Haparandabanan Norrbotten, Nederkalix och Nedertorneå socken, Kalix och Haparanda kommun* (Riksantikvarieämbetet. UV GAL, analysrapport 2008: 24). Stockholm: Riksantikvarieämbetet.

GRANDIN, L. & O. STILBORG. 2010. *Järnframställningsplatsen vid Järnbacken. Analys av järnavfall, slagger och infodringsmaterial från en ugn från förromersk järnålder. Norrbotten, Nederkalix socken, fornlämning 842.* (Riksantikvarieämbetet. UV GAL, analysrapport 2010: 15). Stockholm: Riksantikvarieämbetet.

HEIMANN, R.B., U. KREHER, I. SPAZIER & G. WETZEL. 2001. Mineralogical and chemical investigations of bloomery slags from prehistoric (8th century BC to 4th century AD) iron production sites in Upper and Lower Lusatia, Germany. *Archaeometry* 43: 227–52. https://doi.org/10.1111/1475-4754.00016

Historical Metallurgical Society. 2021. Glossary of terms. Available at: https://historicalmetallurgy.org/glossary/ (accessed 2 November 2020).

LANTING, J.N., A.T. AERTS-BIJMA & J. VAN DER PLICHT. 2001. Dating of cremated bones. *Radiocarbon* 43: 249–54. https://doi.org/10.1017/S0033822200038078

LINDÉN, M., P. MÖLLER, S. BJÖRCK & P. SANDGREN. 2006. Holocene shore displacement and deglaciation chronology in Norrbotten, Sweden. *Boreas* 35: 1–22. https://doi.org/10.1080/03009480500359160

OGENHALL, E. 2015. *Slagg, järn och teknisk keramik från Jukkasjärvi. Järnhantering i nordligaste Sverige. Norrbottens län, Lappland, Kiruna kommun, Jukkasjärvi socken, Vivungi, RAÄ 723:1* (Riksantikvarieämbetet. AU GAL Rapport 2015: 03). Stockholm: Riksantikvarieämbetet.

OGENHALL, E. & L. GRANDIN. 2017. *Järnframställning i Vivungi, Jukkasjärvi. Arkeometallurgiska analyser av slagg, malm, stål och teknisk keramik. Vedartsanalyser av träkol samt resultat från 14C-dateringar. Norrbottens län, Lappland, Kiruna kommun, Jukkasjärvi socken, Vivungi, RAÄ 723:1* (Riksantikvarieämbetet. UV GAL, analysrapport 2017: 05). Stockholm: Riksantikvarieämbetet.

REIMER. P.J. *et al*. 2020. The IntCal20 Northern Hemisphere radiocarbon age calibration curve (0–55 cal kBP). *Radiocarbon* 62: 725–57. https://doi.org/10.1017/RDC.2020.41